“Bereitstellung thermodynamischer Daten für die Auswahl des Arbeitspaares bei Absorptionskältemaschinen”

zur Erlangung des akademischen Grades eines
DOKTORS DER INGENIEURWISSENSCHAFTEN (Dr.-Ing.)

der Fakultät für Chemieingenieurwesen und Verfahrenstechnik des
Karlsruher Institut für Technologie (KIT)

genehmigte
DISSERTATION

von
Dipl.-Ing. Hendryk Rudolph
aus Berlin

Referent:	Prof. Dr. habil. rer. nat. Sabine Enders
Korreferent:	Prof. Dr.-Ing. habil. Jadran Vrabec
Tag der mündlichen Prüfung:	09.06.2017

Danksagung

Im Rahmen meiner Arbeit welche zwischen März 2013 und Dezember 2016 entstand wurde ich von vielen Menschen unterstützt, sodass eine Aufzählung hier den Rahmen sprengen würde. Allerdings möchte ich einige besonders heraus heben, da ihre Hilfe besonders wichtig für den Erfolg dieser Arbeit war.

An erster Stelle soll dabei natürlich meine Doktormutter Prof. Dr. rer. nat. habil. Sabine Enders stehen. Sie unterstützte mich nicht nur im Rahmen meiner Bearbeitung des Dissertationsthemas und meiner Projektarbeit sondern schenkte mir auch ihr Vertrauen durch die Übertragung von Lehraufgaben.

Des Weiteren möchte ich allen wissenschaftlichen und technischen Mitarbeitern der Institute in Berlin und Karlsruhe bedanken mit denen ich im Rahmen meiner Promotion zusammen gearbeitet habe. Besonderen Dank möchte ich dabei Tommy Grunert, Kai Langenbach, Udo Dorn und Markus Bücherl zukommen lassen, mit denen ich immer wieder über wissenschaftliche und manchmal auch nicht ganz so wissenschaftliche Dinge reden und philosophieren konnte. Außerdem möchte ich einen Extra-Dank an Christoph Walowski und Christian Bühl aussprechen, die mir manche Hotelnacht in Karlsruhe erspart haben. Außerdem möchte ich Karin Daniel danken, die mir die eigene als auch die Betreuung der studentischen Arbeit in den Laboren der TU immer wieder deutlich vereinfacht hat.

Auch ohne die Unterstützung meiner Familie wäre der Erfolg dieser Arbeit wohl nicht möglich gewesen. Besonders meine Eltern Ute Rudolph und Heiner Wolf sowie meine Freundin Mareike Margraf waren immer für mich da.

Außerdem gilt mein Dank Holger Gödecker, Fabian Fleischer und Antje Fleischer, die es auf sich genommen haben, diese Arbeit von Fehlern zu bereinigen. Eine Arbeit die sie gerne und gründlich gemacht haben und sich damit meinen ewigen Dank verdient haben.

Für die finanzielle Unterstützung danke ich der TU Berlin, dem KIT und dem Bundesministerium für Bildung und Forschung (E-Norm).

Abstract

Since the cooling of e.g. produced goods or rooms is common and essential to modern life, the potential in energy savings even from minor optimizations is a given. One field of potential optimization for absorption chillers is the choice of an efficient working pair. A promising group for the absorbents are the so-called ionic liquids. By smartly choosing the cation and anion, it is possible to tailor-make the ionic liquid to the desired specifications, combined with an alcohol as cooling agent, even to cooling temperature lower than 0°C. Since these specifications are hard to predict, an extensive screening process is usually needed. In this work, a method is established to quickly gain first information about the performance of a working pair. To achieve this, PC-SAFT parameters are fitted to experimental results of the density which can be gathered reliably in a timely manner. Together with already established parameters for the alcohols, the VLE-behaviour and from that the possible cooling temperature can be determined. Also the possibility of a liquid-liquid-equilibrium can be evaluated which is of course a knock out criterion for a working pair. With additional experimental results for the heat capacity of the ionic liquids, the efficiency of the absorption process can be predicted. The evaluation of the influence of the non-idealities shows, that for a better prediction of the efficiency and cooling temperatures, these can't be neglected. For a possible simulation of the absorption process which includes the transport processes, an improved method for the calculation of self- and binary diffusion coefficients based on the Chapman-Enskog-theory is presented. This method is only applicable for non-associating molecules, yet.

In summary, this work presents a new method to quickly and efficiently gain first information in the selection process for a working pair consisting of an ionic liquid and an alcohol. The possible cooling temperature and the efficiency can be predicted by relying only on a few quickly accessible experimental results and therefore avoiding a huge and time-consuming screening process.

Kurzfassung

Die Bereitstellung von Kälte, z.B. für die Haltbarmachung von Lebensmitteln oder die Klimatisierung von Räumen, benötigt Energie und ist für unser Leben essenziell und weit verbreitet. So können bereits kleine Optimierungen große Energieeinsparungen zur Folge haben. Bei der Benutzung von Absorptionskältemaschinen liegt ein Einsparungspotential in der Auswahl des sogenannten Arbeitspaares. Eine vielversprechende Gruppe für das Absorbenz ist dabei die der ionischen Flüssigkeiten. Die Kombinationsmöglichkeiten von Anion und Kation ermöglichen eine Maßschneiderung der Flüssigkeit an die gewünschten Eigenschaften. Gemeinsam mit einem Alkohol als Kühlmittel kann so eine Kältemaschine ermöglicht werden, die Effizient auf Temperaturen unter 0°C kühlt. Da die Voraussage von Eigenschaften der Ionischen Flüssigkeiten problematisch ist kommt man um ein ausführliches Screening nicht herum. In dieser Arbeit wird aufgezeigt, wie bereits am Anfang des Auswahlprozesses schnell erste wichtige Erkenntnisse zu einem Arbeitspaar gewonnen werden können. Dazu werden PC-SAFT Parameter an Dichtemesswerte, welche schnell und verlässlich ermittelt werden können, angepasst. Zusammen mit etablierten PC-SAFT Parametern für die Alkohole lassen sich sowohl das VLE Verhalten, und daraus maximal mögliche Kühltemperaturen, vorhersagen, als auch die eventuelle Existenz von Flüssig-Flüssig-Gleichgewichten, welche den Einsatz eines Arbeitspaares bereits ausschließen können. Mit zusätzlichen Messwerten der Wärmekapazität der ionischen Flüssigkeiten lassen sich weiterhin Aussagen über die Effizienz der Kältemaschinen machen. Die Untersuchung des Einflusses der Nichtidealitäten auf die Effizienz zeigt, dass eine wirkliche Beurteilung nur mit experimentellen Daten zum Mischungsverhalten möglich ist. Für eine spätere Simulation eines Absorptionsprozesses inklusive der Transportprozesse wird eine neue, verbesserte Möglichkeit der Berechnung der Selbst- und binären Diffusionskoeffizienten mittels Chapman-Enskog-Theorie aufgezeigt welche bisher aber nur auf nicht assoziierende Stoffe angewendet werden kann.

Zusammengefasst zeigt diese Arbeit eine neue Methode schnell und effizient erste Informationen über ein Arbeitspaar für Absorptionskälteprozesse bestehend aus einer ionischen Flüssigkeit und einem Alkohol zu bestimmen. Dabei können Aussagen zu Kühltemperaturen und Effizienz mit wenigen Messwerten gemacht und somit ein aufwendiges Screening umgangen werden.

Table of Contents

Nomenclature

Symbols

$A(T)$	substitution function for ideal gas heat capacity
A_{D}	correctional parameter for diffusion coefficient
a_i, b_i	universal model constants
c	circulation ratio
C_1	compressibility expression
c_{P}	heat capacity at constant pressure
c_{v}	heat capacity at constant volume
D	Diffusion coefficient
d_i	temperature dependent segment diameter
$D_{\mathrm{k}}, D_{\mathrm{l}}$	damping factor for correction of combining rules
D_{M}	mean deviation
f	Helmholtz energy
g_{ii}	radial distribution function
I_1, I_2	power series of integrals of perturbation theory
$\mathrm{k_B}$	Boltzmann constant
k_{ij}	correction of combining rules for interaction energies
l_{ij} l	correction of combining rule for segment diameter
L_i	components of a vector in a polar crystal
m	segment number
M_A	molecular weight of species A
M_i	number of association sites in molecules of species i
N	number of molecules in a volume element
$\mathrm{N_{AV}}$	Avogadro constant
P	pressure

p	polynomial for correction of density
T	temperature
u	speed of sound
w	weight fraction
x_i	mole fraction of species i
X^A	mole fraction of molecules not bonded at site A

Greek Symbols

Δ^{AB}	association strength
ε	dispersion interaction energy
$\varepsilon_{\mathrm{LJ}}$	Leonard-Jones interaction energy
ε^{AB}	association interaction energy
η	reduced density
γ	surface tension
κ	adjustable parameter for surface tension
$\boldsymbol{\kappa}^{(1)}, \boldsymbol{\kappa}^{(2)}$	tensors reflecting crystal symmetry
κ^{AB}	association volume
π	circle number
ρ	density
σ	segment diameter
$\zeta_1, \zeta_2, \zeta_3$	variations of density ($\zeta_3 = \eta$)

Superscripts

association	associations contribution
chain	chain contribution
disp	dispersion contribution (SAFT-framework)
dispersion	dispersion contribution (PC-SAFT framework)
hard-chain	hard-chain contribution
hs	hard-sphere contribution
ideal gas	ideal gas contribution
res	residual

||

seg	segment contribution
VL	at saturated vapor level

Subscripts

0	pure component contribution
E	derived from Chapman-Enskog theory
HS	hard-sphere diffusion
i	species of molecule
k	correction of combining rules for interaction energy
l	correction of combining rules for segment diameter
R	reduced

Abbreviations

BACK	Boublik-Alder-Chen-Kreglewski
COP	Coefficient of Performance
COSMO	Conductor like Screening Model
DGT	density gradient theory
EOS	equation of state
IL	ionic liquid
LLE	liquid liquid equilibrium
MD	molecular dynamics
NRTL	non-random two liquid model
PCP-SAFT	perturbed chain polar-self associating fluid theory
PC-SAFT	perturbed chain-self associating fluid theory
PFG-NMR	pulsed field gradient-nuclear magnetic resonance
RTIL	room temperature ionic liquid
SAFT	self-associating fluid theory
TLV	threshold limit value
VLE	vapor liquid equilibrium
VR	variable range

Ionic liquid abbreviations

[EMIM][OAc]	1-ethyl-3-methylimidazolium acetate
[BMIM][BF4]	1-butyl-3-methylimidazolium tetrafluoroborate
[OMIM][BF4]	1-octyl-3-methylimidazolium tetrafluoroborate
[BMIM][CF3SO3]	1-butyl-3-methylimidazolium Trifluoromethanosulfonate
[BMIM][PF6]	1-butyl-3-methylimidazolium hexafluorophosphate
[HMIM][PF6]	1-hexyl-3-methylimidazolium hexafluorophosphate
[OMIM][PF6]	1-octyl-3-methylimidazolium hexafluorophosphate
[BMMIM][PF6]	1-butyl-2.3-dimethylimidazolium hexafluorophosphate

1 Introduction

In recent years, it has become more and more evident, that massive, unrestricted energy consumption could pose a huge problem for humanity. With oil reservoirs of the world emptying [1], the short term environment costs of coal [2,3] and the long term environment costs of nuclear energy being very problematic [4] and renewable energies being in the fielding stages, possibilities for conserving energy are not only highly desirable but possibly existential for humanity. The consumption of energy occurs in many different aspects of life, e.g. in the production of goods, transport of goods and people and of course in the temperature control of again goods and people alike, be it heating like the tempering of rooms in the winter or cooling of these rooms in summer or even in the winter, e.g. the cooling of sensitive foods that need to be frozen at any time before consumption [5]. This task has been the subject of constant improvement from early forms like the harvesting of ice in frozen lakes in the north and transporting it to the south to be utilized for cooling, to the first compression chillers and refrigerators, able to provide cold anywhere with a power source. An alternative to the compression chiller is the concept of absorption chillers, using two chemicals, one being the cooling agent which is evaporated and the latent heat of evaporation being used to cool its surrounding, and one being the absorbent, as the name implies, absorbing the evaporated cooling agent and together being pumped to a higher pressure level before the cooling agent is desorbed and condensed, starting the absorption cycle again. A schematic of a typical so-called “single-effect”-absorption cooler is pictured in Figure 1. One of the advantages of this process is the possibility of utilizing waste heat as the heat medium needed to desorb the cooling agent from the diluted solution in the so-called desorber, pictured in the top left in Figure 1. This possibility of using waste energy normally simply disposed off into the environment has made huge inroads for this concept in the cooling of storage rooms adjacent to production facilities. The list of the possible combinations of cooling agent and absorbent, together forming a working pair, that have been examined, is long [6], but only two systems are widely used [7]. One is water + lithium bromide (LiBr) with water being the cooling agent and LiBr being the absorbent and the other one being ammonia + water with this time water being the absorbent and ammonia being the cooling agent. While these combinations have several drawbacks, such as corrosiveness, crystallization and toxicity [8], one of the biggest has to be, that the

incorporation of water into the working pairs limits the achievable cooling temperatures to be above the solidification temperature of water, meaning the freezing of goods is not possible.

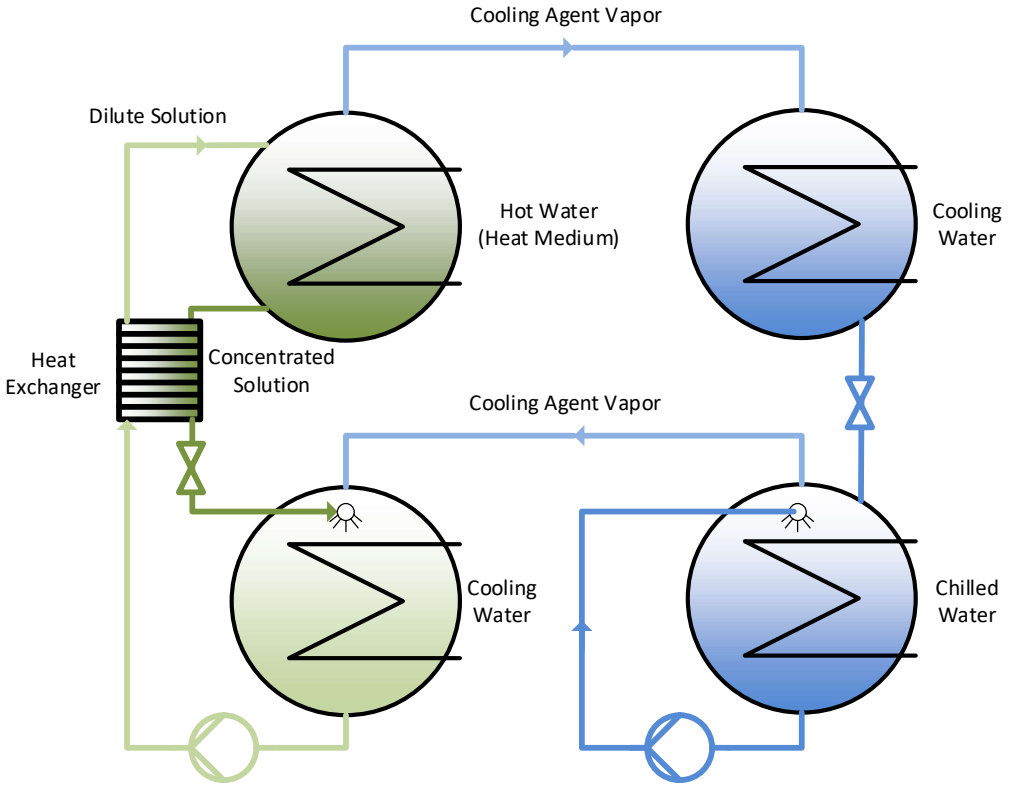

Figure 1: Schematic of a single effect absorption chiller.

A possible solution for this problem could be the use of alcohol as a cooling agent, since the solidification temperatures are much lower than with water. To complete the working pair, a suitable absorbent has to be chosen. A possible co-fluid for alcohol as cooling agent might be found in a recently more and more popular group of solvents, the so called room temperature ionic liquids. A salt mostly composed of an organic cation and a non-organic anion which is in the liquid state at ambient temperature and pressure. These ionic liquids have many favourable properties that benefit them to be the absorbent in an absorption cycle. They have a negligible vapor pressure, making it possible to retrieve a pure cooling agent in the desorber. Depending on the combination of ions, they are of low toxicity and corrosivity. Since there is a nearly endless combination of possible cations and anions with a wide variety of properties, ionic liquids are often said to possibly be “tailor-made” for specific purposes. These purposes are not limited to absorption chillers, ionic liquids have been proposed for a wide variety of fields, from gas purification [9] over the aforementioned absorption

cycles (for cooling and of course for heating) to simply being used as a fine tuneable lubricant [10]. To really tailor the ionic liquid for the purpose in mind (in this work, as absorbent), it is necessary to predict different properties of the ionic liquid correctly and reliably. To calculate the performance of an absorption cycle, even when the modelling is done by a simple energy balance around the whole cycle, omitting any non-idealities, it is necessary to calculate the vapor liquid equilibrium (VLE) of the working pair and the enthalpies or heat capacities of the pure cooling agent as well as of the dilute and concentrated mixtures. For more sophisticated simulations, more complex characteristics are needed such as the transport properties. The development of suitable predication methods is hindered by the amount of possible ion combinations since the experimental data is sparse and scattered over the variety of the ionic liquids [11,12]. Therefore, to truly know about the performance of a working pair, experimental work is still necessary. Since this experimental work is laborious and time- and money-consuming, a simple method with as little experimental data as possible to give a first idea of the possibility of utilizing an alcohol + ionic liquid combination is highly desirable. In this work, the approach of using Perturbed Chain Statistical Associating Fluid Theory (PC-SAFT) to calculate the VLE, the enthalpies in the different states and following the coefficients of performance is examined. The parameters for the PC-SAFT Equation of State (EOS) are fitted to liquid densities, as they can be measured with a good accuracy and a reasonable effort in time and money. With these parameters, the presence of process hindering liquid liquid equilibria (LLE) will be examined and also a first step to describing the transport property diffusion coefficient will be done. The goal of this work is the compilation and theoretical evaluation of a quick and reliable method to examine working pairs consisting of alcohol and ionic liquid, suspending working pairs with LLEs and assess working pairs that are feasible for an absorption refrigeration process with a cooling temperature lower than T=273.15K. This will of course not give a realistic outlook of the performance of a real life absorption refrigerator, as any non-idealities in the process itself are omitted, e.g. losses at the heat exhchanger, pressure drops in the pipes and the degree of efficiency of the pumps. But it can provide valuable information in the field stages of the selection of a specific working pair.

2 State of the art

2.1 Absorption chillers and ionic liquids

Ionic liquids are defined as the combination of a cation and an anion, i.e. a salt, that is in the liquid state at temperatures below T=373.15K. Since the ionic liquids tend to have long complicated names, these names are in general shortened. But since no universally agreed way to abbreviate the names exists, every author is free to choose their own. To avoid any misunderstandings, the abbreviations for the ionic liquids used in this work are listed under the nomenclature. A branch of these ionic liquids are the so called room temperature ionic liquids (RTIL), that are, as the name says, in the liquid state at room temperature and sometimes even lower. Melting points lower than T=200K are reported [13]. Interest for these substances rose in the last decades, which can yield the impression of the IL being a relatively newly discovered substance, but this impression would be wrong. While the first discovered ionic liquid as well its discoverer are unknown, it can be said, that one of the first reports was by Gabriel and Weiner and their paper on derivatives of propylamins [14] where they described ethanolammonium nitrate. With a melting point around T=325K, this was of course no room temperature ionic liquid. One of the first RTIL that was reported by Walden in 1914 [15], with the ionic liquid being ethylammonium nitrate showing a melting point around T=285K. RTILs usually consist of an organic and bulky cation and a mostly an-organic anion [16]. The bulky cation is hindering the electromagnetic interactions between the molecules and together with its steric effects lowers the melting point of the salt, making it an ionic liquid. Since these cations and anions are freely combinable, a huge number of possible combinations with a huge number of different physical and chemical properties can be generated. This gave rise to the view of ionic liquids being “tailor-made” compounds that can be combined to suit nearly every possible desire. This was one of the reasons for the peaking interest in recent time, along with favorable characteristics such as low volatility, non-toxicity, thermic stability and others, all of course subject to the actual cation+anion combination. Since the large number of possible combinations yields a large number of widely varying properties, ionic liquid use has been proposed in many different fields such as the production of fuel cells (e.g. [17,18]), the production of bio fuels (e.g. [19,20,21]), as entrainers in extractive distillation (e.g. [22]) or in the azeotrope distillation (e.g. [23]). To truly tailor an ionic liquid for a single purpose, the physical

properties of the combination have to be predictable. Coutinho et al. [24] found that the predictive models are hindered by a lack of reliable data for the properties of the ionic liquids, which may be attributed to a large number of combinations which seems to be the disadvantage of the large number of possible cations and anions.

Plechkova and Seddon [25] point out, that the possibility of tailoring special solvents for special purposes increases dramatically by allowing for mixtures of ionic liquids, but it is this authors believe that this is a task for the future, when the properties of a single ionic liquid are completely understood and predictable.

One of the most often mentioned functions of ionic liquids is their usage as an absorbent. Their low volatility helps recapturing the previously absorbed substance without losing too much of the absorbent. This is why ionic liquids are seen as very promising tools in CO_2-capture [26,27]

Another one of the most mentioned uses for the ionic liquids and the focus of this work is the use of ionic liquids as the absorbents in absorption chillers. As one can imagine, there is a huge variety of ionic liquids proposed as the absorbents, as there is a huge variety of anion and cation combinations, but there is also a variety of cooling agents proposed, for example water, ammonia and several hydrocarbons. And these various combinations of ionic liquids and cooling agents get treated with a variety of approaches to calculate their states. Many groups have put a lot of work and effort into this field, publishing a series of works mostly on special IL + cooling agent combinations. Wang et al. [28] examined absorption chillers with 1-ethyl-3-methylimidazolium tetrafluoroborate ([EMIM][BF4]) + 2,2,2-trifluoroethanol (TFE) and 1,3-dimethylimidazolium chloride ([DMIM][Cl]) + water, calculating the vapor pressures with a combination of non-random-two-liquid model in combination with an antoine-type equation for the pure cooling agent. Zhang and Hu [29,30] calculated 1-ethyl-3-methylimidazolium dimethylphosphate ([EMIM][DMP]) + water as well as lithium bromide + water and TFE + tetraethylenglycol dimethylether, predicting the coefficients of performance (COPs) for the IL + water system at around $\mathrm{COP} = 0.72...0.75$. They reported a connection of the temperature in the evaporator and the COP with the COP decreasing with a decreasing temperature in the evaporator [29]. Yokozeki and Shiflett [31,32,33] evaluated 12 ionic liquids, including [BMIM][PF6] and [BMIM][BF4], and LiBr with water as a cooling agent. Based on the model proposed by Yokozeki [34], Yokozeki and Shiflett [33] modelled the absorption

cycle with an Redlich-Kwong type equation of state with parameters for the ILs fitted to binary VLE data and calculated COPs in the range of $COP = 0.525...0.691$. Kim et al., Kim and Gonzalez and Kim and Kohl [35,36,37,38,39] examined 7 ionic liquids including [BMIM][PF6] with 5 hydrocarbons as cooling agents by utilizing NRTL equations as well as Redlich-Kwong type EOS. They reported COPs up to 0.8. Preißinger et al. [40], Swarnka et al. [41] and Weith et al. [42] examined the possibilities of an ionic liquid + water absorption cycle. Swarnka et al. [41] were trying to improve the cycle by adding ammonia, thereby creating a ternary system. Using NRTL within the process simulation software AspenPlus no significant drop in the COP but a lower circulation ratio was calculated. Weith et al. [42] also used AspenPlus in combination with NRTL looking for improvements by switching from single-effect to double-effect absorption cycles which means adding a second condenser and desorber to allow for more refrigerant being desorbed from the solution. Preißinger et al. [40] again used AspenPlus together with NRTL but reported that they expect deviations between their calculations and possible experimental results as AspenPlus always assumes a small percentage of ionic liquid in the cooling agent stream. Ruiz et al. [43] did simulations of 6 different ionic liquids and ammonia for a simple absorption cycle similar to the one in Figure 1 but without the heat exchanger between the concentrated and diluted solutions. They [43] were using the COSMO framework, reporting COPs of $COP = 0.54...0.67$. Kurnia et al. [44] also utilized the COSMO framework and screened for the ionic liquids with the highest water solubilities and therefore for an ideal ionic liquid for a water based absorption cycle. They [44] suggested the use of dianionic IL, e.g oxalate. Mozurkewich et al. [45] used a Langmuir-like model to examine the possibilities of an absorption cycle with a theoretical cofluid to CO_2 as a cooling agent and therefore creating a molecular design guidance for ionic liquids that could be tailored after the theoretical cofluids.

In 1988 Jackson et al. [46] and Chapman et al. [47,48] developed the SAFT framework to calculate the states of a hard sphere liquid. It follows the concept of a perturbation theory, as it summarizes contributions perturbing the state of the original reference system. To account for associating substances, they [46,47,48] implemented the Wertheim contribution [49,50,51,52]. For non-associating molecules, the substance is described with 3 parameters, for associating molecules,

2 additional parameters are needed. This framework has led to many deviations to either improve on shortcomings of the original model or include substances with interactions not originally included.

In 1997, Gil-Vilega et al. [53] and Galindo et al, [54] developed the SAFT-VR EOS where the reference fluid consisted of not of hard spheres but of spheres with a variable attraction range (VR=variable range). Since the range of attraction is another variable in the equation, an associating molecule needs 6 parameters to be described.

In 1998 Adidharma and Radosz [55] developed the heterosegmental SAFT EOS for polymers, which Ji and Adidharma evolved for electrolytes [56,57,58]. In this framework, the ions of the ionic liquid are treated as separate fluids, each one described with 5 parameters bringing the total of parameters for a single ionic liquid up to 10.

In 2001 and 2002 Gross and Sadowski [59,60] developed the PC-SAFT framework, where the reference system is now described as hard chains. The number of parameters for an associating fluid is 5, as in the original SAFT framework.

In 2001 Blas and Vega [61] introduced their soft-SAFT approach. In this framework, the reference fluid is a Lennard-Jones type. Just as SAFT and PC-SAFT, an associating molecule can be described with 5 parameters.

In 2002, Hu et al. [62] combined the BACK-Equation of Boublik-Alder-Chen-Kreglewski EOS [63] with the Wertheim contribution for associating molecules establishing the SAFT-BACK framework. An associating molecule is described in the framework with 7 parameters, therefore needing 2 more than SAFT, PC-SAFT and soft-SAFT.

As an extension of the PC-SAFT framework for electrolytes, in 2005 Camaretti et al. [64] developed the ePC-SAFT framework. The ionic interactions are modelled with the Debye-Hückel theory that was developed for strong electrolytes. In the case of ionic liquids, the association is neglected, but since the ions are treated as separated molecules, a single ionic liquid is described with 6 parameters. The different SAFT-Versions, its contributions and number of parameters per pure ionic liquid is summarized in Table 1.

Name	Contributions	Parameter per pure IL	Source
SAFT	$f = f^{HS} + f^{MF} + f^{association}$	5	[46,47,48]
SAFT-VR	$f^{res} = f^{Mono} + f^{Chain} + f^{association}$	6	[53,54]
Heterosegmental SAFT	$f^{\mathrm{res}} = f^{\mathrm{HS}} + f^{\mathrm{disp}} + f^{\mathrm{chain}} + f^{\mathrm{association}}$	10	[55]
PC-SAFT	$f^{res} = f^{\mathrm{hard\,chain}} + f^{\mathrm{dispersion}} + f^{\mathrm{association}}$	5	[59,60]
Soft-SAFT	$f^{\mathrm{res}} = f^{\mathrm{LJ}} + f^{\mathrm{chain}}$	5	[61]
SAFT-BACK	$f^{\mathrm{res}} = f^{\mathrm{rep}} + f^{\mathrm{att}} + f^{\mathrm{association}}$	7	[62]
ePC-SAFT	$f^{\mathrm{res}} = f^{\mathrm{hard\,chain}} + f^{\mathrm{dispersion}} + f^{\mathrm{association}} + f^{ion}$	6	[64]

Table 1: SAFT and Deviations with their respective contributions and number of parameters for a single ionic liquid.

These different SAFT variations have been used in combination with ionic liquids.

The SAFT framework with some minor variations has already been used for ionic liquids [65,66]. Seyfi et al. [65] used the SAFT framework with a different hard-sphere equation for electrolytes while treading the ions as individual species and Guzman et al. [66] combined the SAFT framework with a mean spherical approximation to calculate the vapor-liquid-equilibrium VLE of pure ionic liquids and compared them with MC-simulations both reaching good agreements. Polichuk [67,68,69] combined the SAFT-framework with a cubic equation of state and compared it to a cubic-plus-association (CPA) approach, a SAFT version generalized for heavy compounds (GSAFT) plus a cubic EOS and PC-SAFT for ionic liquids including [BMIM][PF6]. While all approaches yielded good results, the GSAFT approach worked best for ionic liquids. But as this approach is specially built for heavy molecules, it cannot be utilized for the short-chain alcohols of methanol and ethanol that are the subject of this work. The 5 pure component parameters for the CPA were taken from Maia et al. [70] and are showing deviations with speed of sound and density predictions. The PC-SAFT parameters are taken directly from Paduszynski et al. [71], they show deviations in the prediction of heat capacities but this may be attributed to the treatment of the ideal gas contribution.

The SAFT-VR equation [53,54] was utilized for the calculation of electrolytes [72,73]. Also several variations of the SAFT-VR have been used like the SAFT-VR-Mie

equation [74,75], a special SAFT-VR version for electrolytes (SAFT-VRE) [76] or the SAFT-γ group contribution expansion [77] which has also been used in the context of ionic liquids [78]. In the SAFT-VR framework, ILs are treated as individual ions, too. Association is neglected. This means that a single IL is described by 6 pure component parameters (3 per ion) and 2 temperature dependent interaction parameters. With these parameters the CO_2-solubility can be described well, but deviations in the calculations of the density occur.

The heterosegmental SAFT framework was utilized for ionic liquids by Ji and Adidharma [56,57,58], where the cation was modeled as a chain with one segment as the ionic head and a chain of different segments as the alkyl remainder and the anion as a single spherical segment. It was used to calculate the mixture of CO_2 and ionic liquids including [BMIM][BF4] [79]. This SAFT version performed well for the calculation of densities and CO_2-solubilities, but as the ions of the ionic liquids are treated as individual species, one ionic liquid needs fitting of 10 pure component parameters.

The PC-SAFT framework has been widely used to describe ionic liquids. Domanska et al. [80,81], Paduszynski et al. [82,83,84,85,86,87,88,89], Paduszynski and Domanska [52,90] and Lukoshko et al. [91] examined several association schemes for treating the ionic liquids, from the 2B [83,90], a 3 donor and 3 acceptor scheme (“3+3”) [85,86,87,91], a “4+4” scheme [84,86] and a “5+5” scheme [71,80,81,82,88,89] depending on the anion in the examined ionic liquid. They report that they observed deviations for the different schemes in [71] but do not supply the data to support the claim. Krolikowska et al. [92] even utilized a “7+7” scheme for the ethylsulfate anion. Other groups have also successfully implemented the PC-SAFT framework with the calculations of ionic liquids [93,94,95,96,97,98,99,100,101,102], most of them utilizing the “2B” association scheme but also calculations using a “5+5” scheme [97,98,99]. Comparison between the different schemes is problematic since because of the variety of the available ionic liquids, same ionic liquids are seldom used with different schemes. [BMIM][NTf2] was calculated by Mahato et al. [93] and by Curras et al. [96] with a 2B association scheme with reported average absolute deviations (AAD) for the calculated densities of AAD=0,12% and AAD=0.2% respectively while Paduszynski and Domanska calculated the densities with the “5+5” model reporting an AAD=0.16% for all ILs following [C_NMIM][NTf2] with N=1-

10,12,14. From this it can be concluded, that the influence of the association scheme is negligible. Joshipura [103] calculated the vapor pressures of pure ionic liquids with a cubic equation of state by combining it with a self-developed cohesion factor expression and reached good results compared to PC-SAFT calculations and COSMO based models. Alvarez and Saldana [104] utilized an artificial neural network (ANN) with COSMO-SAC parameters as input to calculate the VLE of ILs + CHF_3/CO_2. The calculations were compared to PC-SAFT calculations without an association contribution. The calculations did show that the association contribution is necessary and PC-SAFT without it is not suitable for ionic liquids. Khelassi-Sefaoui et al. [105] and Chen et al. [106,107,108] calculated CO_2-solubilities. They did not specify the association scheme used in the calculations, the association parameters were set to fixed values just as in the works of e.g. Andreu and Vega [122,123]. They [105,106,107,108] also had some deviations in the calculations of the pure IL densities.

The so called soft-SAFT equation where the reference fluid is composed of a Lennard-Jones fluid, hence the “soft”-prefix, was utilized for ionic liquids by several authors. Pereira et al. [109,110,111], MacDowell et al. [112], Oliveira et al. [113,114,115], Lovell et al. [116,117,118,119,120], Vega et al. [121], Andreu and Vega [122,123] calculated densities of ionic liquids and mixtures of ionic liquids with several organic and non-organic gases. The parameters related to association were set to fixed values and the remaining parameters were fitted to the IL densities with good results overall but small deviations for the calculations of pure IL densities.

The SAFT-BACK equation, a combination of the Boublik-Alder-Chen-Kreglewski framework [63] and the SAFT framework was evolved for ionic liquids by Magheri et al. [124,125,126,127] with which they reached good results for the calculation of the speed of sound in ionic liquids but had deviations to the vapor pressures [128,129] that were estimated by Paulechka et al. [130) and Kabo et al. [131]. To achieve these results, the SAFT-BACK version made use of 7 pure component parameters.

The ePC-SAFT framework developed by Camaretti et al. [64] is an extension of the PC-SAFT framework for electrolytes based on the Debye-Hückel theory accounting for the long range electromagnetic interactions of the ions. Held et al. [132] and Held and Sadowski [133] utilized this electrolyte framework for the electrolytes and following from there the framework was used to calculate a lot of ionic liquids and

mixtures containing them. Shen et al. [134,135,136] reached good results for the calculation of surface tension and speed of sound predictions but also had some deviations in the prediction of heat capacity. This may again be attributed to the ideal gas contribution as it was treated similar to the works of Polichuk [67]. Ji et al. [137] were successful in modelling the densities of pure ionic liquids and their binary mixtures. Neves et al. [138] did successful calculations of the solubilities of ionic liquids in water. Verevkin et al. [139] calculated viscosity and CO_2-solubility with ionic liquids. The results were again good. The same goes for the calculations of Ji et al. [140,141]. The ePC-SAFT framework has also successfully been utilized by other groups [142]. But since the ionic liquids are again treated as individual ions, a single ionic liquid is described by 6 pure component parameters.

The performance of several SAFT and SAFT-based frameworks has also been reviewed by Vega and Llovell [143] for aqueous solutions including ionic liquids. They pointed out the importance of the inclusion of the association interaction into the framework and also suggested that the approach of keeping the association sites to a minimum might be a physically more reasonable approach. Tan et al. [144] reviewed SAFT framework and its advancements for complex systems including ionic liquids pointing out that the incorporation of different interactions made the framework a powerful scientific and engineering EOS.

In this work the PC-SAFT framework with the 2B association scheme is utilized. This keeps the number of pure component parameters for the description at 5 which is in line with this works goal to find a quick and simple method to evaluate the ionic liquids. The SAFT and the soft-SAFT approach do also need only 5 parameters per pure component. But in the literature, the SAFT approach has only been used to calculate ionic liquids after modification. And the goal of this work is to find an equation of state, that can treat the ionic liquid and the cooling agent the same. Therefore, an EOS modified specifically for ionic liquids is not useful. The soft-SAFT approach did show deviations in the calculation of the densities. Since the densities play a key role in the method laid out in this work. So the soft-SAFT EOS is omitted, too. The PC-SAFT approach with contribution for the association is able to calculate ionic liquids and cooling agents with a satisfiable accuracy. To correctly calculate the densities, the association parameters are not being set to a fixed value but being fitted to the experimental data as well. Since ionic liquids are electrolytes, the

question arises if the description can be improved by incorporating the electrolyte interactions as in the ePC-SAFT framework. But as said earlier, the interactions are described on the basis of the Debye-Hückel theory, which was developed for strong electrolytes. Ionic liquids however can be expected to be weak electrolytes [145]. Since many authors were successful in describing ionic liquids with PC-SAFT with the association contribution (e.g [83,93]), this will be done in this work, too.

While to the best of this author's knowledge, the combination of modelling an absorption cycle in combination with the Perturbed Chain-Self Associating Fluid Theory (PC-SAFT) framework or some other SAFT derivatives (e.g. ePC-SAFT, Soft-SAFT) has not yet been examined, the modelling of ionic liquids and mixtures including them with the SAFT family is not a new subject.

2.2 Chapman-Enskog Theory

The transport properties are of particular importance for the modelling of several technical processes like rectification, extraction, drying (air or solids) or gas purification and of course absorption processes. So it is of no wonder, that the determination of these transport properties is often the subject in the literature. This determination can be divided into three greater columns, the experimental determination, the calculated determination utilizing an underlying theory and Monte-Carlo type or molecular dynamics (MD) simulations which fall kind of in-between the first two.

An often used experimental method is the pulsed field gradient nuclear magnetic resonance (PFG-NMR) technique [146,147,148,149,150,151,152]. In the PFG-NMR, the nuclei of a molecule are exposed to a magnetic field pulse which they absorb and then re-emit. This re-emission can be measured and in combination with a field gradient, can be translated into location information of the molecules which ultimately lead to self-diffusion coefficients. Another experimental method is the quasi-elastic incoherent neutron scattering in which neutrons are fired at the nuclei and the scattered neutrons are measured. These scattered neutrons can be interpreted, under the assumption of quasi-elastic scattering, to calculate the molecular motions and therefore the diffusion coefficients. This method has also been used in the literature [153]. Collections of the available experimental results can be found in the literature [152,154,155,156,157].

Other than the experimental methods, Monte-Carlo simulations [158] and molecular dynamic simulations [159,160,161,162] are a computerized method of determining the diffusion coefficients without the use of an underlying theory of diffusion. The computerized nature of the methods yield a wide range of temperature and pressure in which the method is feasible. This method has been used to determine the diffusion coefficients of non-polar fluids like noble gases [163], cycloalkanes [164] or several organic and non-organic gases [165]. The methods are of a special interest in the case of examining strong polar fluids like water [166,167,168] and alcohols [166,169]. The works of Guevara-Carrion et al. [169] are of special importance for this work with their predictions of the diffusion coefficients of methanol and ethanol and their mixtures at atmospheric pressure over a wide range of temperature. The predictions were in a good agreement with experimental data they took from literature.

Since the experimental work is time consuming and laborious and the Monte-Carlo and MD simulations come with a high demand of computing power and are therefore time consuming themselves, a calculative model for the prediction of the diffusion coefficients from data that is less elaborate in the determination is highly desirable. After the division of the estimation methods into three columns earlier, the methods of the calculative estimation can again be divided into two frameworks [170,171]. For the first framework it can be said, that the diffusion is determined by the excess entropy [172]. This framework is quite popular and many extensions have been made [173,174,175,176,177,178,179,180,181]. Another way to look at the transport properties is to acknowledge that the transport processes are mainly due to short range repulsive interactions namely hard sphere collisions. On this foundation, Chapman and Enskog individually developed their theory [182,183]. Since the theory was developed for diluted gases, one limitation is that it is only viable for low densities. This limitation was the target of many extensions [184,185,186,187,188,189,190,191,192,193,194,195,196,197,198,199,200]. The possibility to incorporate an equation of state directly into the Chapman-Enskog theory was also examined [201], in this case for the Peng-Robinson EOS. The Chapman-Enskog theory together with its modifications for the density was then also applied to examine mixtures [202,203,204,205,206,207,208]. But since most of these approaches utilize an interaction potential with parameters fitted to the transport

coefficients, these methods are not predictive and the laborious experimental work of measuring the diffusion coefficients is still needed.

The incorporation of EOS is of course not limited to Peng-Robinson as done by Sheng et al. [201], and one of the most successful EOS of the last decades has been the Perturbed-Chain-Polar–Statistical Association Fluid theory (PCP-SAFT) as developed by Gross and Sadowski [59,60] and extended by Gross [209] and Gross and Vrabec [210]. With this PCP-SAFT EOS it is possible to model a wide variety of substances like polar and non-polar fluids carrying a dipole or a quadrupole and associating and non-associating fluids. The SAFT, a predecessor of the PC-SAFT, and PC-SAFT framework was used to calculate the diffusion coefficients [211,212,213]. The SAFT of PC-SAFT-EOS was used to calculate the excess entropy [211,212] or in combination with extensions for the density inside of the Chapman-Enskog theory [189,214] to directly calculate the diffusion coefficients successfully [213].

Liu et al. [190] did review the different predictions and correlations of the diffusion coefficients and their performance in describing the experimental data. Although many different methods for the determination of the diffusion coefficients are available, no single method can truly excel at time and work consumption and accuracy, so the area can still be considered a work in progress. In this work, the possibility of predicting the diffusion coefficients from pure component parameters, fitted to liquid densities and vapor pressures, inside of the PCP-SAFT framework and integrated in the Chapman-Enskog theory, is examined to allow for the possibility to include the diffusion coefficient predictions in more sophisticated future absorption cycle simulations.

3 Theoretical methods

3.1 PC-SAFT EOS

Jackson et al. [46] and Chapman et al. [47,48] developed an EOS for a system consisting of hard spheres forming a chain combining it with the Wertheim theory [49,50,51,52] and therefore being able to treat associating hard spheres. This is known as the statistical associating fluid theory (SAFT). Within this framework it is possible to calculate the residual Helmholtz energy as the energy of the reference system and adding differences due to perturbation as additional terms. They [46,47,48] defined the reference system as a fluid consisting of hard spheres which is perturbed by the spheres building chains, dispersion and association interactions. The residual Helmholtz energy has therefore the mathematically form of [e.g.48]:

$$f^{\mathrm{res}} = f^{\mathrm{seg}} + f^{\mathrm{chain}} + f^{\mathrm{association}} \tag{1}$$

The individual contributions are calculated in the form of [48]:

$$f^{\mathrm{seg}} = f_{\mathrm{o}}^{\mathrm{seg}} \sum_i x_i m_i = \left(f_{\mathrm{o}}^{\mathrm{hs}} + f_{\mathrm{o}}^{\mathrm{disp}} \right) \sum_i x_i m_i \tag{2}$$

$$\frac{f_{\mathrm{o}}^{\mathrm{hs}}}{\mathrm{R}T} = \frac{4\eta - 3\eta^2}{(1-\eta)^2} \tag{3}$$

$$f_{\mathrm{o}}^{\mathrm{disp}} = \frac{\varepsilon_{\mathrm{LJ}} \mathrm{R}}{\mathrm{k_B}} \left(f_{\mathrm{o1}}^{\mathrm{disp}} + \frac{f_{\mathrm{o2}}^{\mathrm{disp}}}{T_{\mathrm{R}}} \right) \tag{4}$$

In these equations (2), (3) and (4), x_i is the mole fraction, m_i is the segment number, with i being the species of the molecule, $\varepsilon_{\mathrm{LJ}}$ is the Leonard-Jones interaction energy, η is the reduced density $\eta = \frac{\pi \mathrm{N_{AV}}}{6} \rho d^3 \sum_i x_i m_i$ and T_R is the reduced temperature $T_{\mathrm{R}} = \frac{\mathrm{k_B} T}{\varepsilon_{\mathrm{LJ}}}$. The segment equation consists of, for the hard spheres, a conventional Carnahan-Starling contribution [215] and for the dispersion of two terms $f_{\mathrm{o1}}^{\mathrm{disp}}$ and $f_{\mathrm{o2}}^{\mathrm{disp}}$ which are correlations from molecular simulation for a Lennard-Jones-Fluid. Chapman et al. [47,48] used an approach by Cotterman et al. [216]. The chain contribution f^{chain} in equation (1) is calculated as follows:

$$f^{\mathrm{chain}} = \sum_i x_i (1 - m_i) \ln \left(g_{ii}^{\mathrm{hs}} (d_{ii}) \right) \tag{5}$$

In this equation g_{ii} is the radial distribution function for hard spheres.

$$g_{ij}^{\mathrm{hs}} = \frac{1}{(1-\zeta_3)} + \left(\frac{d_i d_j}{d_i + d_j}\right)\frac{3\zeta_2}{(1-\zeta_3)^2} + \left(\frac{d_i d_j}{d_i + d_j}\right)^2 \frac{2\zeta_2^2}{(1-\zeta_3)^3} \quad \textbf{(6)}$$

$$\zeta_n = \frac{\pi}{6}\rho\sum_i x_i m_i d_i^n \quad \textbf{(7)}$$

$$d_i = \sigma_i\left[1 - 0.12\cdot\exp\left(-3\frac{\varepsilon_i}{\mathrm{k_B}T}\right)\right] \quad \textbf{(8)}$$

The contribution due to the association $f^{association}$ in equation (1) is described as Wertheim suggested [49,50,51,52] with the following equation:

$$\frac{f^{\mathrm{association}}}{\mathrm{R}T} = \sum_i x_i\left[\sum_{A_i}\left[\ln X^{A_i} - \frac{X^{A_i}}{2}\right] + \frac{1}{2}M_i\right] \quad \textbf{(9)}$$

In equation (9) M_i represents the number of association sites of a molecule of the species i and X^{A_i} represents the mole fraction of molecules not bonded at the association site A of the molecule of the species i. This mole fraction is highly dependent on the overall number of association sites, the nature of the individual sites, being donor or acceptor, and the bonding strength of the sites. This information is usually combined in so called association schemes. For the 8 most occurring schemes, Huang and Radosz [217] have derived equations to directly calculate the mole fractions. One scheme will be highlighted here, since it is the one used to describe the association of the cooling agent, alcohol, and the ionic liquid. This scheme is the so called 2B model, meaning we assume 2 association sites, one a donor, and one an acceptor, (A and B) with only interaction between A and B, but not A and A or B and B. This yields that the mole fraction of the molecules not bonded on site A or B are calculated as follows:

$$X^{A_i} = X^{B_i} = \frac{-1 + \left(1 + 4\rho\Delta^{A_i B_i}\right)^{0.5}}{2\rho\Delta^{A_i B_i}} \quad \textbf{(10)}$$

With the association strength $\Delta^{A_i B_j}$ given by:

$$\Delta^{A_iB_j} = {d_{ij}}^3 g_{ij}^{\mathrm{hs}}(d_{ij})\kappa^{A_iB_j}\left[\exp\left(\frac{\varepsilon^{A_iB_j}}{\mathrm{k_B}T}\right)-1\right] \quad \textbf{(11)}$$

To further improve the SAFT-EOS, Gross and Sadowski [59,60] proposed the possibility of changing the reference system to a fluid of hard, square-well chains and therefore including the influence of the chain length on the attractive dispersion interactions. This modification is known as the perturbed chain self-associating fluid theory (PC-SAFT). The chains in this framework consist of spherical segments. The PC-SAFT EOS is composed of contributions for the ideal gas, the hard-chains, dispersive and associating interactions. Mathematically, it has the form of equation (12) [59].

$$f = f^{\text{ideal gas}} + f^{\text{hard chain}} + f^{\text{dispersion}} + f^{\text{association}} \quad \textbf{(12)}$$

In the case of a non-associating fluid, the pure component is described by three parameters, the segment diameter σ_i, the depth of the square-well potential ε_i and the number of segments m_i. In the case of associating molecules, it is necessary to include two more parameters for the interaction energy related to the association energy ($\varepsilon^{A_iB_i}$) and for the association volume ($\kappa^{A_iB_i}$). With these parameters all the individual contributions in equation (12) can be calculated. The ideal gas contribution is given by:

$$f^{\text{ideal gas}} = \mathrm{R}T\ln\left(\rho\mathrm{R}T\right) + \mathrm{R}T\sum_i x_i \ln x_i \quad \textbf{(13)}$$

In equation (13) ρ is the molar density and x_i is the mole fraction. The hard chain contribution is given by the following equation

$$\frac{f^{\text{hard chain}}}{\mathrm{R}T} = \bar{m}\cdot f^{\mathrm{hs}} - \sum_i x_i\left(m_i - 1\right)\ln\left(g_{ii}^{\mathrm{hs}}\left(d_{ii}\right)\right) \quad \textbf{(14)}$$

$$f^{hs} = \frac{1}{\zeta_0}\left[\frac{3\zeta_1\zeta_2}{\left(1-\zeta_3\right)} + \frac{{\zeta_2}^3}{\zeta_3\left(1-\zeta_3\right)^2} + \left(\frac{{\zeta_2}^3}{{\zeta_3}^2} - \zeta_0\right)\ln\left(1-\zeta_3\right)\right] \quad \textbf{(15)}$$

with $\bar{m}$ being the mean segment diameter.

$$\frac{f^{\text{dispersion}}}{\mathrm{R}T} = -2\pi\mathrm{N_{AV}}\rho I_1\left(\eta,\bar{m}\right)\overline{m^2\varepsilon\sigma^3} - \pi\mathrm{N_{AV}}\rho\bar{m}C_1 I_2\left(\eta,\bar{m}\right)\overline{m^2\varepsilon^2\sigma^3} \quad \textbf{(16)}$$

In equation (16) the integrals of the pair potential and its derivative with respect to the density being given by Gross and Sadowski [59] are a power series in the form:

$$I_1(\eta,\bar{m}) = \sum_{i=0}^{6} a_i(\bar{m})\eta^i \quad \textbf{(17)}$$

$$I_2(\eta,\bar{m}) = \sum_{i=0}^{6} b_i(\bar{m})\eta^i \quad \textbf{(18)}$$

In the equations (17) and (18) a_i and b_i being:

$$a_i(\bar{m}) = a_{0i} + \frac{\bar{m}-1}{\bar{m}}a_{1i} + \frac{\bar{m}-1}{\bar{m}}\frac{\bar{m}-2}{\bar{m}}a_{2i} \quad \textbf{(19)}$$

$$b_i(\bar{m}) = b_{0i} + \frac{\bar{m}-1}{\bar{m}}b_{1i} + \frac{\bar{m}-1}{\bar{m}}\frac{\bar{m}-2}{\bar{m}}b_{2i} \quad \textbf{(20)}$$

In the equations (19) and (20) a_{Ni} and b_{Ni}, where $N=1,2,3$, are the universal model constants [59]. The other terms in equation (16) being:

$$\overline{m^2\varepsilon\sigma^3} = \sum_i\sum_j x_i x_j m_i m_j \left(\frac{\varepsilon_{ij}}{\mathrm{k_B}T}\right)\sigma_{ij}{}^3 \quad \textbf{(21)}$$

$$\overline{m^2\varepsilon^2\sigma^3} = \sum_i\sum_j x_i x_j m_i m_j \left(\frac{\varepsilon_{ij}}{\mathrm{k_B}T}\right)^2\sigma_{ij}{}^3 \quad \textbf{(22)}$$

$$C_1 = \left[1 + \bar{m}\frac{8\eta-2\eta^2}{(1-\eta)^4} + (1-\bar{m})\frac{20\eta-27\eta^2+12\eta^3-2\eta^4}{\left[(1-\eta)(2-\eta)\right]^2}\right]^{-1} \quad \textbf{(23)}$$

In these equations the segment diameter of the mixture σ_{ij} and the depth of the square well potential of the mixture ε_{ij} are given by the following combining rules:

$$\sigma_{ij} = 0.5\cdot(\sigma_{ii}+\sigma_{jj})(1-l_{ij}) \quad \textbf{(24)}$$

$$\varepsilon_{ij} = \sqrt{\varepsilon_{ii}\varepsilon_{jj}}\left(1-k_{ij}^{\mathrm{dispersion}}\right) \quad \textbf{(25)}$$

In the two equations (24) and (25) l_{ij} and $k_{ij}^{\mathrm{dispersion}}$ being the binary interaction parameters to correct the combining rules for the temperature independent segment diameter and the depth of the square well potential respectively.

The association contribution based on Wertheim [49,50,51,52] follows the framework of Jackson et al. [46] and Chapman et al. [47,48] and is therefore already given in

equation (9). With the combining rules for the association volume of the mixture $\kappa^{A_iB_j}$, the association interaction energy of the association sites $\varepsilon^{A_iB_j}$ and the temperature dependent segment diameter of the mixture d_{ij} being [60]:

$$d_{ij} = 0.5 \cdot \left(d_{ii} + d_{jj} \right) \tag{26}$$

$$\varepsilon^{A_iB_j} = 0.5 \left(\varepsilon^{A_iB_i} + \varepsilon^{A_jB_j} \right) \left(1 - k_{ij}^{\text{association}} \right) \tag{27}$$

$$\kappa^{A_iB_j} = \sqrt{\kappa^{A_iB_i} \kappa^{A_jB_j}} \left(\frac{\sqrt{\sigma_{ii}\sigma_{jj}}}{0.5\left(\sigma_{ii} + \sigma_{jj} \right)} \right)^3 \tag{28}$$

where $k_{ij}^{\text{association}}$ being the binary interaction parameter to correct the combining rules for the association energy.

3.2 Interfacial Properties

Interfacial properties are becoming more and more vital for process simulations since they are a key part in every transport process from one phase to another. But the interest in these properties is not new. One of the first to examine the area between to bulk phases was van der Waals [218]. He conceptualized the interface as an area between the phases with a continuous varying density. Based on these ideas, Cahn and Hilliard [219] rediscovered the so-called Density Gradient Theory (DGT) to calculate the density profiles in the interface and the consequential interfacial tension by varying one variable inside of the interface. They [219] did build their framework on the assumption, that the gradients of the density inside of the interface are small against the reciprocal value of intermolecular distance and therefore the density and its gradients can be treated like independent variables. A Taylor series expansion in these variables yields:

$$\begin{aligned} f\left(\rho, \nabla\rho, \nabla^2\rho, \ldots \right) &= f_0\left(\rho \right) + \sum_i L_i \left(\frac{\partial \rho}{\partial z_i} \right) + \ldots \\ \ldots &+ \sum_{i,j} \kappa_{ij}^{(1)} \left(\frac{\partial \rho}{\partial z_i \partial z_j} \right) + \frac{1}{2} \sum_{i,j} \kappa_{ij}^{(2)} \left(\frac{\partial \rho}{\partial z_i} \right) \left(\frac{\partial \rho}{\partial z_j} \right) + \ldots \end{aligned} \tag{29}$$

In the equation (29) L_i are components of a vector in a polar crystal and $\kappa_{ij}^{(1)}$ and $\kappa_{ij}^{(2)}$ are tensors reflecting the crystal symmetry and may not be confused with the

association volume $\kappa^{A_iB_j}$. For an isotropic fluid, the following simplifications can be made:

$$L_i = 0 \tag{30}$$

$$\kappa_{ij}^{(1)} = \left(\frac{\partial f}{\partial \nabla^2 \rho} \right)_0 \text{ for } i = j \text{ and } \kappa_{ij}^{(1)} = 0 \text{ for } i \neq j \tag{31}$$

$$\kappa_{ij}^{(2)} = \left(\frac{\partial^2 f}{\left(\partial \nabla^2 \rho \right)^2} \right)_0 \text{ for } i = j \text{ and } \kappa_{ij}^{(2)} = 0 \text{ for } i \neq j \tag{32}$$

Together with equation (29) this yields:

$$f\left(\rho, \nabla\rho, \nabla^2\rho, \ldots \right) = f_0\left(\rho \right) + \kappa_{ij}^{(1)} \nabla^2 \rho + \frac{\kappa_{ij}^{(2)}}{2} \left(\nabla\rho \right)^2 \tag{33}$$

To receive the whole Helmholtz energy of a volume, equation (33) is integrated and gives us the equation:

$$f = N \int_v \left(F_0\left(\rho \right) + \kappa_{ij}^{(1)} \nabla^2 \rho + \frac{\kappa_{ij}^{(2)}}{2} \left(\nabla\rho \right)^2 \ldots \right) dv \tag{34}$$

Here N is the number of molecules in one volume element. Under the assumption of a flat surface, the Gauss theorem can be utilized:

$$\int_v \left(\kappa_{ij}^{(1)} \nabla^2 \rho \right) dv = -\int_v \left(\frac{\partial \kappa_{ij}^{(1)}}{\partial \rho} \left(\nabla\rho \right)^2 \right) dv + \int_s \kappa_{ij}^{(1)} \nabla\rho n ds \tag{35}$$

Because the effects on bent surfaces can be omitted, the limits of the integral are chosen in a way, that the term $\nabla\rho n = 0$. This simplifies the equation (35) to:

$$f = N \int_v \left(F_0\left(\rho \right) + \kappa \left(\nabla\rho \right)^2 \ldots \right) dv \tag{36}$$

$$\kappa = -\left(\frac{\partial \kappa_{ij}^{(1)}}{\partial \rho} \right) + \frac{\kappa_{ij}^{(2)}}{2} \tag{37}$$

Since the width of the interfacial area is very small against the plane of the interface, the problem can be further simplified to a one dimensional problem. This yields the equation:

$$f = N \int_{-\infty}^{\infty} F_0(\rho) + \kappa \left(\frac{\partial \rho}{\partial z} \right)^2 dz \tag{38}$$

In equation (38) z is the coordinate that is perpendicular to the interface. The interfacial tension γ is per definition the difference of the Helmholtz energy over the interface with the energy of the equilibrium subtracted. This yields the equation:

$$\gamma = N \int_{-\infty}^{\infty} \left(\Delta\omega(\rho) + \kappa \left(\frac{\partial \rho}{\partial z} \right)^2 \right) dz \tag{39}$$

In equation (39) ω is the grand thermodynamic potential and $\Delta\omega$ is the difference of the potential between in the interfacial area and in the bulk phases. Substituting the integrand of equation (39) in the Euler equation results in a differential equation with the solution being, assuming the system is at equilibrium:

$$\Delta\omega(\rho) + \kappa \left(\frac{\partial \rho}{\partial z} \right)^2 = \text{const.} = \mathrm{C} \tag{40}$$

Because of the fact, that the gradient has to reach zero for $z \to \pm\infty$ the constant equals $\mathrm{C} = 0$. With equation (40) the gradient of equation (39) can be eliminated, yielding:

$$\gamma = 2 \int_{\rho^l}^{\rho^v} \sqrt{\kappa \Delta\omega}\, d\rho \tag{41}$$

Since the equation (41) is utilized to calculate the surface tension of an ionic liquid, the density of the vapor phase is set to $\rho^v = 0$ because the vapor pressure of the ionic liquid is negligible and it can be treated as non-volatile. The parameter κ is treated as a fittable parameter and needs to be set with one surface tension at one temperature, yielding the surface tensions at all the other temperatures. The DGT has been combined with ePC-SAFT by Shen et al. [134] and with soft-SAFT by Oliveira et al. [115]. But to the best of this author's knowledge, it has not yet been combined with PC-SAFT for ionic liquids.

3.3 Chapman-Enskog theory for the diffusion

For diluted gases with spherical molecules, which means that the intermolecular distance is significantly larger than the size of the molecules, Chapman and Enskog

[182,183] separately derived an equation for the self-diffusion from the Boltzmann equation. They both developed the following equation:

$$D_E = \frac{3}{8\rho_N d^2 g_{ii}(d_{ii})}\sqrt{\frac{\mathrm{k_B}T}{\pi M_m}} \quad \textbf{(42)}$$

In this equation ρ_N is the number density and M_m is the mass of one molecule. The rest of the variables are as described earlier in the PC-SAFT framework.

To correct the equation for higher densities, many expansions were incorporated [184,185,186,187,188,189,190,191,192,193,194,195,196,197,198,199,200]. Mostly, these extensions were in the form of polynomials dependent on the reduced density $\rho^* = 6\eta/\pi$ with η being the packing fraction as described in the PC-SAFT framework earlier. According to Ruckenstein and Liu [191] the equation (42) is valid for packing fractions for up to $\eta = 0.1$, and they [191] as well as Yu and Gao [189] suggested a correction for densities higher than $\eta = 0.1$ in the form of

$$D_{\mathrm{HS},\eta<1} = D_{\mathrm{E}} p(\rho^*) \quad \textbf{(43)}$$

with the polynomial $f(\rho^*)$ being [189,191]:

$$p(\rho^*) = 1 + 0.94605(\rho^*)^{1.5} + 1.4022(\rho^*)^3 - 5.6898(\rho^*)^5 + 2.66262(\rho^*)^7 \quad \textbf{(44)}$$

This polynomial in equation (44) was derived from molecular dynamics simulations of a Lenard-Jones fluid by Erpenbeck and Wood [160]. According to Ruckenstein and Liu [191] only argon can be treated as a Lenard-Jones fluid. Other components are either just approximated as a Lenard-Jones fluid or are simply incompatible with it, especially for non-spherical molecules. While it is possible to fit Lenard-Jones parameters to the experimental data of the diffusion, these parameters do not yield any predictive capabilities. To include real gas effects in the model, it is possible to include 2nd and 3rd virial coefficients in a method that is called the modified Chapman-Enskog theory [188,220]. These virial coefficients can be derived from the PC-SAFT framework, but since the PC-SAFT-EOS is directly implemented in the model in this work, it is not necessary here.

This equation is derived and valid for diluted, spherical gases. Since most gases that are encountered in applied problems are non-spherical, the equation (42) needs to

be corrected according to that. This can be done in the form of a correctional factor A_D for the hard sphere diffusion coefficient.

$$D = A_{\mathrm{D}} D_{\mathrm{HS}}(\rho, \sigma) \tag{45}$$

Gross [221] proposed this factor to be $A_{\mathrm{D}} = 1/m$ with m being the segment number of the PC-SAFT framework. The corrected equation from the combination of equations (42) and (45) can be extended to the binary mixture yielding:

$$D = \frac{3}{32 m \rho d_{ij}^2 g_{ij}\left(d_{ij}\right)} \sqrt{\frac{8 \mathrm{k_B} T}{\pi}\left(\frac{1}{M_A} + \frac{1}{M_B}\right)} \tag{46}$$

All parameters in equation (46) can directly be derived from the PC-SAFT framework as described earlier and therefore the self-diffusion coefficients of the pure components and the mutual diffusion coefficients of the binary mixtures can be derived directly.

3.4 Absorption chillers

Since the second law of thermodynamics forbids an energy exchange in the form of heat from a cooler reservoir to a hotter reservoir, this exchange has to be forcefully done with the application of outside energy. The two most commonly used mechanisms are the compression cycles were a cooling agent in its gaseous state is compressed by a mechanical pump, then condensed and expanded and finally evaporated, making it possible to take energy from a low temperature reservoir. This method is usually used in the common household refrigerators. For the cooling of much larger reservoirs, like in air conditioning of rooms or cooling houses, the cooling is often done by the use of an absorption cycle, were the cooling agent is absorbed in an absorbent before a pump compresses the liquid to a higher pressure. Since the external energy for this cycle can be provided in the form of low level heat, these absorption cycles can be driven by excess energy from other processes usually available at a producing plant with the need for cooling houses. This brings up the need for identifying so called working pairs of a cooling agent and an absorbent that fulfil certain specification. The cooling agent needs to have a fitting vapor pressure, making it possible to condense it while cooling the agent against the environment and evaporating it at a temperature that makes it possible to cool the reservoir to a certain temperature. To this cooling agent, a suiting absorbent is needed, making it possible to absorb the vaporous cooling agent and desorbing it at higher temperature.

In this work, the possibilities of creating an absorption cycle with the ability to cool a reservoir like a cooling house to a temperature below the freezing point of water are investigated. An often used working pair for absorption chillers is water + lithium bromide, which of course cannot cool to a temperature lower than T = 273 K since the cooling agent would solidify. Another often used working pair is the combination ammonia + water. Since water works as the absorbent, and ammonia as the cooling agent, this absorption cycle has got the ability to reach cooling temperatures lower than the solidifying temperature of water. However, the toxicity off the ammonia together with its high volatility makes it a hazardous substance to work with. A less toxic cooling agent would therefore be highly desirable. In this work, the use of alcohols, namely methanol and ethanol are proposed. While these are not completely

safe either, the Institute for the Occupational Safety and Health of Germany gives a threshold limit value (TLV) for the methanol of TLV = 270 [mg/m³] and a TLV = 960 [mg/m³] for the ethanol which are substantially higher than for the ammonia with a TLV = 14 [mg/m³], showing the toxicity of the ammonia is far more severe than that of the alcohols [222].

To find a suitable absorbent for the alcohols, in this work the use of ionic liquids is proposed. Ionic liquids have a negligible vapor pressure allowing for a clean desorption of the cooling agent from the absorbent. The large number of possible combinations of anion and cation is allowing for the possibility of tailoring the ionic liquid to the needs of the specific absorption cycle. This creates the need for a huge screening of the possible ionic liquids, of course. It would be highly desirable to perform this screening with a minimum of experimental results. A possible solution would be the fitting of the PC-SAFT pure component parameters to properties that are quick and effortless to measure. In this work, the pure component parameters are fitted to the liquid densities.

To identify the most suitable working pair, two parameters are of particular importance. First, the possible cooling temperature, since the goal of this work is to find a working pair with the ability to cool to a temperature lower than the freezing point of water. And second the coefficient of performance (COP), of course, since the energy efficiency is an important point in the selling of absorption chilling machines. The COPs calculated with the simple model used in this work are of course not comparable to experimental results, since a lot of simplifications are made as was discussed in the introduction. To the best of this author's knowledge, no experimental results for the COP of absorption chillers utilizing alcohol and ionic liquids is available. For ionic liquids + water and ionic liquids + NH_3 the COPs are in the area of 0.5 to 0.6 [223].

To evaluate the two key properties of the considered working pairs, the following steps were taken. First, it was necessary to set some key parameters that would be consistent for all considered working pairs. To utilize any cooling against the environment, the temperature in the condenser and in the absorber are set to T=300K. The ionic liquid concentration in the diluted solution is set to x_{IL} = 0.7 since this is a usual value for the absorbent concentration [224]. The concentration in the

concentrated solution is given by the circulation ratio $c = \frac{x_{diluted}}{x_{diluted} - x_{concentrated}} = 11$ which is a typical value for absorption chillers [224]. By calculating the vapor pressure in the absorber for x_{IL} = 0.7 and T = 300 K, which is also the vapor pressure for the pure cooling agent in the evaporator, the possible cooling temperature is determined. The calculation of the rest of the absorption is straightforward. With knowing the temperatures, pressures and concentrations in the working points, the enthalpies can be determined and therefore the heat exchanges and consequentially the COP can be calculated.

4 Results

4.1 Pure component systems

4.1.1 Fitting of the parameters

Since the ionic liquids are assumed to be self-associating fluids in this work, 5 parameters have to be fitted to correctly describe them in the PC-SAFT framework. The cooling agent is either methanol or ethanol, so they are both described with the 2B association scheme given in equation (10). It is assumed, that the ionic liquid does have one donor site and one acceptor site as well, which stems from the ionic bond in this case. So the ionic liquid will be described with the 2B model, too. The parameters for the pure ionic liquid are fitted to experimental results for the liquid density. A commonly used procedure is to fit the parameters to the liquid density and the vapor pressure (for example [59]). This obviously can't be done for the ionic liquid, since the vapor pressure is negligible and therefore not measureable. It was decided to fit the parameters only to the liquid density. Although it would be possible to fit to other measurable pure component properties like heat capacity or speed of sound, the experiments are often laborious and time consuming. Measurements of the liquid density can be done in a short time span and are most likely to be already available when considering an ionic liquid.

Since a lot of authors have measured the densities of ionic liquids, a lot of measured data has to be considered. Because it would be too complex to depict all the data in the graphs, only a selected group of the data will actually be drawn out. To make the selection, first a linear interpolation of the mean average of the available data is calculated in the form of the equation:

$$\frac{\rho(T)}{\mathrm{mol}/\mathrm{cm}^3} = A \cdot \frac{T}{\mathrm{K}} + B \tag{47}$$

and a mean deviation is selected so only data located inside the deviation will be considered in the graphs and data outside of the deviation will be omitted. This is done exemplary for the ionic liquid [EMIM][OAc]. For the remaining ionic liquids, the selection process is being done in the appendix A.1.

For the ionic liquid [EMIM][OAc] the linear interpolation of all the found experimental data (Table 2) yielded parameters of $A = -0.6016$ and $B = 1279.1$.

The sources for the experimental data and the mean deviation from the linear interpolation can be seen in Table 2.

Author	Mean deviation D_M in [1]	Temperature range in [K]
Araujo et al. [225]	0.0014	283.15 – 343.15
Castro et al. [226]	0.0006	278.15 – 338.15
Fröba et al. [227]	0.0001	273.15 – 363.15
Freire et al. [228]	0.0004	278.15 – 363.15
Oliveira et al. [229]	0.0012	298.15 – 323.15
Pereiro et al. [230]	0.0009	298.15 - 333.15
Pinkert et al. [231]	0.0078	278.15 – 358.15
Pinto et al. [232]	0.0008	298.15 – 358.15
Quijada-Maldonado et al. [233]	0.0019	303.15 – 343.15
Rabari et al. [234]	0.0015	293.15 – 328.15
Rosenboom et al. [235]	0.0018	293.15 – 358.15
Shiflett et al. [236]	0.0026	298.1 – 373.1

Table 2 Sources of experimental data for the density of [EMIM][OAc] with mean deviation from linear interpolation (equation (47)).

Since the data sets from Pinkert et al. [231] and from Shiflett et al. [236] are showing a mean deviation greater than $D_{\mathrm{M}} = 0.002$ and are therefore more deviating than the rest of the data sets, they will be omitted in this work. Pinkert et al. [231] do mention in their work, that the conventional drying of the ionic liquids is problematic and can lead to higher water contents, so this may be an explanation for their deviations. Shiflett et al. [236] do not mention any problems.

Since the fitting process for the PC-SAFT parameters to all experimental data that satisfies the selection critrerium described above, would be too time consuming only one data set is selected for the fit. In the early stages of selecting a new working pair, it is unlikely that experimental data is available in abundance. The data that is not used to fit the parameters is used as a comparison for the calculated data. In the case of the [EMIM][OAc], the data set of Quijada-Maldonado et al. [233] is selected for the fitting process. They report a very low water content of w=0.0013. They [233] are reporting, that the water content could not be lowered significantly after drying for 1 day at T=343 K due to the strong hydrophilic nature of the [EMIM][OAc]. Most other

articles report higher water contents. Castro et al. [226] report a slightly lower water content of a mass fraction of w_{water}=0.0012, although they do not describe the drying process in detail. For example the duration of the drying is not mentioned. Shiflett et al. [236] are reporting water contents similar to Quijada-Maldonado et al. [233]. But since they [236] dried the ionic liquids for 5 days at T=343 K and therefore significantly longer than Quiada-Maldonado et al. [233] without better results, their [236] data is omitted for the fitting process as thermal decomposition is more likely due to the longer drying under high temperatures.

For the [BMIM][PF6], the data set of Troncoso et al. [237] was chosen, as the they report the ionic liquid was especially pure at purchase (>99.8%) while other authors (e.g. [238,239]) report lower purities (>98% for [238], 99,56% for [239]). For the remaining ionic liquids, the data sets of Gardas et al. [240] was used as they report very low water contents (lower than w_{water}=0.0005 for all considered ionic liquids) and provided the dara for several ionic liquids summarized.

The fitting procedure was conducted in the following way. For each of the parameters an initial value was chosen. Then the value for the segment number m_i was varied to minimize the failure function $\left(\frac{\partial \text{failure}}{\partial m_i}\right)_{\sigma_i, m_i, \varepsilon_i, \varepsilon^{A_iB_i}, \kappa^{A_iB_i}} = 0$. This value was set as the new initial value for m_i. Now, the values of the segment number m_i and the temperature independent segment diameter σ_i were varied to minimize the failure function $\left(\frac{\partial^2 \text{failure}}{\partial m_i \partial \sigma_i}\right)_{m_i, \varepsilon_i, \varepsilon^{A_iB_i}, \kappa^{A_iB_i}} = 0$ and the yielded results were set as the new initial values. This was continued while adding the depth of the square well potential ε_i, then the association energy $\varepsilon^{A_iB_i}$ and finally the association volume $\kappa^{A_iB_i}$ to the varied parameters until finally all parameters were fitted altogether.

The experimental results were all in a temperature range where the ionic liquid would not undergo any phase transformation and are not weighted in any way. The experimental results that were used to fit the parameters and the calculated densities with these parameters are shown in Figure 2.

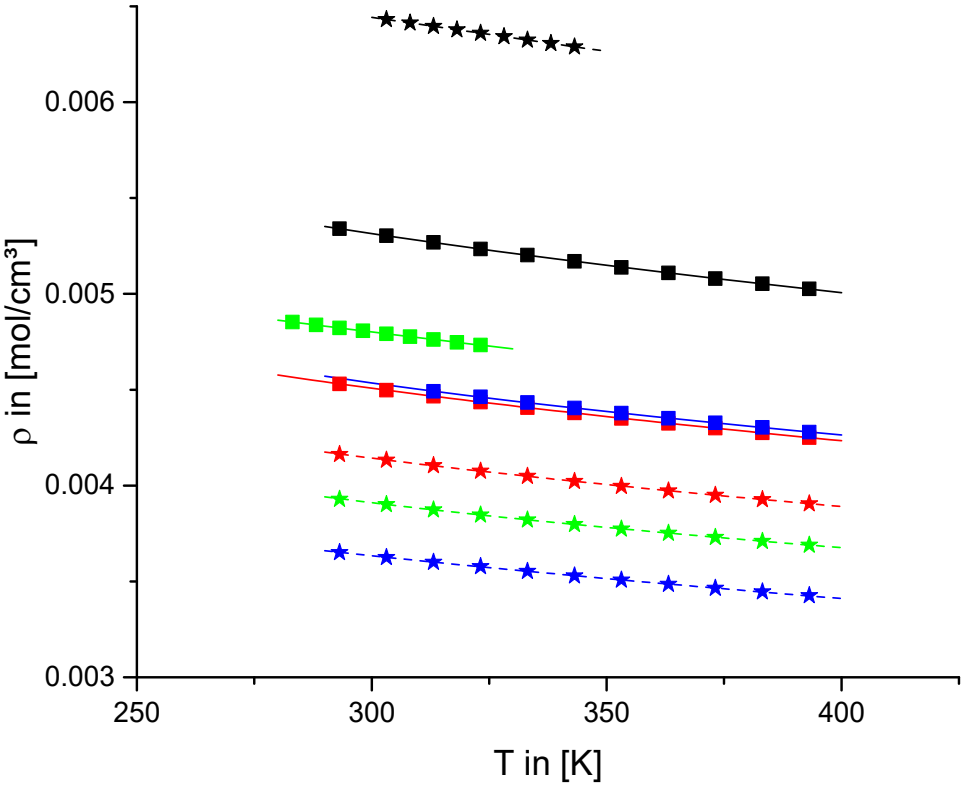

Figure 2: Densities used to fit the parameters and calculated density functions at P = 1 bar. The calculations are represented by the lines drawn: solid black = [BMIM][BF4], solid red = [BMIM][CF3SO3], solid green = [BMIM][PF6], solid blue = [BMMIM][PF6], dashed black = [EMIM][OAc], dashed red = [HMIM][PF6], dashed green = [OMIM][BF4], dashed blue = [OMIM][PF6]. The squares and stars represent the experimental results: black stars = [EMIM][OAc] from Quijada-Maldonado et al. [233], green squares = [BMIM][PF6] from Troncoso et al. [237], black square = [BMIM][BF4], red squares = [BMIM][CF3SO3], blue squares = [BMMIM][PF6], red stars = [HMIM][PF6], green stars = [OMIM][BF4], blue stars = [OMIM][PF6], all from Gardas et al. [240].

The individual parameters for each of the ionic liquids are summarized in Table 3.

Ionic liquid	m in [1]	σ in [Å]	ε/k_B in [K]	ε^{AB}/k_B in [K]	κ^{AB} in [1]
[EMIM][OAc]	1.794	5.116	634.434	820.7367	0.0011
[BMIM][BF4]	3.45866	4.49741	679.011	711.394	0.0271946
[OMIM][BF4]	4.0013	4.7685	694.3388	698.1816	0.0016387
[BMIM][CF3SO3]	4.0512	4.4817	595.1145	698.8589	0.0037
[BMMIM][PF6]	3.9173	4.5685	693.3995	724.1226	0.004745
[OMIM][PF6]	3.4164	5.0598	562.1529	918.0661	0.010126
[HMIM][PF6]	4.1171	4.6063	629.8929	730.7385	0.0037
[BMIM][PF6]	2.7866	4.5995	566.2996	665.0153	0.0014864

Table 3: PC-SAFT Parameters for the considered ionic liquids.

For the ionic liquids [BMIM][BF4] and [BMIM][CF3SO3] more than one PC-SAFT parameter set has been fitted, the comparison of them are in Table 4 for [BMIM][BF4] and in Table 5 for [BMIM][CF3SO3].

Source	m in [1]	σ in [Å]	ε/k_B in [K]	ε^{AB}/k_B in [K]	κ^{AB} in [1]
This work	3.45866	4.49741	679.011	711.394	0.0271946
Chen et al. [108]	3.62	4.33	426.7	3450	0.00225
Curras et al. [96]	8.1885	3.2724	356.98	240.83	0.089610

Table 4: Comparison of PC-SAFT parameters from this work with parameters from literature for [BMIM][BF4].

Source	m in [1]	σ in [Å]	ε/k_B in [K]	ε^{AB}/k_B in [K]	κ^{AB} in [1]
This work	4.0512	4.4817	595.1145	698.8589	0.0037
Chen et al. [108]	3.92	4.43	392	3450	0.00225
Passos et al. [100]	8.1368	3.3037	206.85	189.21	0.144

Table 5: Comparison of PC-SAFT parameters from this work with parameters from literature for [BMIM][CF3SO3].

In the work of Chen et al. [108] the association energy and the association volume were set to a fixed value taken from 1-alkanols. It can be seen, that the association energy is much higher than the one fitted in this work. Passos et al. [100] fitted their parameters to liquid densities and water activities and VLE for the aqueous solutions. Interaction energies are lower than the ones established in this work and the segment numbers are much bigger. Curras et al. [96] fitted the parameters only to liquid densities and also estimate the interaction energies at lower values and the segment number at higher values. To assure that the parameters fitted are in accordance with experimental data, the calculated liquid densities were compared with the experimental data from literature that was selected above. The results for [EMIM][OAc], [BMIM][BF4], [BMIM][CF3SO3] and [OMIM][BF4] can be seen in Figure 3.

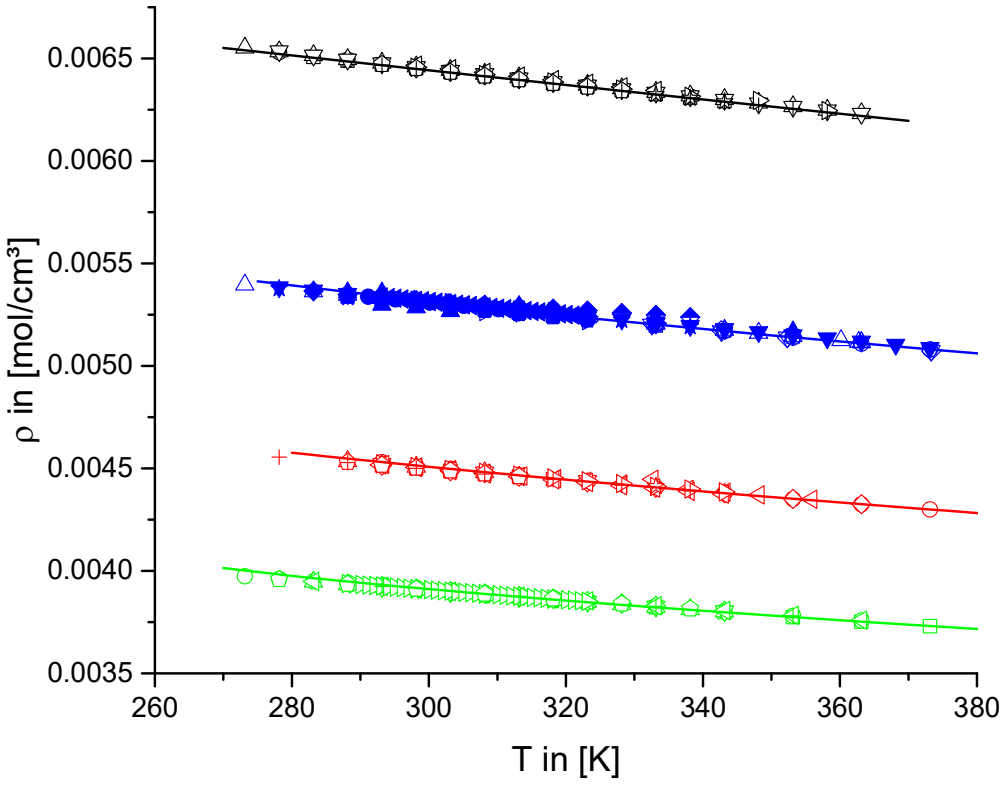

Figure 3: Comparison of calculated densities (solid lines) and experimental results (symbols) at P=1bar data, for [EMIM][OAc] (black lines and symbols), [BMIM][BF4] (blue lines and symbols), [BMIM][CF3SO3] (red lines and symbols) and [OMIM][BF4] (green lines and symbols). [EMIM][OAC] references (black): open square ([225]), open circle ([226]), open triangle up ([227]), open triangle down ([228]), open diamond ([229]), open triangle left ([230]), open triangle right ([232]), open star ([233]), open pentagram ([234]), plus sign ([235]). [BMIM][BF4] references (blue): open square ([241]), open circle ([240]), open triangle up ([242]),open triangle down ([243]), open diamond ([244]), open triangle left ([245]), open triangle right ([246]), open star ([247]),open pentagram ([238]), plus sign ([248]), full square ([249]), full circle ([250]), full triangle up ([251]), full triangle down ([252]), full diamond ([253]), full triangle left ([254]), full triangle right ([255]), full star ([256]), full pentagram ([257]), half full square ([258]), half full circle ([259]), half full triangle up ([260]), half full triangle down ([261]), half full diamond ([262]), half full star ([263]). [BMIM][CF3SO3] references (red): open square ([264]), open circle ([240]), open triangle up ([265]), open triangle down ([266]), open diamond ([243]), open triangle left ([267]), open triangle right ([268]), open star ([258]),open pentagram ([259]), plus sign ([269]). [OMIM][BF4] references (green): open square ([240]), open circle ([270]), open triangle up ([271]), open triangle down ([238]), open diamond ([272]), open triangle left ([273]), open triangle right ([254]), open star ([274]), open pentagram ([256]), plus sign ([275]). Lines are PC-SAFT calculations with the parameters from Table 3.

It can be seen, that the calculated densities for [EMIM][OAc], [BMIM][BF4], [BMIM][CF3SO3] and [OMIM][BF4] are in a good agreement with the experimental data taken from literature. The comparison for other four ionic liquids, namely [BMIM][PF6], [BMMIM][PF6], [HMIM][PF6] and [OMIM][PF6], can be seen in Figure 4.

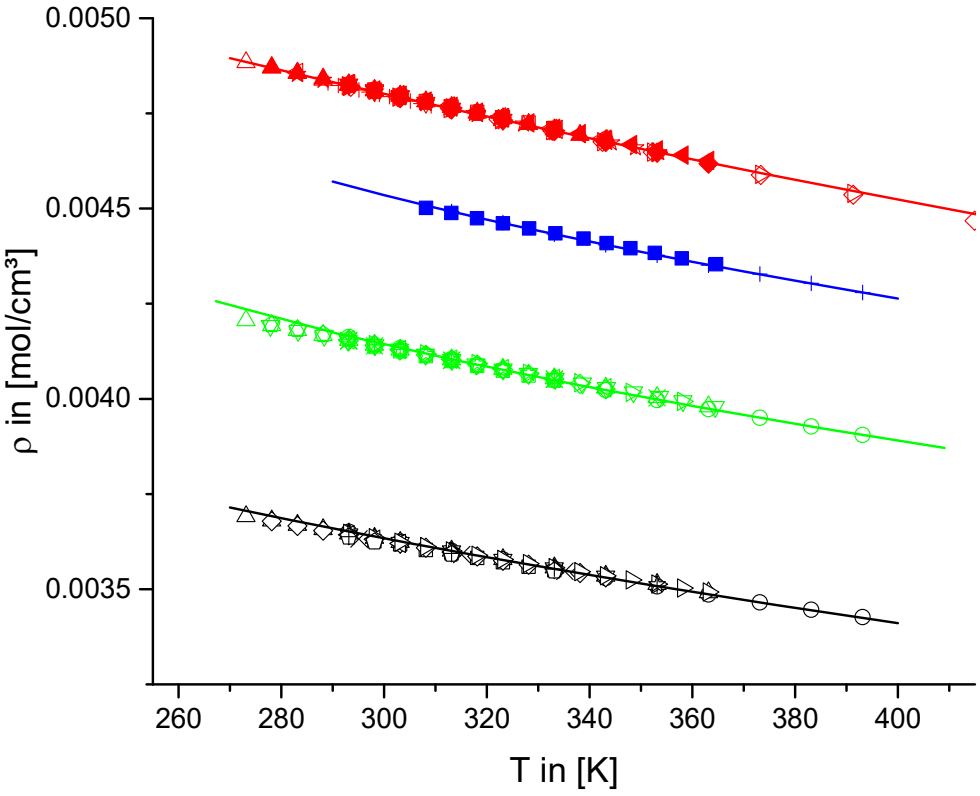

Figure 4: Comparison of calculated densities (solid lines) and experimental results (symbols) at P=1bar data, for [BMIM][PF6] (red lines and symbols), [BMMIM][PF6] (blue lines and symbols), [HMIM][PF6] (green lines and symbols) and [OMIM][PF6] (black lines and symbols). [BMIM][PF6] references (red): open square ([276]), open circle ([277]), open triangle up ([278]), open triangle down ([279]), open diamond ([280]), open triangle left ([281]), open triangle right ([244]), open star ([239]), plus sign ([282]), full square ([283]), full circle ([238]), full triangle up ([284]), full triangle down ([285]), full diamond ([286]), full triangle left ([287]), full triangle right ([260]), full star ([237]), full pentagram ([288]). [BMMIM][PF6] references (blue): full square ([289]), plus sign ([240]). [HMIM][PF6] references (green): open square ([276]), open circle ([289]), open triangle up ([290]), open triangle down ([291]), open diamond ([292]), open triangle left ([238]), open triangle right ([293]),open star ([272]), open pentagram ([294]), plus sign ([295]), X ([296]), Asterisk ([258]). [OMIM][PF6] references (black): open squares ([276]), open circle ([240]), open triangle up ([270]), open triangle down ([238]), open diamond ([284]), open triangle left ([285]), open triangle right ([287]), open star ([296]), open pentagram ([258]), plus sign ([297]), X ([298]). Lines are PC-SAFT calculations with the parameters from Table 3.

Figure 4 shows just as Figure 3 that the calculations for the liquid densities are in a good agreement with the literature data selected in the appendix. To further investigate the capabilities of the parameters to make predictions over a pressure range, the liquid densities were calculated with a pressure of P = 100 bar. The results were then compared to experimental data from literature. For the ionic liquids [BMIM][BF4], [BMIM][CF3SO3] and [OMIM][BF4] this can be seen in Figure 5.

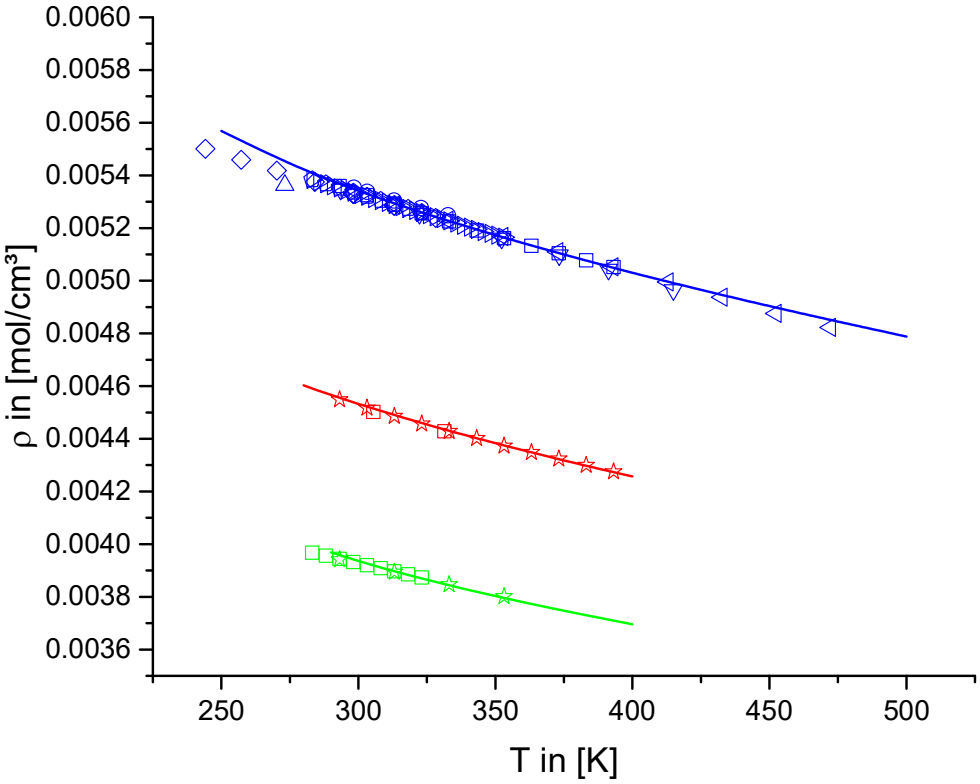

Figure 5: Comparison of calculated densities (solid lines) and experimental results (symbols) at P=100bar, data for [BMIM][BF4] (blue lines and symbols), [BMIM][CF3SO3] (red lines and symbols) and [OMIM][BF4] (green lines and symbols. [BMIM][BF4] references (blue): open square ([240]), open circle ([299]), open triangle up ([242]), open triangle down ([280]), open diamond ([300]), open triangle left ([301]), open triangle right ([302]), open star ([303]), open pentagram ([254]), plus sign ([304]). [BMIM][CF3SO3] references (red): open squares ([305]), open stars ([240]). [OMIM][BF4] references (green): open square ([253]), open star ([275]).

It can be seen in Figure 5, that the agreement between the experimental data and the data predicted from the pure component parameters is quite good. There are minor deviations at lower temperatures, but this temperature range is not of interest in this work, since the temperature of the ionic liquids will be above T = 300 K at all times due to the boundaries set for the calculations of the absorption cycles, and for this temperature range, the agreement is very good. For the ionic liquids [BMIM][PF6], [BMMIM][PF6], [HMIM][PF6] and [OMIM][PF6], the comparison between the experimental data from literature and the calculations are depicted in Figure 6.

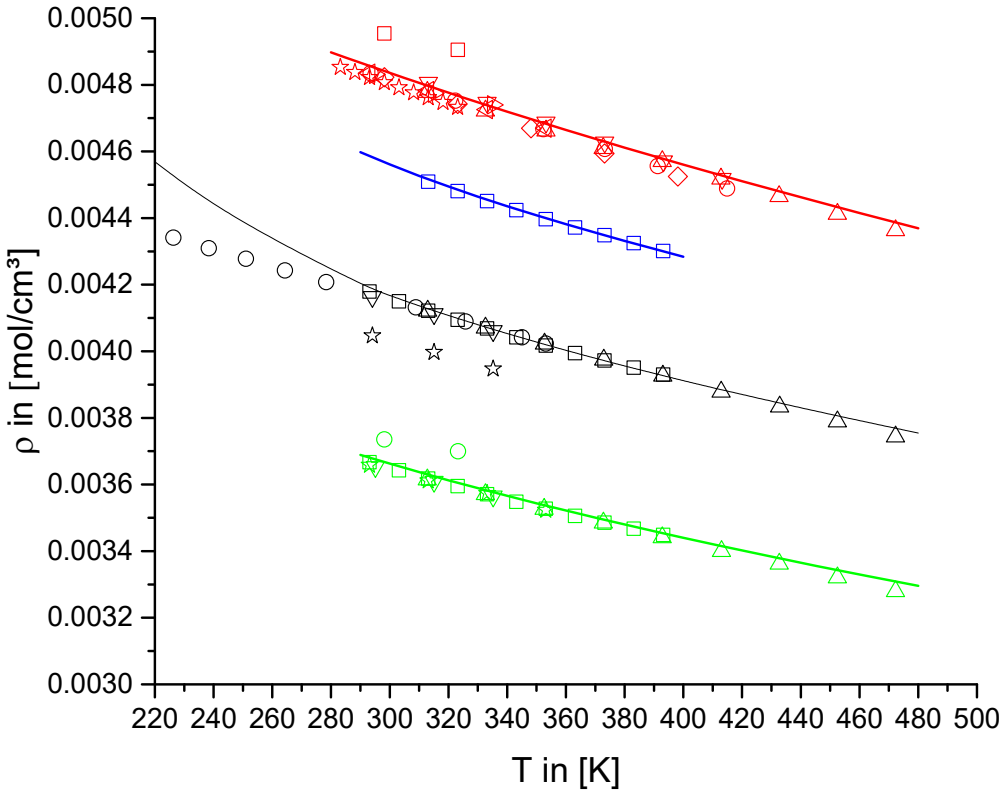

Figure 6: Comparison of calculated densities (solid lines) and experimental results (symbols) at P=100bar, data for [BMIM][PF6] (red lines and symbols), [BMMIM][PF6] (blue lines and symbols), [HMIM][PF6] (black lines and symbols) and [OMIM][PF6] (green lines and symbols). [BMIM][PF6] references (red): open squares ([306]), open circle ([280]), open triangle up ([301]), open triangle down ([307]), open diamond ([308]), open triangle left ([260]), open triangle right ([298]), open stars ([237]). [BMMIM][PF6] references (blue): open squares ([240]). [HMIM][PF6] references (black): open squares ([240]), open circles ([291]), open triangle up ([296]), open triangle down ([298]), open star ([297]). [OMIM][PF6] references (green): open squares ([240]), open circles ([306]), open triangle up ([296]), open triangle down ([298]), open stars ([297]).

Again, Figure 6 shows, just as Figure 5, that the agreement is quite good between the predictions and the experimental data. In Figure 6 we can see the deviations for lower temperatures quite more prominent for the ionic liquid [HMIM][PF6]. But all bigger deviations occur only for temperatures lower than T = 300 K except for the deviations with the results of Gu et al. [306] and Tomida et al. [297]. Tomida et al. [297] attributed it to water impurities in the ionic liquids. The deviations are therefore not relevant for the calculations in this work. The pressures in the absorption cycle are of course lower than P = 1 bar. But no experimental data for the density of ionic liquids could be found for pressures below P = 1 bar. Since the deviations between the predictive calculations at P = 100 bar from the pure component parameters fitted

at P = 1bar and the experimental results are negligible, it is assumed, that the calculations for lower pressure than P = 1 bar will be reliable as well.

4.1.2 Surface tension

To further evaluate the reliability of the predictions from the fit to only liquid densities, the surface tension as a derivative will be examined. As described earlier it is possible to calculate the interfacial tension of a liquid utilizing the DGT with equation (41), if the influence parameter κ is fitted to a single surface tension measured by a specified temperature. In this work, these fitting processes were done by hand and not to a specific temperature as these calculations are only done as a plausibility test for the pure component parameters and therefore no extensive fitting process was necessary. The fitted influence parameters for the ionic liquids can be found in Table 6. For substances like [OMIM][BF4], where the experimental data has deviations between the different authors, the fitting was done to the experimental data that was in the best agreement with the mean average. Many authors (e.g. [309,310]) mention the high influence of impurities such as water on the results, so the deviations between the different data sets may be attributed to these impurities.

Ionic liquid	Experimental results used to fit	κ in $\left[\frac{\mathrm{Nm}^3}{\mathrm{mol}}\right]$
[BMIM][BF4]	Freire et al. [309]	4.6e-7
[BMIM][CF3SO3]	Freire et al. [309]	2.95e-7
[EMIM][OAc]	Almeida et al. [310]	1.26e-6
[OMIM][BF4]	Sanchez et al. [273]	2.1e-7
[BMIM][PF6]	Law and Watson [311]	7.5e-7
[BMMIM][PF6]	Freire et al. [309]	3.5e-7
[HMIM][PF6]	Freire et al. [309]	2.43e-7
[OMIM][PF6]	Freire et al. [309]	1.8e-7

Table 6: Influence parameters for the calculation of the surface tensions of the ionic liquids and experimental data used to fit them.

For the ionic liquids [EMIM][OAc], [BMIM][BF4], [BMIM][CF3SO3] and [OMIM][BF4] this is depicted in Figure 7.

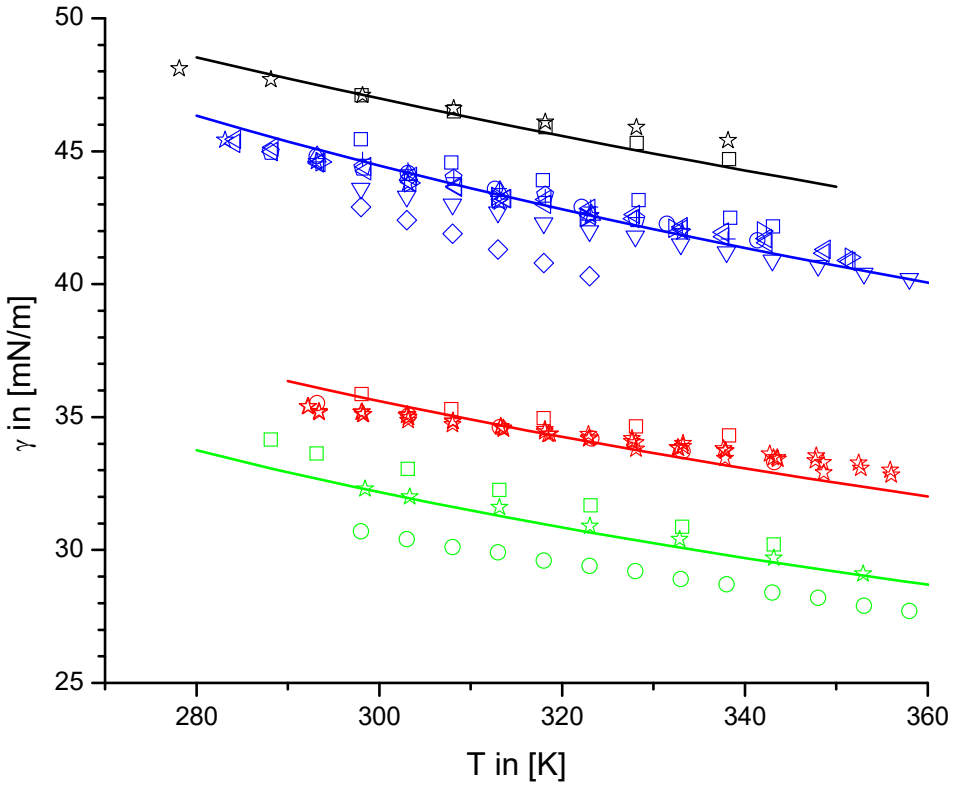

Figure 7: Comparison of calculated (with influence parameters from Table 6, solid lines) and experimental (symbols) interfacial tensions at P=1bar, data for [EMIM][OAc] (black lines and symbols), [BMIM][BF4] (blue lines and symbols), [BMIM][CF3SO3] (red lines and symbols) and [OMIM][BF4] (green lines and symbols) with experimental data from literature. [EMIM][OAc] references (black): black squares ([310]), open stars ([226]). [BMIM][BF4] references (blue): open squares ([310]), open circle ([309]), open triangle up ([312]), open triangle down ([313]), open diamond ([314]), open triangle left ([315]), open triangle right ([273]), open star ([316]), open pentagram ([317]), plus sign ([262]). [BMIM][CF3SO3] references (red): open squares ([310]), open circle ([309]), open stars ([318]). [OMIM][BF4] references (green): open squares ([309]), open circle ([313]), open stars ([273]).

It can be seen in Figure 7 that the calculations for the whole temperature range are in good agreement with the experimental results. For the ionic liquids containing the [PF6]-anion, the graph was distributed to two graphs for clarity reasons. For the ionic liquids [BMIM][PF6] and [OMIM][PF6] the surface tensions of the calculations and experiments from literature are depicted in Figure 8.

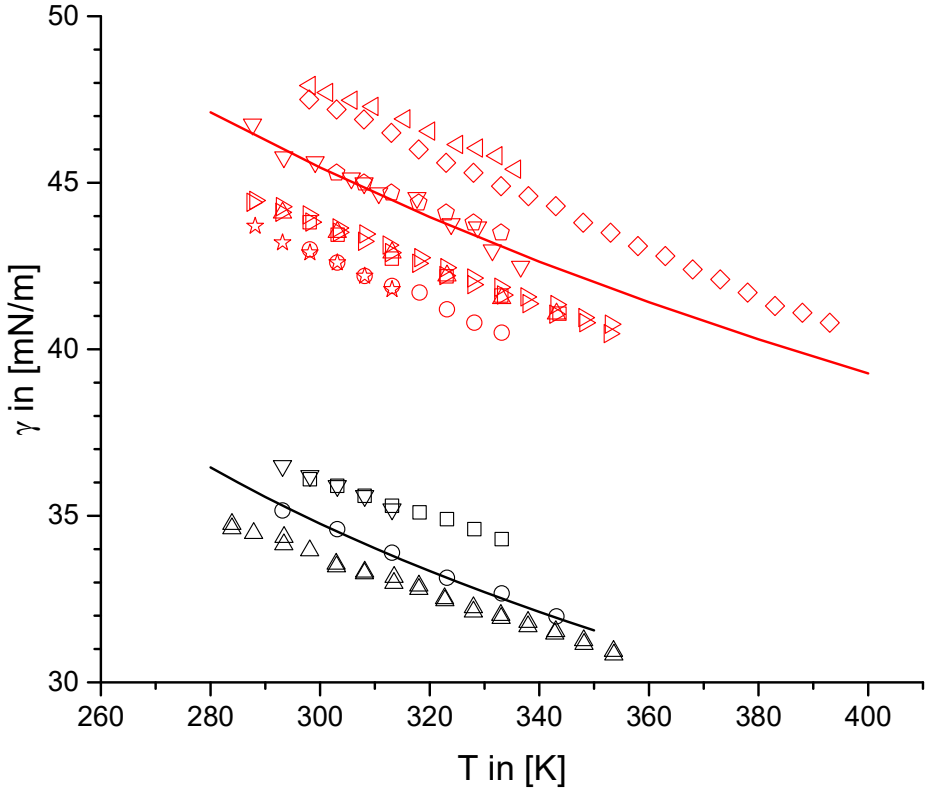

Figure 8: Comparison of calculated (with influence parameters from Table 6, solid lines) and experimental (symbols) interfacial tensions at P=1bar, data for [OMIM][PF6] (black lines and symbols), [BMIM][PF6] (red lines and symbols). [OMIM][PF6] references (black): open squares ([276]), open circles ([309]), open triangle up ([319]), open triangle down ([284]). [BMIM][PF6] references (black): open squares ([310]), open circle ([276]), open triangle up ([309]), open triangle down ([320]), open diamond ([313]), open triangle left ([321]), open triangle right ([319]), open star ([284]), open pentagram ([322]).

In Figure 8 it can be seen, that the calculated data is again in a good agreement with the experimental data. Although the experimental results deviate, the slope of the interfacial tension with the temperature is in a good agreement with all the experimental results. And this slope is derived from the density function so these comparisons are a good indicator for the reliability of the parameter fits. For the ionic liquids [BMMIM][PF6] and [HMIM[PF6] the calculated and experimental surface tensions can be seen in Figure 9.

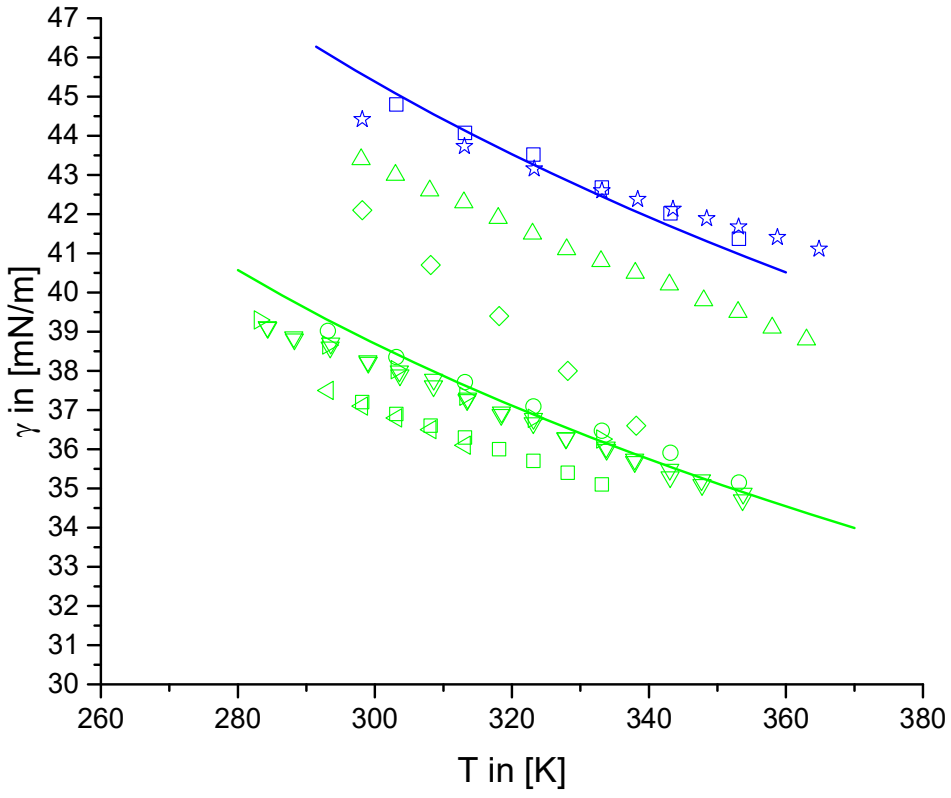

Figure 9: Comparison of calculated (with influence parameters from Table 6, solid lines) and experimental (symbols) interfacial tensions at P=1bar, data for [BMMIM][PF6] (blue lines and symbols), [HMIM][PF6] (green lines and symbols). [BMMIM][PF6] references (blue): open squares ([309]), open stars ([323]). [HMIM][PF6] references (green): open squares ([276]), open circle ([309]), open triangle up ([313]), open triangle down ([319]), open diamond ([293]), open triangle left ([284]), open triangle right ([316]).

In Figure 9 we can again see that the calculated data is in a good agreement with the experimental data despite the deviations of the individual experimental results, especially for the slope. Apart from the confirmation of the reliability of the parameter fit, the data additionally shows that the surface tension of an ionic liquid can be reliably calculated if the influence parameter κ can be fitted to a single interfacial tension at a specified temperature. This may be of importance for simulations of absorption processes incorporating the mass transfer over the interface. Since the deviations between the individual experimental data sets is a clear sign for the complicated and susceptible experimental methods for the determination of interfacial tensions, a reliable calculation method for the interfacial tensions is highly desirable. The DGT-method may be this method.

4.1.3 Calculation of the heat capacity at constant pressure

As mentioned before (chapter 2.1), different SAFT-versions have been used to calculate the heat capacities of ionic liquids e.g. [67,129,134]. The calculations come with deviations that are mostly attributed to the lack of data for the ideal gas contribution. In the literature, the ideal gas contribution is often taken directly from statistical thermodynamics e. g. [130]. Because the goal of this work is to predict the applicability and performance of absorption cycles with ionic liquids in a quick and low effort way, an approach founded in statistical thermodynamics would be undesirable. For this work, a different approach has been used. The calculation of the heat capacity in the PC-SAFT framework follows the equation

$$c_p = c_p^{\text{ideal gas}} + c_p^{\text{res}} \tag{48}$$

where c_p^{res} is the residual heat capacity directly calculable from the pure component parameters already determined and $c_p^{\text{ideal gas}}$ being the contribution to the heat capacity by the component at ideal gas state. Since the vapor pressure of the ionic liquids is negligible and the organic ions decompose long before the liquids even evaporate, it is impossible to experimentally determine the ideal gas contribution to the heat capacity. In this work, the $c_p^{\text{ideal gas}}$ contribution was fitted to experimental data for the heat capacity of the liquid and therefore the ideal gas contribution is given by a substitution function $A(T) = c_P^{\text{ideal gas}}$, yielding also a good agreement of the calculations to the experimental data used to fit. To account for the possibility of necessary extrapolation from the temperature range of the experimental data, the substitute function was chosen as a linear function to eliminate the threat of the approach function breaking away outside of the considered temperature range. The experimental data taken from literature for the fitting process can be seen in Table 7 together with the resulting substitution functions. For [BMIM][BF4] and [OMIM][BF4] the data from Sanmamed et al. [324] was selected because only they report a very low water content of w=0.001 for [BMIM][BF4] and w=0.002 für [OMIM][BF4], describe the purification process in detail and provide enough points for a sound fitting process. For [BMMIM][PF6], the data of Hu et al. [325] is used for the fitting since Fredlake et al. [326] only provide 2 data points. For [BMIM][PF6] Kabo et al. [239] and Nieto de Castro et al. [327] are reporting the lowest water content. But only Kabo et al. [239] are describing their drying process and are therefore selected as

the provider of the fitting data set. For [HMIM][PF6] only the data of Li et al. [292] comes with description of the drying process and the water content, so it is selected as the fitting data set.

Ionic liquid	**Experimental results used to fit the approach function**	**Substitution functions for $A(T)$**
[BMIM][BF4]	Sanmamed et al. [324]	$0.594 \cdot T + 89.1506$
[EMIM][OAc]	Freire et al. [228]	$0 \cdot T + 285.8287$ (only 1 data point)
[OMIM][BF4]	Sanmamed et al. [324]	$0.953 \cdot T + 96.991$
[BMIM][PF6]	Kabo et al. [239]	$0.6001 \cdot T + 165.9317$
[BMMIM][PF6]	Hu et al. [325]	$0.8659 \cdot T + 48.9550$
[HMIM][PF6]	Li et al. [292]	$0.8168 \cdot T + 60.8043$

Table 7: Substitution function for ideal gas contribution for the heat capacity at constant pressure and experimental data used to fit the parameters of the functions.

No experimental heat capacity at constant pressure data for [BMIM][CF3SO3] and [OMIM][PF6] was found, therefore the substitution function $A(T)$ could not be fitted and the absorption cycles for these two systems were not calculated. For the ionic liquid [EMIM][OAc], only Freire et al. [228] did provide experimental data for the heat capacity at constant pressure and they only did measure one point. Therefore no linear function could be fitted. For this ionic liquid, it was assumed, that the contribution of the substitute function $A(T)$ is constant over temperature. The deviation stemming from this simplification should be small since all other substitute functions $A(T)$ had a slope of less than $\frac{dA}{dT} < 1 \frac{\mathrm{J}}{\mathrm{mol\,K^2}}$ while the value of the heat capacity is around $c_\mathrm{p} = 300 \frac{\mathrm{J}}{\mathrm{molK}}$. The temperature range of the ionic liquids should be around 50 K. This means, that there is of course a deviation that comes with the simplification, but it should not render the calculation useless. With the substitution function for the ideal gas contribution the full heat capacity can now be calculated:

$$c_P = A(T) - RT^2\left(\frac{\partial^2 F}{\partial T^2}\right)_{V,n} - 2RT\left(\frac{\partial F}{\partial T}\right)_{V,n} - T\frac{\left(\partial P/\partial T\right)^2_{V,n}}{\left(\partial P/\partial V\right)_{T.n}} - Rn \quad \textbf{(49)}$$

For the ionic liquids [EMIM][OAc], [BMIM][BF4] and [OMIM][BF4], the calculated heat capacities from PC-SAFT and the substitution functions from Table 7 and experimental results can be seen in Figure 10.

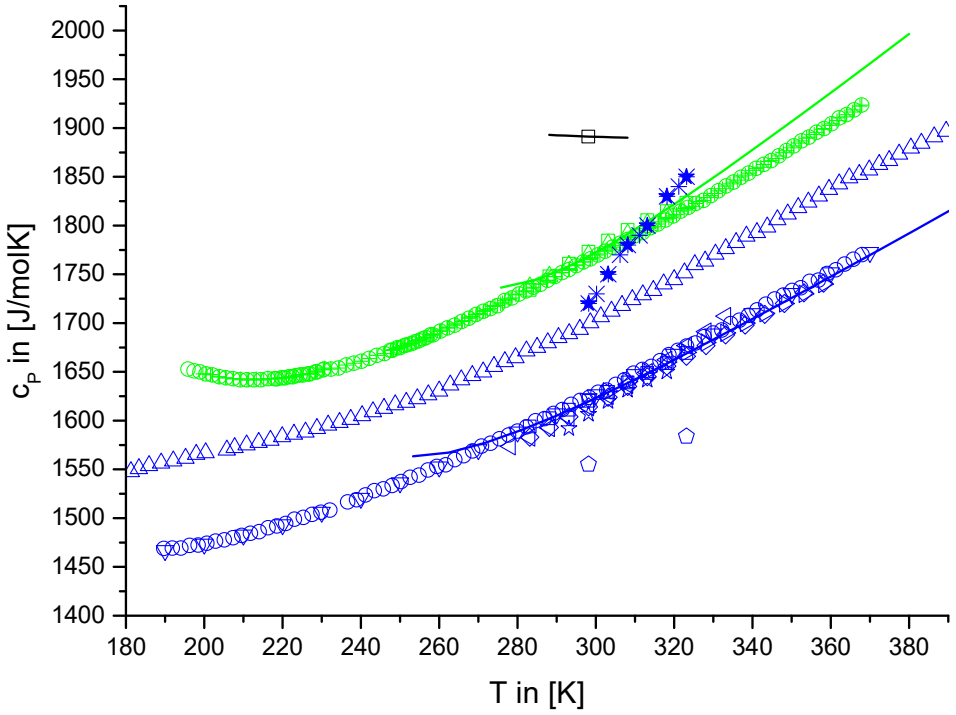

Figure 10: Heat capacity at constant pressure from PC-SAFT calculations (solid lines) with substitution function from Table 7 and experimental results (symbols) for [EMIM][OAc] (black lines and symbols), [BMIM][BF4] (blue lines and symbols] and [OMIM][BF4] (green lines and symbols). [EMIM][OAc] references (black): open square ([228]). [BMIM][BF4] references (blue symbols): open square ([324]), open circles ([328]), open triangle up ([329]), open triangle down ([330]), open diamond ([331]), open triangle left ([332]), open triangle right ([333]), open star ([334]), open pentagram ([326]), plus sign ([335]), asterisk ([336]). [OMIM][BF4] references (green symbols): open squares ([324]), open circle ([328]), open triangle up ([337]), open triangle down ([338]), plus sign ([330]).

It can be seen, that the experimental results have some deviations for the ionic liquid [BMIM][BF4]. Deviations may be attributed again to water content as it has led to deviations for the densities and surface tensions before. Neither Zhang et al. [329], Fredlake et al. [326] nor Kim et al. [336] give an explanation for the deviations. For [BMIM][BF4] and [OMIM][BF4] it can be seen, that the calculations are in a good agreement with the experimental results, especially for the temperature range from T = 280 K to T = 350 K. For the [EMIM][OAc], as said before, only one data point for

the heat capacity at constant pressure could be found. For the ionic liquids [BMMIM][PF6] and [HMIM][PF6] the calculated heat capacities from PC-SAFT and the substitution functions from Table 7 and experimental results can be seen in Figure 11.

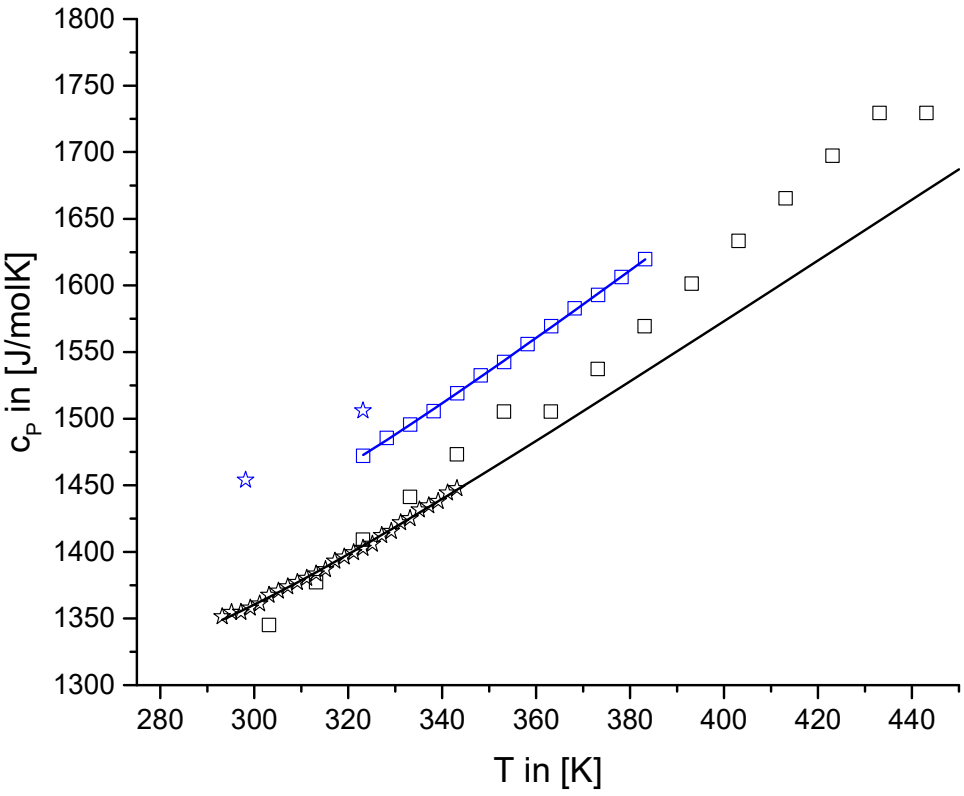

Figure 11: Heat capacity at constant pressure from PC-SAFT calculations (solid lines) with substitution function from Table 7 and experimental results (symbols) for [BMMIM][PF6] (blue lines and symbols) and [HMIM][PF6] (black lines and symbols). [BMMIM][PF6] references (blue symbols): open squares ([325]), open stars ([326]). [HMIM][PF6] references (black symbols): open squares ([339]), open stars ([292]).

For both [BMMIM][PF6] and [HMIM][PF6], it can be seen in Figure 11 that the agreement of the calculations and the experimental results is again quite good, especially for the temperature range of T = 300 – 400 K. For the ionic liquid [BMIM][PF6] the calculated heat capacities from PC-SAFT and the substitution functions from Table 7 and experimental results can be seen in Figure 12.

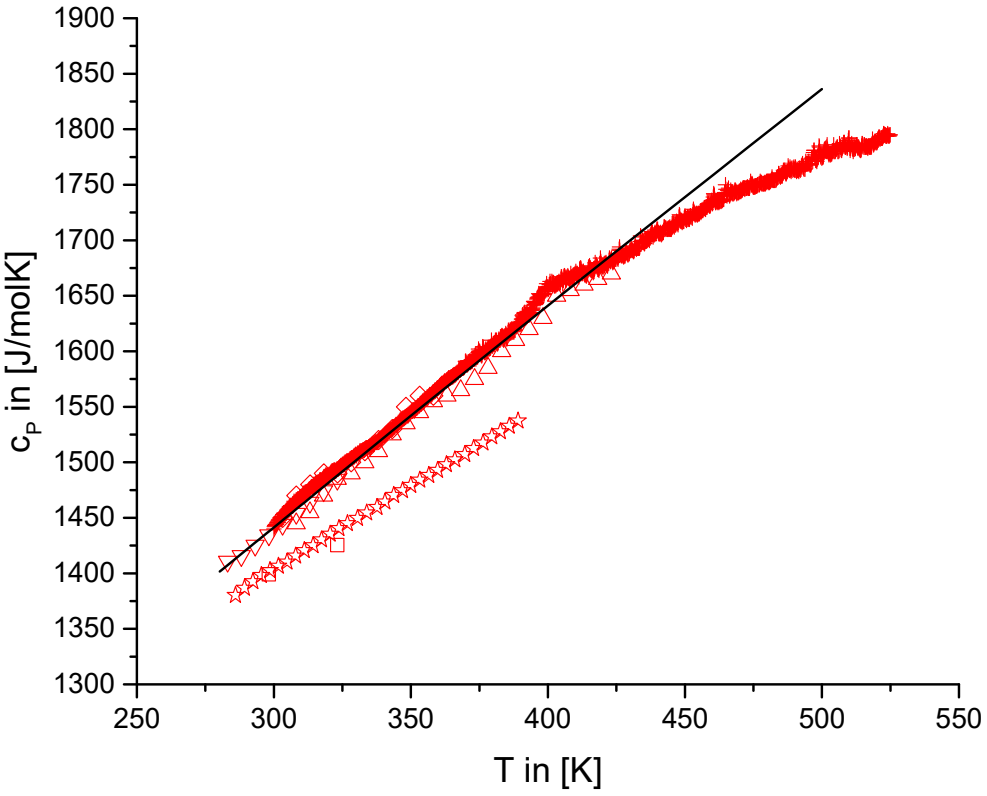

Figure 12: Heat capacity at constant pressure from PC-SAFT calculations (solid lines) with substitution function from Table 7 and experimental results (symbols) for [BMIM][PF6]. Open square ([326]), plus sign ([239]), open triangle up ([327]), open triangle down ([237]), open diamond ([333]), open star ([340]).

In Figure 12 it can be seen, that there are some deviations between the experimental results. The calculated results are in a good agreement with the majority of the experimental results for a temperature range from T = 280 K to over T = 400 K.

For the calculation of the COPs of the absorption cycles, the heat capacity at constant pressure for the cooling agents, namely methanol and ethanol, are needed. Since it is possible to measure the ideal gas heat capacities, there is no need for a substitution function. The ideal gas contribution is fitted as a polynomial to experimental data [341].

4.1.4 Speed of sound

As a final test of the fitted parameters, the speed of sound for the various ionic liquids was calculated. For a real liquid, the speed of sound can be calculated with the equation:

$$u = \sqrt{\frac{c_\mathrm{P}}{c_\mathrm{v}} \left(\frac{\partial P}{\partial \rho} \right)_T} \qquad \textbf{(50)}$$

The heat capacity at constant pressure c_P is calculated as shown in the paragraph before. Since the heat capacity at constant pressure contribution of the ideal gas was calculated as an substitution function fitted to experimental data, the value of the heat capacity at constant volume has to be calculated a different way.

$$c_\mathrm{v} = c_\mathrm{P} - T \frac{\left(\partial^2 P / \partial T^2 \right)_v}{\left(\partial P / \partial v \right)_T} \qquad \textbf{(51)}$$

The calculations of the speed of sound rely on the calculations of the heat capacities which themselves rely on the calculations of first and second derivations of the Helmholtz energy and first and second derivations of the pressure. Because of the complexity of the calculations, deviations of the calculation, which are predictions of the speed of sound from the pure component parameters for the PC-SAFT equation and the substitution function for the ideal gas contribution of the heat capacity at constant pressure, and experimental results are to be expected. The calculations can only be executed for ionic liquids with a fitted substitution function for the ideal gas contribution for the heat capacity at constant pressure. No experimental data for the speed of sound of [BMMIM][PF6] could be found. For the ionic liquids [EMIM][OAc], [BMIM][BF4] and [OMIM][BF4] the calculations and experimental data from literature are depicted in Figure 13.

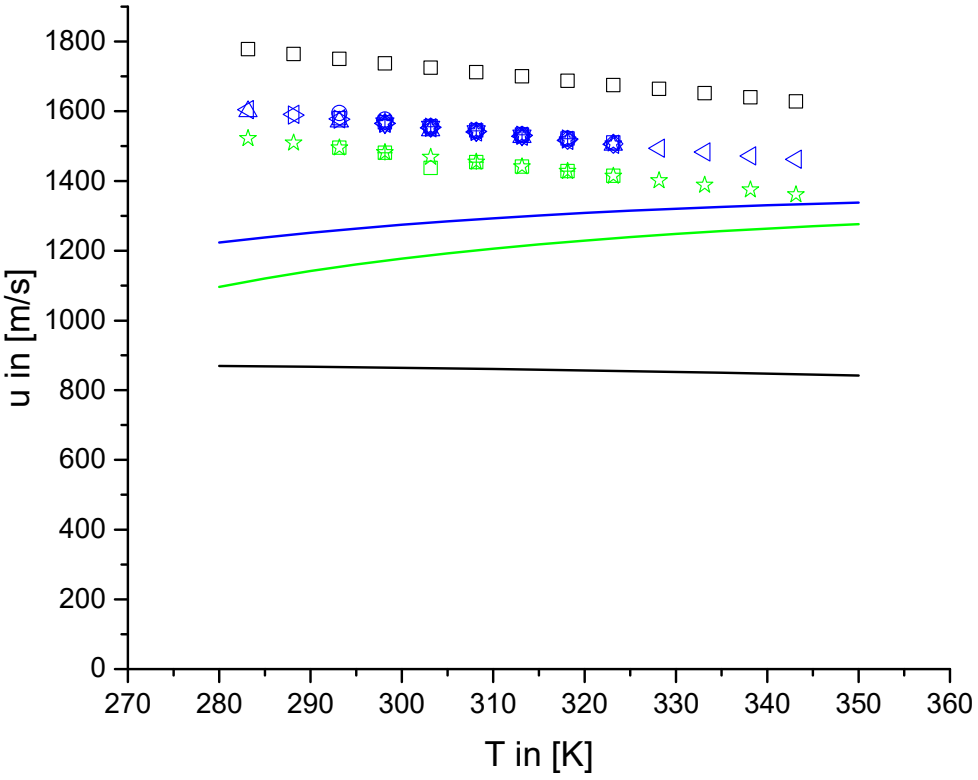

Figure 13: Speed of sound calculated from PC-SAFT (solid lines) and experimental data (symbols) for [EMIM][OAc] (black lines and symbols), [BMIM][BF4] (blue lines and symbols) and [OMIM][BF4] (green lines and symbols). [EMIM][OAc] references (black symbols): open square ([225]). [BMIM][BF4] references (blue symbols): open square ([342]), open circle ([334]), open triangle up ([299]), open triangle down ([245]), open diamond ([247]), open triangle left ([271]), open triangle right ([249]), open star ([257]), plus sign ([288]). [OMIM][BF4] references (green symbols): open square ([343]), open star ([271]), plus sign ([344]).

It can be seen in Figure 13 that there are some deviations between the calculations and the experimental results. The deviations are a bit bigger for [EMIM][OAc] but this may be because of the fact, that the substitution function for the ideal gas contribution of the heat capacity at constant pressure for this ionic liquid had to be fitted to only one data point and is a constant. The deviations for all three ionic liquids are in a range were the fit of the pure component parameters can be considered as reasonable. For the ionic liquids [BMIM][PF6] and [OMIM][PF6] the results of the calculations and experimental data taken from literature are depicted in Figure 14.

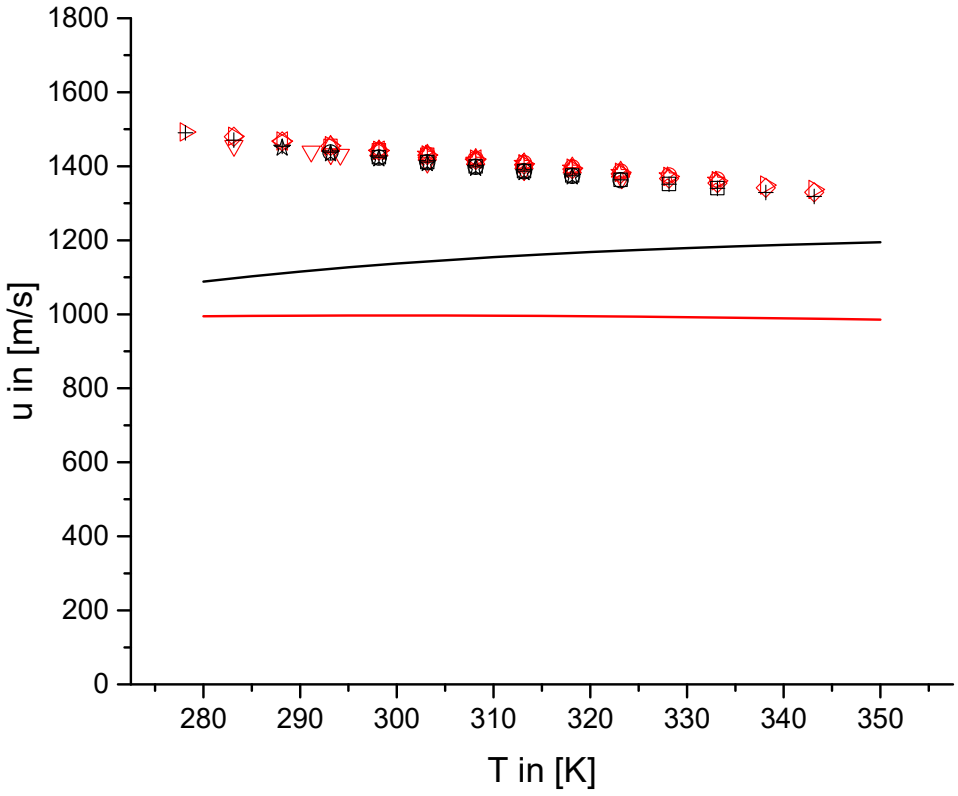

Figure 14: Speed of sound calculated from PC-SAFT (solid lines) and experimental data (symbols) for [BMIM][PF6] (red lines and symbols) and [OMIM][PF6] (black lines and symbols). [BMIM][PF6] references (red symbols): open square ([285]), open circle ([276]), open triangle up ([277]), open triangle down ([299]), open diamond ([271]), open triangle left ([345]), open triangle right ([284]), open star ([322]), plus sign ([346]). [OMIM][PF6] references (black symbols): open square ([276]), open circle ([347]), open star ([348]), open diamond ([285]), plus sign ([284]).

Again, the deviations of the ionic liquids in Figure 14 are in a range, in which the pure component parameters can be considered reasonable. Deviations in the predictions of speed of sound with PC-SAFT is not unusual. For example de Villiers et al. [349] predicted the speed of sound for 1-hexanol and their results did show deviations around 10% even though the parameters for the alcohol could be fitted to liquid densities and vapor pressures, which is not possible for the ionic liquids as mentioned before. Therefore the results for speed of sound of ionic liquids seem satisfiable.

4.1.5 Self-diffusion

The calculations of the diffusion coefficients were done for components already described in the literature. The pure component parameters used and their references are listed in Table A 7 in the appendix. Since the calculations were also

done for polar molecules, an extension to the PC-SAFT framework was incorporated, namely the PCP-SAFT extension specifically accounting for polarities in the molecules developed by Gross [209]. The PCP-SAFT framework was also implemented by Diamantonis et al. [213], but without the quadrupole term, together with the model of Yu and Gao [189] or Reis et al. [214] and compared the results with experimental results by Etesse et al. [350]. They were in a good accordance with the experimental data, but with slightly less deviations for the model of Yu and Gao (equations (43) and (44)). An even better result is achieved with the correction suggested by Gross [221] as depicted in Figure 15.

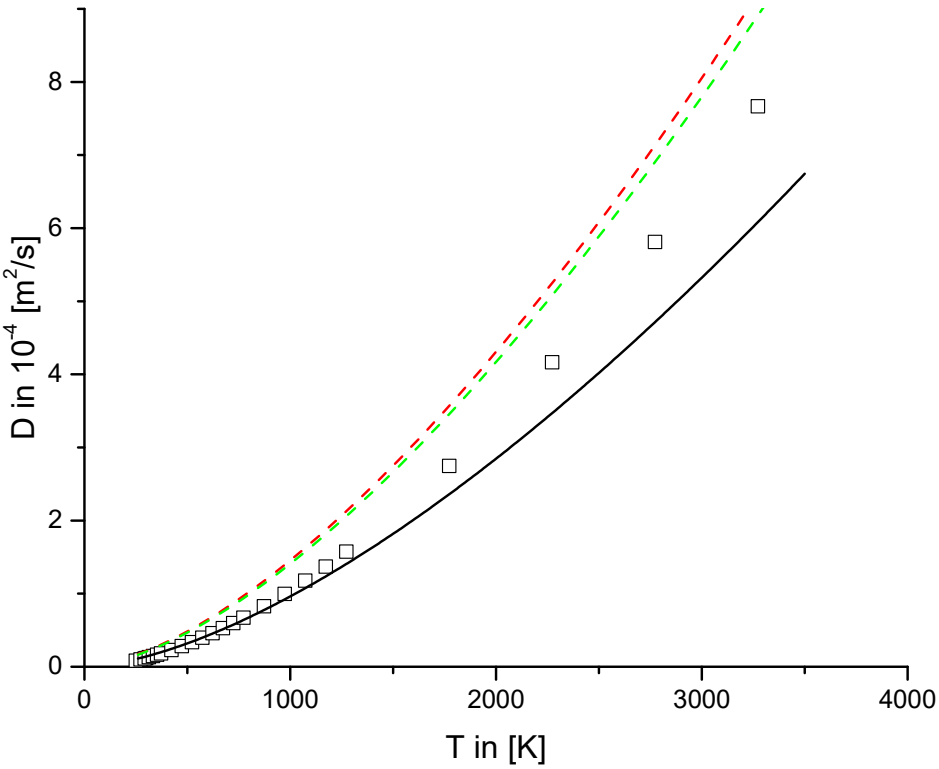

Figure 15: Self-diffusion coefficient of carbon dioxide at atmospheric pressure. Open squares are experimental results by Bouhsehri et al. [154], lines are calculations with PCP-SAFT and equation (42) (red dotted line), equations (43) and (44) (green dashed line) and equation (45) with the correction proposed by Gross [221] (black solid line).

It can be seen in Figure 15, that the correction according to Gross [221] has less deviations than the modification according to Yu and Gao [189] and the unmodified Enskog equation (equation (42)). This leads to the decision, that the following calculations in this work will be done with the correction from Gross [221]. Since the calculations for the temperature dependence of the self-diffusion are satisfiable, the

next step is to examine the pressure dependence. Etesse et al. [350] provided experimental results by PFG-NMR over a wide pressure range. Comparison of the calculations and the experimental results from Etesse et al. [350] are shown in Figure 16.

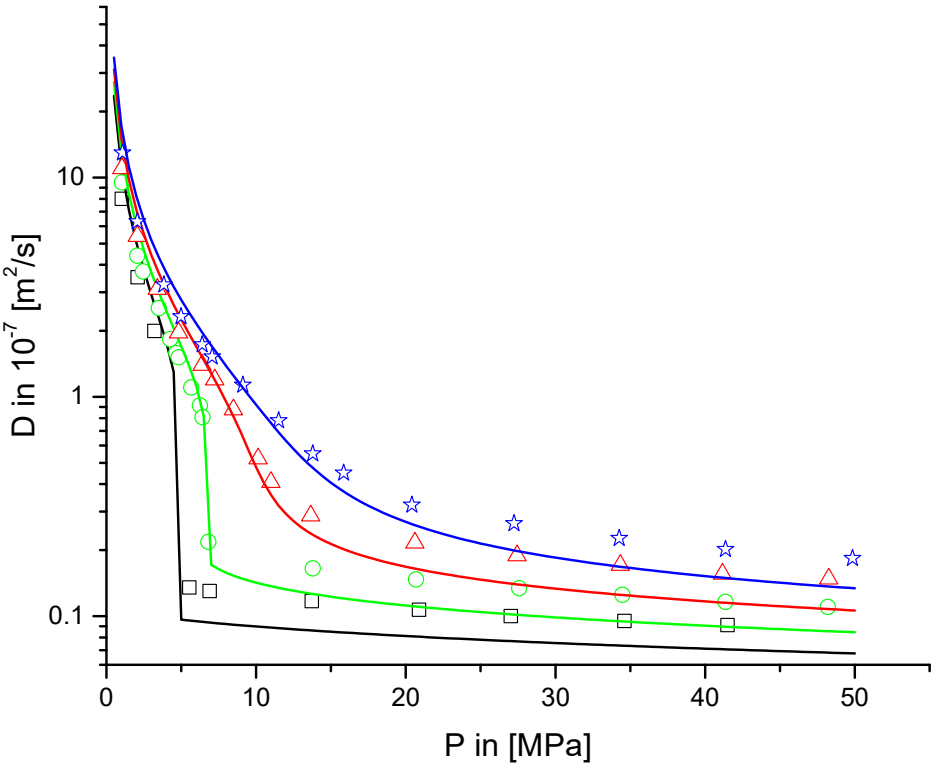

Figure 16:Self-diffusion coefficient of carbon dioxide at T=273.15K (black lines and open squares), T=298.15K (green lines and open circles), T=323.15K (red lines and open triangles) and T=348.15K (blue lines and open stars). Lines are predictions from PCP-SAFT calculations, symbols are experimental results from Etesse et al. [350].

In Figure 16 it can be seen, that the calculations are in a good agreement for lower pressures at the gaseous state. For higher pressures and therefore in the liquid state, these deviations increase. Since the calculation of the self-diffusion heavily depends on the calculation of the densities, it is possible, that the deviations in Figure 16 may be attributed to deviations in the calculation of the densities at very high pressures. To examine this, the densities calculated with PCP-SAFT are compared to a high-precision equation of state developed by Span and Wagner [351]. This comparison is depicted in Figure 17.

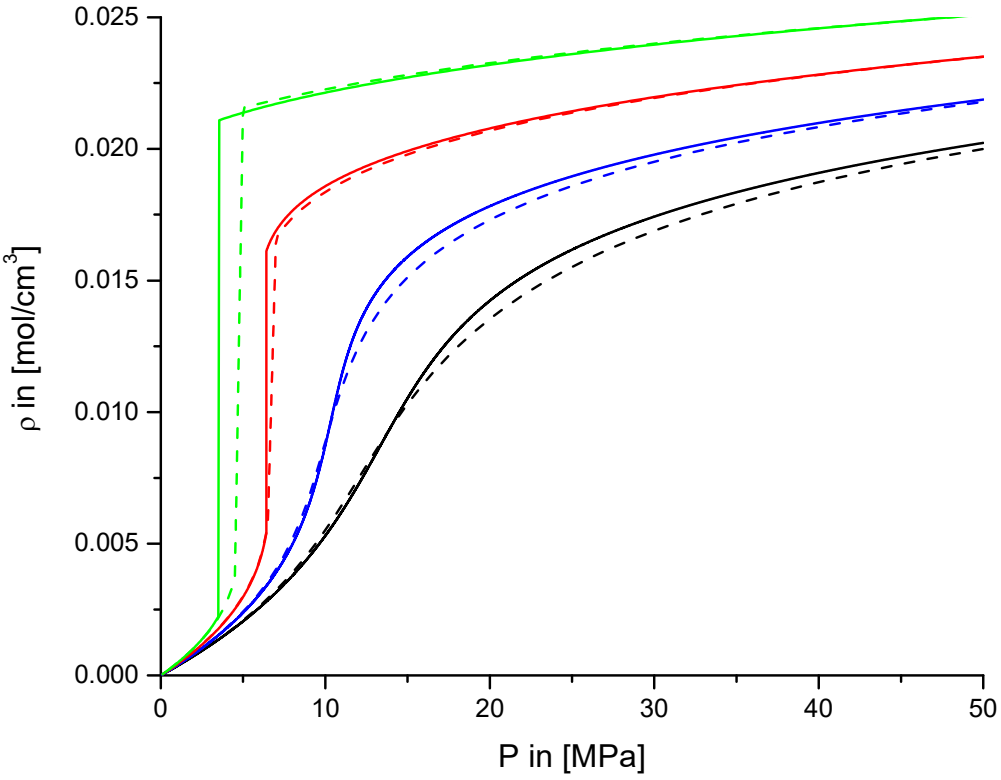

Figure 17: Comparison of calculated densities from PCP-SAFT (dashed lines) and Span and Wagner high precision EOS [351] (solid lines) at T=273.14K (green lines), T=298.15K (red lines), T=323.15K (blue lines) and T=348.15K (black lines).

As can be seen in Figure 17, the deviations between the two calculations are small, but are certainly there especially at higher temperatures. This can be attributed to the fact, that PC-SAFT parameters are usually fitted to saturated liquid densities and vapor pressures. In the case of the here depicted carbon dioxide, the critical pressure is at $P_{crit} = 7.337 MPa$, meaning that any calculations above this pressure have to be treated as a prediction. For both, the pressure and temperature dependency both can be predicted with a good accuracy in the range of the fitting data for carbon dioxide. The temperature dependency of the self-diffusion coefficient of methane can be seen in Figure 18.

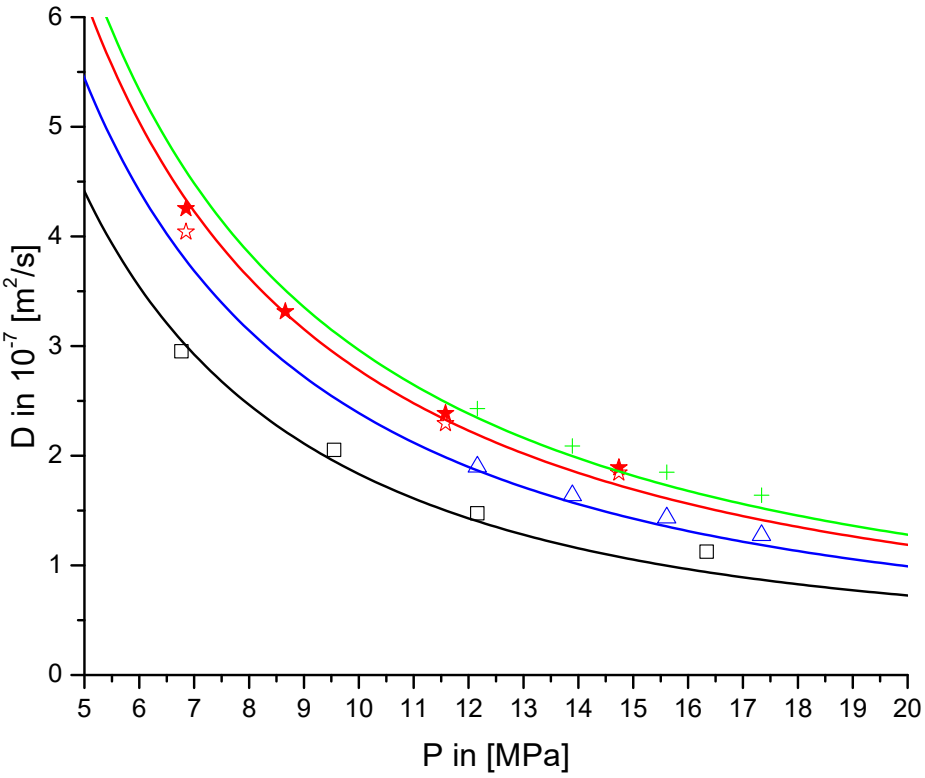

Figure 18: Self-diffusion coefficients for methane at T=298.15K (black lines and symbols), T=330.93K (blue lines and symbols), T=353.7K (red lines and symbols) and T=364.21K (green lines and symbols). Solid lines are predictions of the PC-SAFT calculations, symbols are experimental results: open squares, open triangles, open stars and plus signs [352], solid stars [353].

For methane, the predictions are again in a good agreement with the experimental results, which can be expected since the methane molecule can be considered as nearly spherical. In Figure 18 it becomes clear, that both the temperature and the pressure dependency is in agreement between the experiments and the prediction, but of course, the temperature range is not very large. A comparison of the self-diffusion coefficients for hydrogen can be seen in Figure 19.

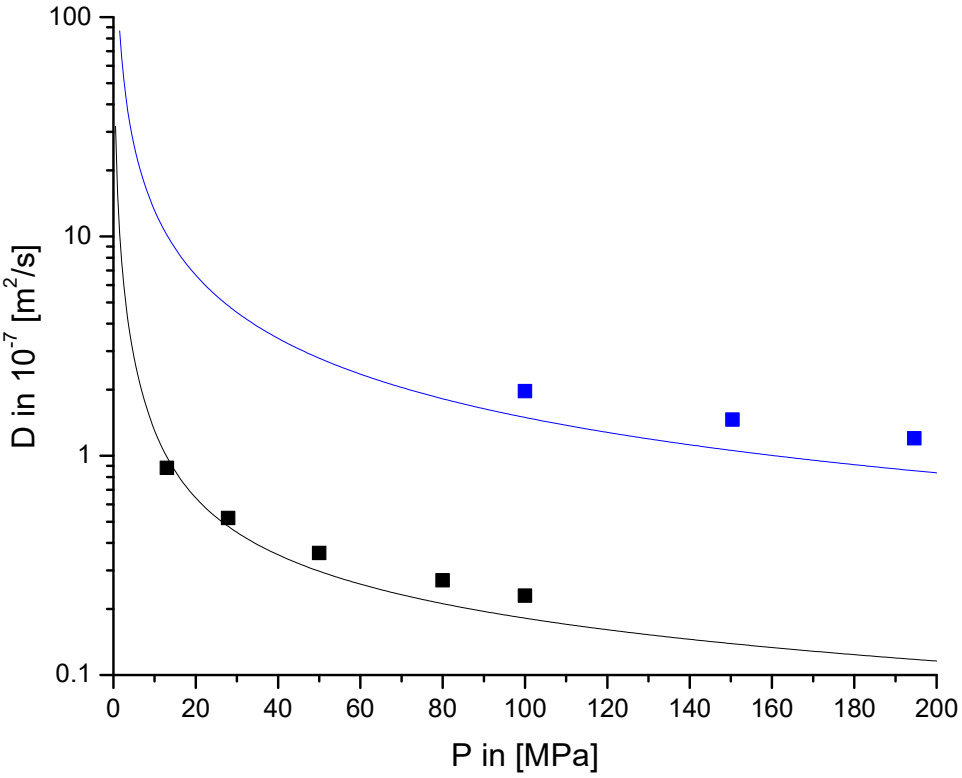

Figure 19: Self-diffusion coefficients for hydrogen at T=293K (black lines and symbols) and T=78K (blue lines and symbols). Solid lines are predictions, solid squares experimental results [153].

For the hydrogen, the deviations between the predictions and the experimental results are again small, just as for the methane in Figure 18. This may again be attributed to the fact, that the hydrogen molecule can also be considered nearly spherical, similar to the methane. Of course, the limitation to spherical molecules would be a major one, therefore the performance of the predictions for non-spherical molecules is of interest.

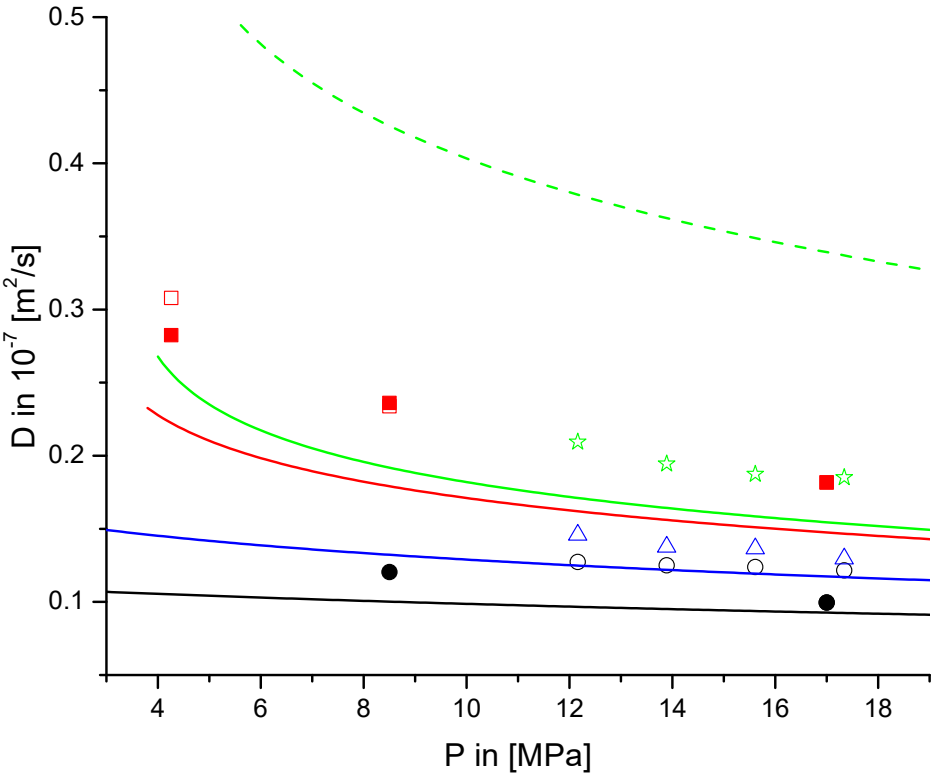

Figure 20: Self-diffusion coefficients of propane at T=298.15K (black lines and symbols), T=330.93K (blue lines and symbols), T=358.7K (red lines and symbols) and T=364.21K (green lines and symbols). Open circles, open triangles, open squares and open stars [353], solid squares and solid circles [354]. The solid lines represent a prediction with correction from equation (45), the dashed line is a prediction with a correction from equation (43).

Figure 20 shows, that the predictions of the self-diffusion coefficients are hindered by the non-spherical form of the molecules. The calculations are in a fair agreement with the experimental data, but underestimate the coefficients when the correction proposed by Gross [221] is utilized. A correction with the equation (43) leads to a huge overestimation of the self-diffusion coefficients. To further look into what is causing these deviations the self-diffusion of ethylene is examined.

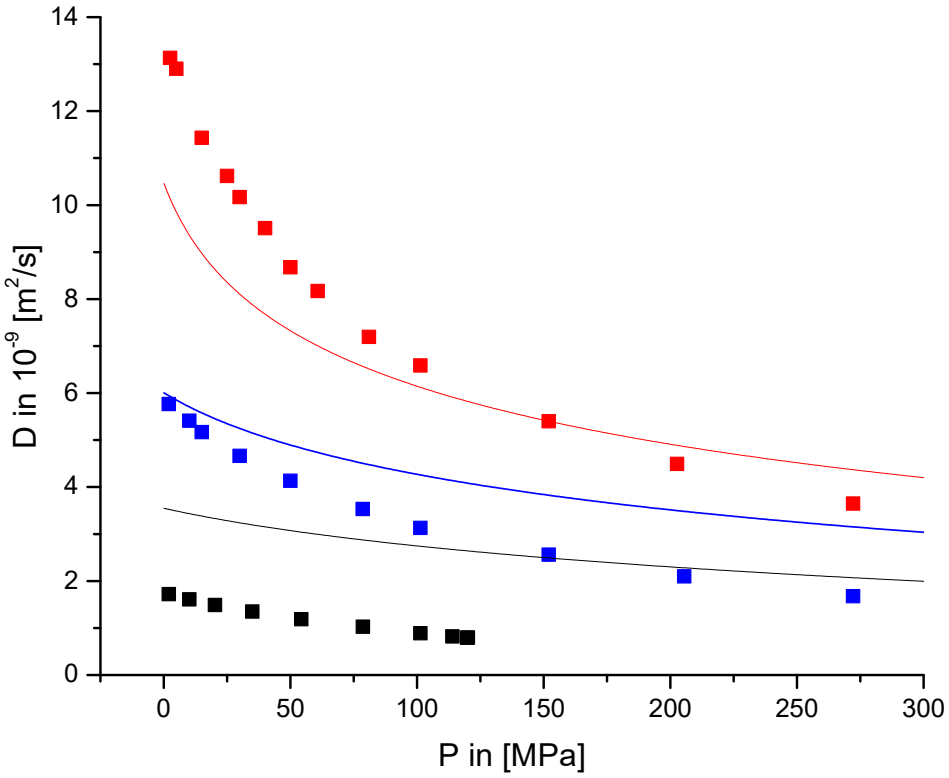

Figure 21: Self-diffusion of ethylene at T=123.15K (black lines and symbols), T=173.15K (blue lines and symbols) and T=223.15K (red lines and symbols). Solid lines are predictions from PC-SAFT calculations. Solid squares are experimental results [148].

In Figure 21 we can again see some deviations between the PC-SAFT predictions and the experimental results. The two possible and already discussed reasons for these deviations are deviations in the density calculations or the fact that the ethylene molecules are not spherical. To examine the first possibility, the calculated densities of the ethylene are compared to experimental results [148] are depicted in Figure 22.

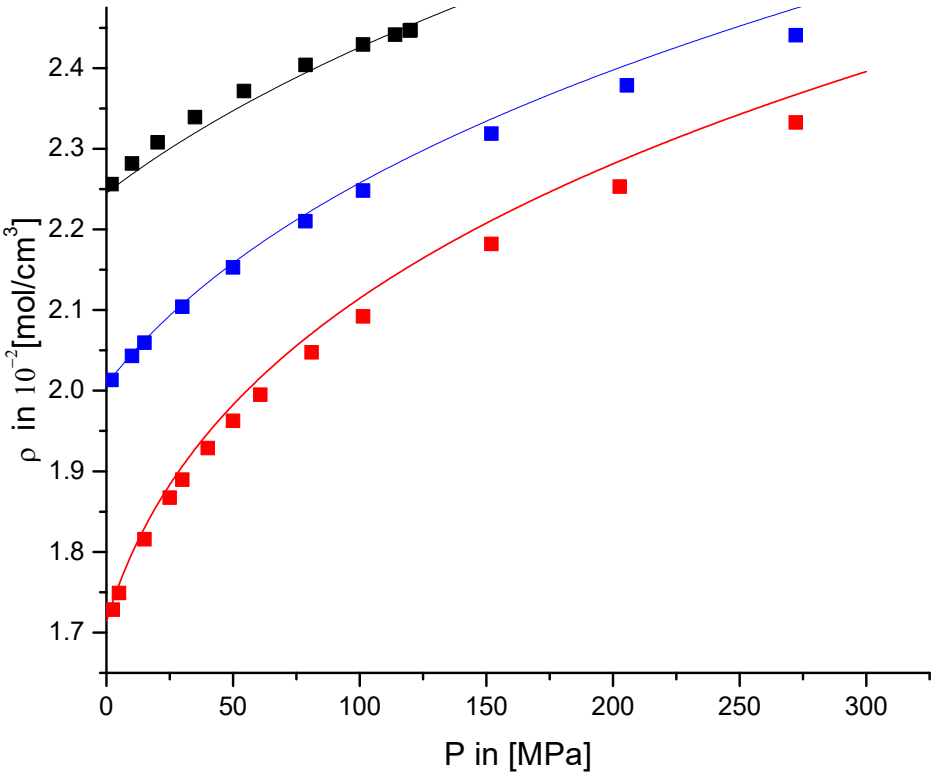

Figure 22: Density of ethylene at T=123.15K (black lines and symbols), T=173.15K (blue lines and symbols) and T=223.15K (red lines and symbols). Solid lines are predictions from PC-SAFT calculations. Solid squares are experimental results [148].

Figure 22 shows, that the calculated results are in a good agreement with the experimental results and therefore cannot be the reason for the deviations of the self-diffusion coefficients in Figure 21. These have probably to be attributed to the correction for the non-spherical shape of the molecule. Perhaps further improvement on the approach suggested by Gross [221] is necessary which will not be discussed in this work. For nearly spherical, non-associating molecules, the results are quite satisfactory as depicted in Figure 23 for the molecules of argon, helium, methane, ethane and ethylene.

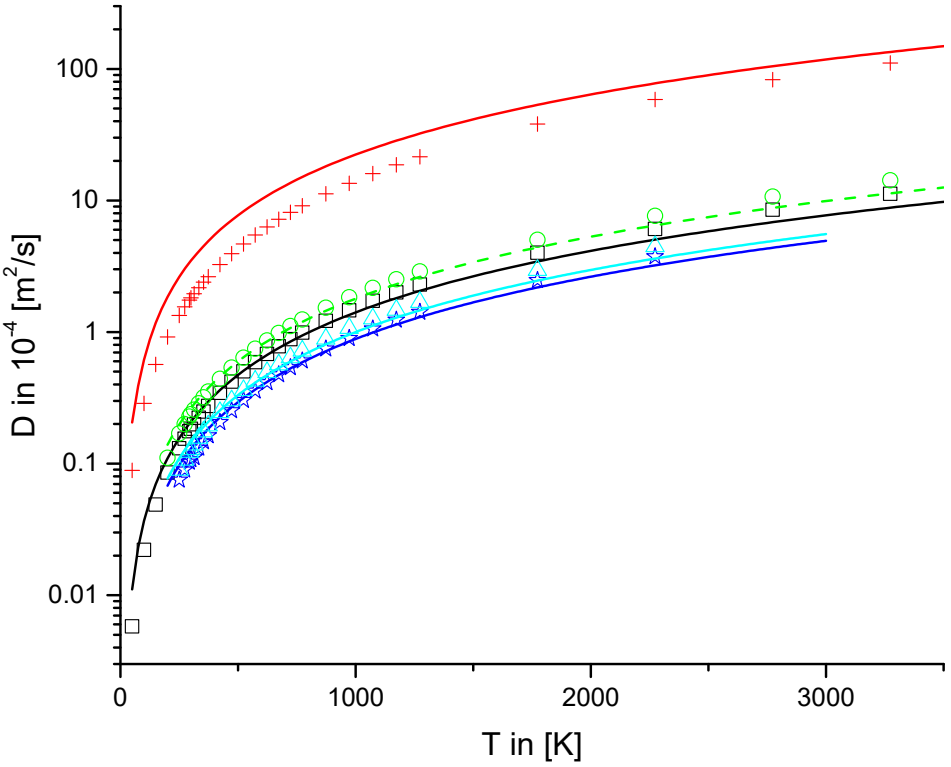

Figure 23: Self-diffusion coefficients at P=1bar of argon (black lines and symbols), helium (red lines and symbols), methane (green lines and symbols), ethane (dark blue lines and symbols) and ethylene (light blue lines and symbols). Symbols are experimental results: plus signs, open stars, open triangles [154]; open squares and open circles [152].

Figure 23 shows that the predictions and the experimental results are in a good agreement with each other. The self-diffusion coefficients for nitrous oxide, nitrogen, oxygen and carbon monoxide are shown in Figure 24.

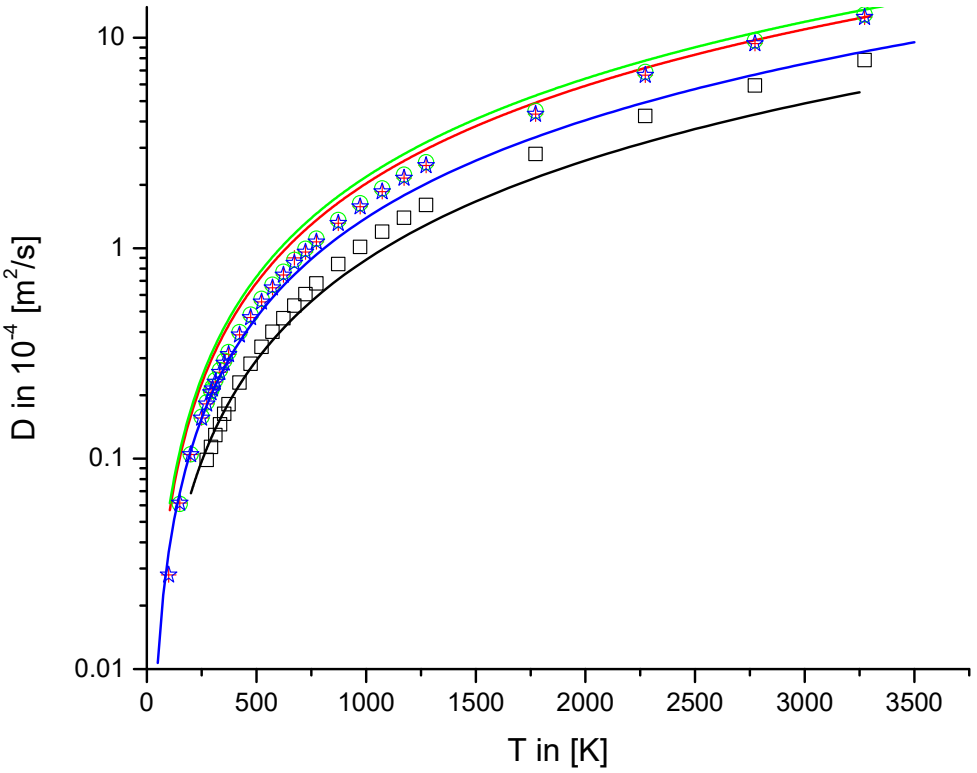

Figure 24: Self-diffusion coefficients at P=1bar of nitrous oxide (black lines and symbols), nitrogen (red lines and symbols), oxygen (green lines and symbols) and carbon monoxide (blue lines and symbols). Symbols are experimental results [154].

Figure 24 shows just as Figure 23, that the predictions for spherical and nearly spherical, non-associating molecules are in a good agreement with the experimental results. Since the major focus of this work is on substances with association forces, the performance of the Enskog-theory with associating molecules is of special interest. With the PC-SAFT framework, the association interactions are already implemented as described in chapter 3.1. Asahi and Nakamura [355] did measurements on methanol vapor for several reduced densities $\rho_r = \rho / \rho_{critical}$ with the critical density of methanol being $\rho_{critical} = 272\, kg/m^3$. These experimental data together with the predictions of the PC-SAFT predictions are shown in Figure 25.

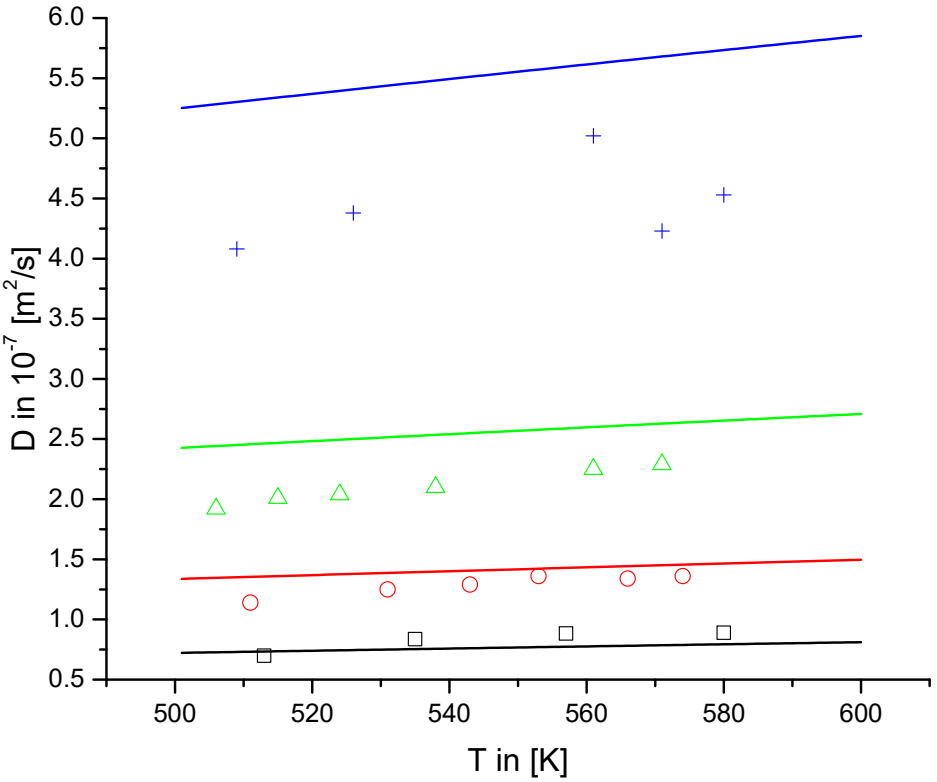

Figure 25: Self-diffusion coefficients of methanol at $\rho_r = 1.008$ (black lines and symbols), $\rho_r = 0.622$ (red lines and symbols), $\rho_r = 0.372$ (green lines and symbols) and $\rho_r = 0.183$ (blue lines and symbols). Lines are predictions from PC-SAFT calculations, symbols are experimental data [355].

Figure 25 shows a good agreement of the predictions at high densities which means at high pressures and a fair agreement at low densities and low pressures. But even with the deviations at low pressures, these are promising results keeping in mind, that the calculations are pure predictions from the parameters fitted to liquid densities and vapor pressures. The effect, that the precision increases with the pressure was attributed by Wallen et al. [356] and by Hoffmann and Conradi [357] to increased hydrogen bonding of the methanol molecules. To further investigate the prediction capabilities of the model for associating molecules, the self-diffusion of water was examined. Yoshida et al. [358,359] provided experimental results and these are compared to the Enskog-model in Figure 26.

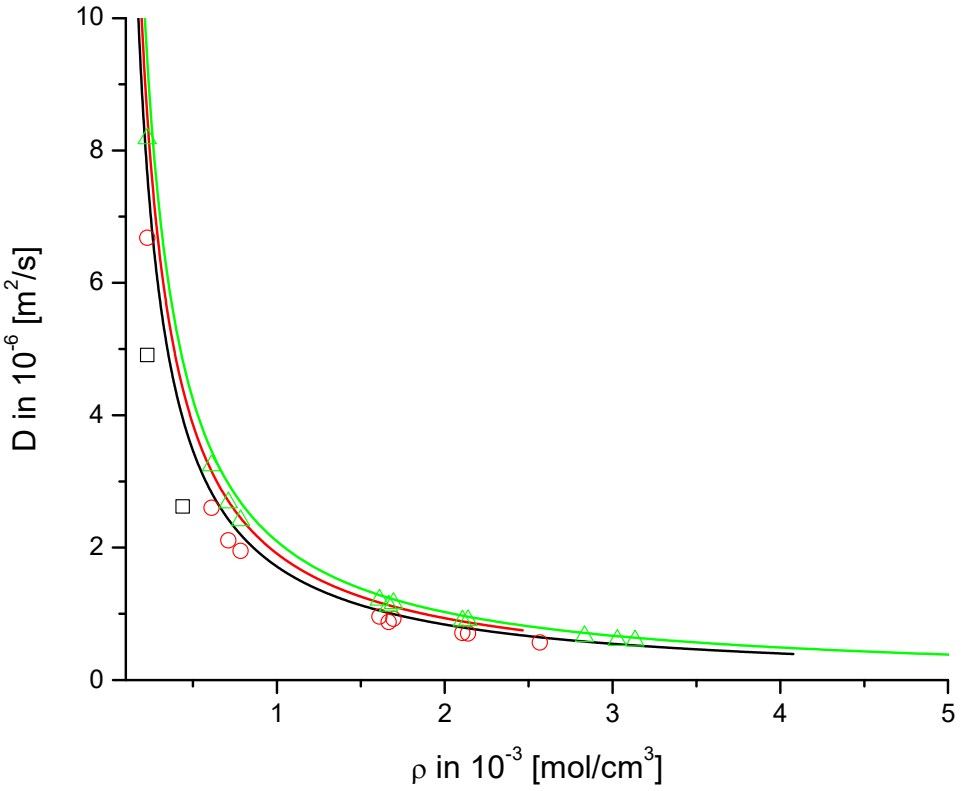

Figure 26: Self-diffusion coefficients for water vapor at T=473.15K (black lines and symbols), T=573.15K (red lines and symbols) and T=673.15K (green lines and symbols). Lines are predictions from PC-SAFT calculations, symbols are experimental data [358,359].

Again, as in Figure 25, Figure 26 the predictions and the experimental results are in a good agreement. It can be concluded, that the Enskog-theory combined with the PCP-SAFT equations of state is able to predict the self-diffusion of associating molecules in the vapor state. Guevara-Carrion et al. [169] examined the self-diffusion of methanol and ethanol by molecular dynamic simulation. Since the data is in a good agreement with experimental results it can be treated as a pseudo-experimental data. Comparing this data with the predictions made with the Enskog model showed that it is not possible to predict the self-diffusion of the liquid molecules with a satisfiable accuracy.

It can be concluded, that the Enskog-model, modified with the corrections suggested by Gross [221] combined with the PC-SAFT framework, or PCP-SAFT framework for polar molecules, can be used to reliably predict the self-diffusion of molecules that are spherical or nearly spherical molecules in the vapor state for associating and non-associating molecules. For the case of non-associating molecules, it is possible

to predict the self-diffusion coefficients with a fairly good agreement in the liquid state but it was not possible to do the same for associating liquids.

4.2 Binary systems

4.2.1 Binary diffusion

As described earlier in chapter 3.3, the Enskog theory can easily be extended to binary mixtures yielding the equation (46). This equation was again combined with the PCP-SAFT framework under the assumption, that the binary interaction parameter for the combining rule of the dispersion interaction $k_{ij}^{dispersion}$ can be set to $k_{ij}^{dispersion} = 0$. This allows for the prediction of the diffusion coefficient for the mixture including its dependency on temperature, pressure and composition. For the equimolar mixture of methane + ethane a comparison between the predicted values and experimental results [360] can be seen in Figure 27.

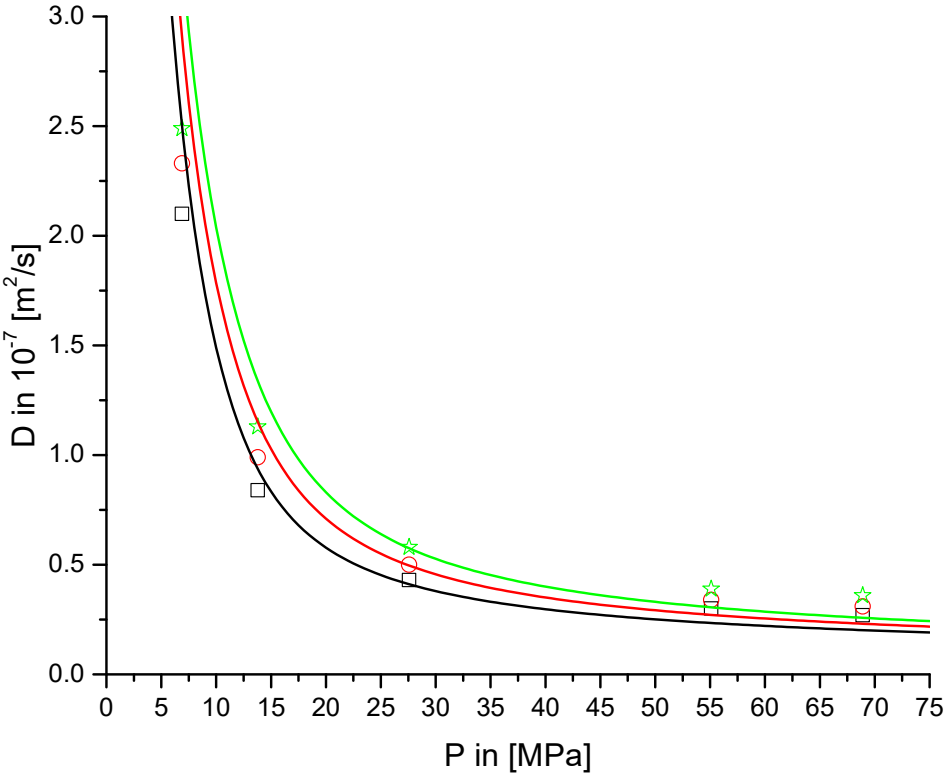

Figure 27: Diffusion coefficients of methane + ethane at $x_{Methane}$=0.8 and temperatures of T=313.15K (black lines and symbols), T=333.15K (red lines and symbols) and T=350.37K (green lines and symbols). Solid lines are predictions and symbols are experimental data [360].

Figure 27 shows a good agreement between the experimental results and the predictions for lower pressures and a fair agreement at higher pressures, similar to the results for the pure component self-diffusion coefficients for nearly spherical shaped molecules before (Figure 15, Figure 16, Figure 18, Figure 23, Figure 24). This means that a good prediction over a pressure range typically used in practice is possible with the model. The temperature dependence of the diffusion coefficient of the equimolar systems carbon monoxide + hydrogen, carbon monoxide + helium and carbon monoxide + argon is examined and shown in Figure 28.

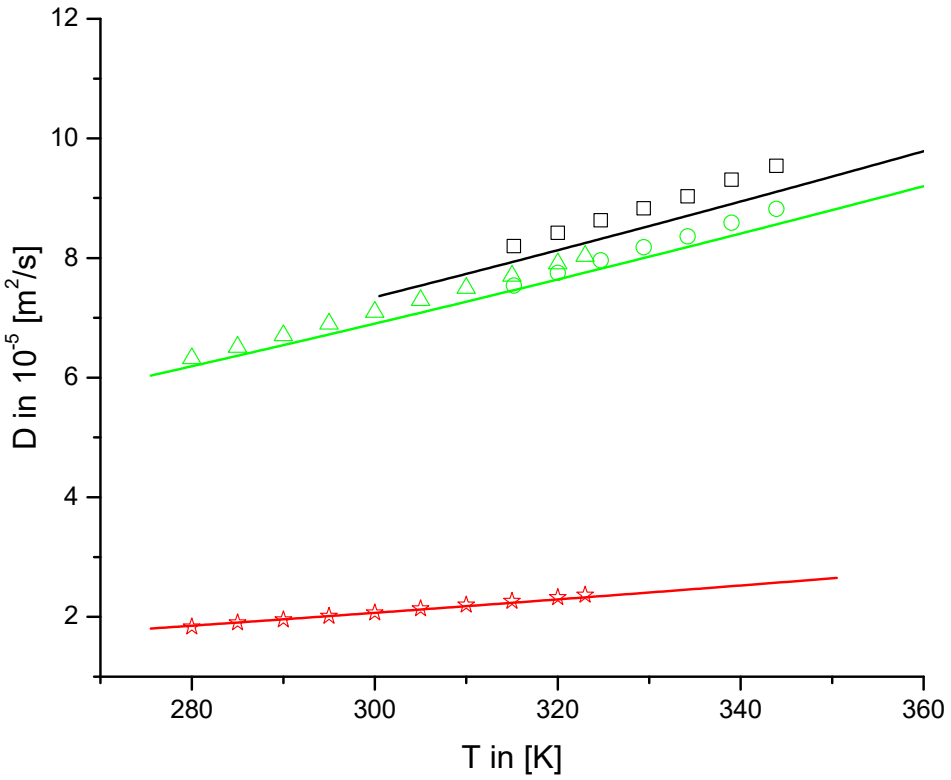

Figure 28: Diffusion coefficients of equimolar mixtures at atmospheric pressure of carbon monoxide + hydrogen (black lines and symbols), carbon monoxide + helium (green lines and symbols) and carbon monoxide + argon (red lines and symbols). Solid lines are predictions and symbols are experimental results: open squares, open circles [186]; open triangles, open stars [361].

Again in Figure 28, as in Figure 27, the predicted diffusion coefficients are in a good agreement with the experimental results. The temperature range in Figure 28 is of course not especially wide. In Figure 29 diffusion coefficients of the equimolar mixtures of argon + butane, ethylene + nitrogen, ethane + nitrogen and carbon dioxide + hydrogen are depicted, partially with wider temperature ranges up to $\Delta T \approx 350K$.

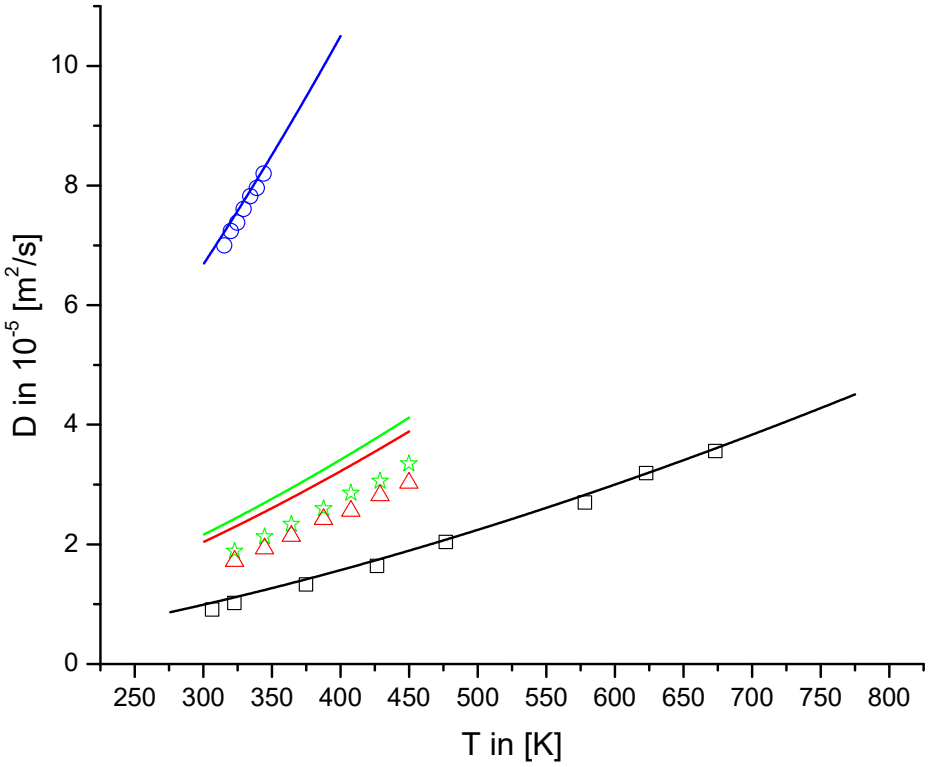

Figure 29: Diffusion coefficients of equimolar mixtures at atmospheric pressure of argon + butane (black lines and symbols), ethylene + nitrogen (green lines and symbols), ethane + nitrogen (red lines and symbols) and carbon dioxide + hydrogen (blue lines and symbols. Solid lines are predictions and symbols are experimental results: open squares [362], open circles [186]; open triangles [363], open stars [364].

A good agreement between predictions and experimental results can be seen for the systems of argon + butane and carbon dioxide + hydrogen. But for the systems ethylene + nitrogen and ethane + nitrogen, the quality of the predictions is only fair. But deviations did already occur for the self-diffusion of nitrogen and ethylene earlier, so deviations in the mixture are to be expected. But it is good to remind oneself, that all the calculated results are predictions from the PC-SAFT parameters as no additional parameters were taken into account. Keeping that in mind, the results for the two systems of ethylene + nitrogen and ethane + nitrogen are still satisfactory. For the equimolar systems of helium + carbon dioxide, oxygen, nitrogen or argon, the predictions and experimental results [186,365] are depicted in Figure 30.

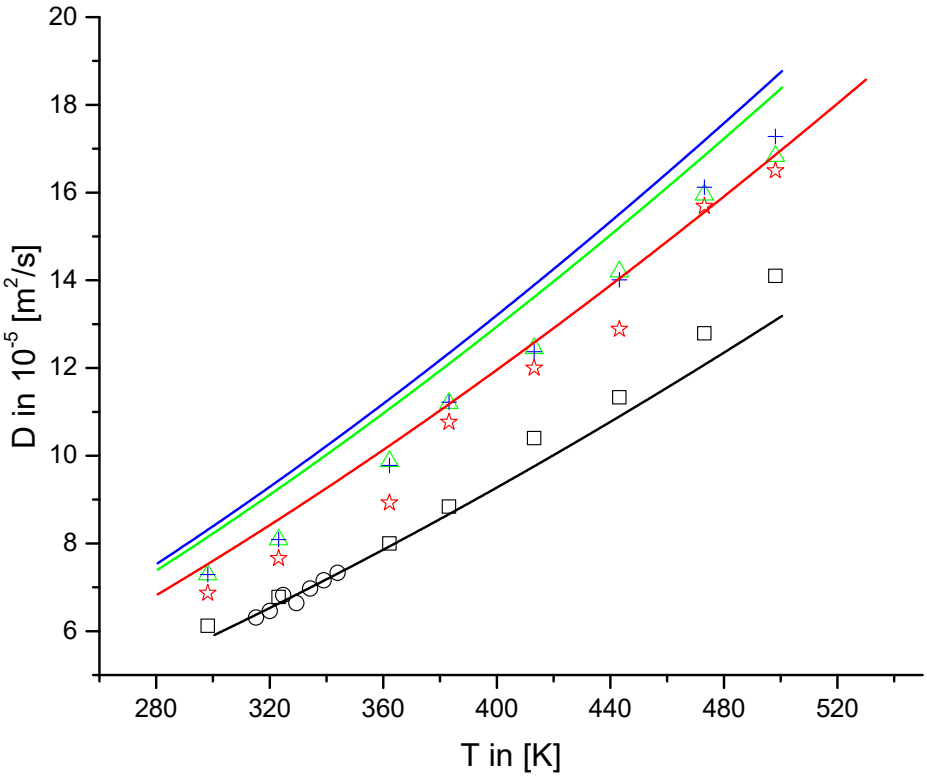

Figure 30: Diffusion coefficients of equimolar mixtures at atmospheric pressure of helium + carbon dioxide (black lines and symbols), helium + oxygen (green lines and symbols), helium + nitrogen (red lines and symbols) and helium + argon (blue lines and symbols. Solid lines are predictions and symbols are experimental results: open squares, open stars, open triangles and plus sign [365]; open circle [186].

In Figure 30, there is a good agreement between the calculations and the experimental results for helium + carbon dioxide. However for helium + oxygen, nitrogen or argon deviations occur. It seems, as if the prediction capability of the model for equimolar mixtures is generally there, but some systems can only be predicted with lower accuracy than others. The occurring deviations can seemingly not be linked to deviations for the pure component systems. At the moment, the reason for the deviations cannot be explained. Additionally, the model seems to overestimate the composition dependency of the diffusion coefficient. Kestin et al. [152] provided experimental results of the diffusion coefficient of the system argon + helium dependent on the composition. The results and the predictions are depicted in Figure 31 together with the pure component self-diffusion coefficients.

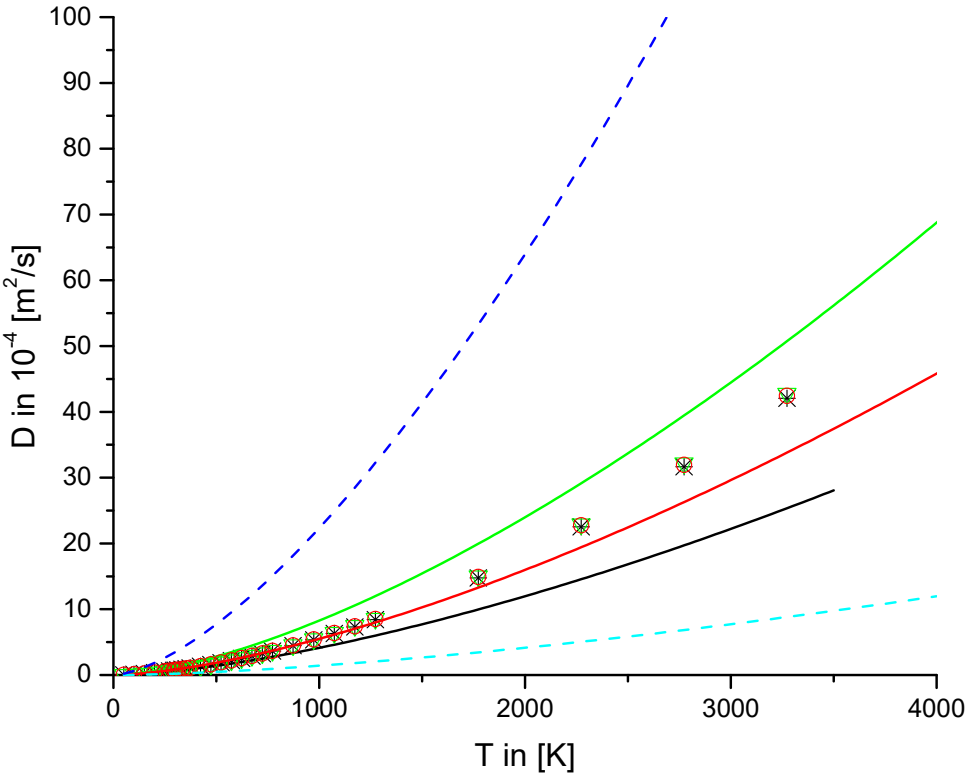

Figure 31: Diffusion coefficients of pure argon (light blue dashed line), pure helium (dark blue dashed line) and mixtures of the two components with composition x_{argon}=0.25 (green line and asterisks), x_{argon}=0.5 (red line and open circle) and x_{argon}=0.75 (black line and stars). Lines are predictions and symbols are experimental data [152].

It can be seen, that the experimental results are showing a very small dependency of the diffusion to the composition. In contrast, the Enskog model is showing a clearly visible dependency.

The Enskog theory with modifications according to Gross [221] in combination with the PCP-SAFT framework seems to be able to predict the diffusion coefficients for equimolar mixtures of spherical and nearly spherical molecules in the gaseous state. To include the model into the calculations of absorption cycles including alcohols and ionic liquids, it needs to be extended to the mixture of liquids additionally to the extension to liquid associating models as discussed in chapter 4.1.5.

4.2.2 Experimental results for the binary equilibria from literature

Since ionic liquids are a relatively new substance and there is a very wide variety to choose from, it can be difficult to find experimental results for a specific working pair. This is, of course, a reason for the desirability of a shortcut method to evaluate the

value of a working pair. For the pairs considered in this work, only few results for the binary systems at equilibrium could be found. Only Revelli et al. [366] provided experimental results for the binary VLE of the systems [BMIM][BF4] + methanol and [BMIM][BF4] + ethanol. They [366] measured the vapor pressures of the systems for several temperatures and concentrations. Therefore it was possible to fit binary interaction parameters ($k_{ij}^{\text{dispersion}}, k_{ij}^{\text{association}}, l_{ij}$) for these two systems. Pereiro and Rodriguez [295] produced experimental results for the LLE equilibrium concentrations at P=1bar for several temperatures for the systems [BMIM][PF6] + ethanol and [HMIM][PF6] + ethanol. Sahandzhieva et al. [367] gathered experimental results of LLE equilibrium concentrations at P=1bar for the system [BMIM][PF6] + ethanol. The LLE data was used to validate the calculations with the pure component parameters and binary interaction parameters. But as mentioned before, it was not used to fit binary interaction parameters.

Source	System	Equilibrium	Temperature range in [K]	x_{IL} range in [1]	Number of points
Revelli et al. [366]	[BMIM][BF4] + methanol	VLE	283.15 - 293.15	0 - 0.9	27
Revelli et al. [366]	[BMIM][BF4] + ethanol	VLE	283.15 - 298.15	0 - 0.9	34
Pereiro and Rodriguez [295]	[BMIM][PF6] + ethanol	LLE	288.2 - 328	-	24
Pereiro and Rodriguez [295]	[HMIM][PF6] + ethanol	LLE	278.15 - 293.15	-	8
Sahandzhieva et al. [367]	[BMIM][PF6] + ethanol	LLE	279.1 – 313.8	-	66

Table 8: Literature sources for experimental results.

4.2.3 VLE of methanol + ionic liquid

For the system of [BMIM][BF4] + methanol, experimental results for the VLE were found. Revelli et al. [366] measured the vapor pressure for 3 temperatures T=283.15, 288.15, 293.15 K over mole fractions from x_{IL}=0 to x_{IL}=0.9. Since the composition in absorption chillers is located around the mole fraction of x_{IL}=0.7–0.8 (apart from the pure ethanol in the evaporator and condenser), the three parameters (l_{ij}, $k_{ij}^{\text{dispersion}}$, $k_{ij}^{\text{association}}$) were fitted to the experimental results in this composition range, in which the parameter to correct the combining rule for the temperature independent segment diameter (l_{ij}) was treated as constant with temperature and the two parameters to correct the mixing rules for the depth of the square-well potential and the association energy ($k_{ij}^{\text{dispersion}}$ and $k_{ij}^{\text{association}}$ respectively) were treated as temperature dependent. The binary interaction parameters are given inTable 9.

Parameter	Value	Equation
l_{ij}	0.0028	(24)
$k_{ij}^{\text{dispersion}}$	$-0.00046 \cdot T/\text{K} + 0.0842$	(25)
$k_{ij}^{\text{association}}$	$-0.0004 \cdot T/\text{K} - 0.0933$	(27)

Table 9 Binary interaction parameters for [BMIM][BF4] + methanol.

The calculated vapor pressures for the ionic liquid concentrations x_{IL}=0.7 and x_{IL}=0.8 (the data used for the parameter estimation) are shown in Figure 32.

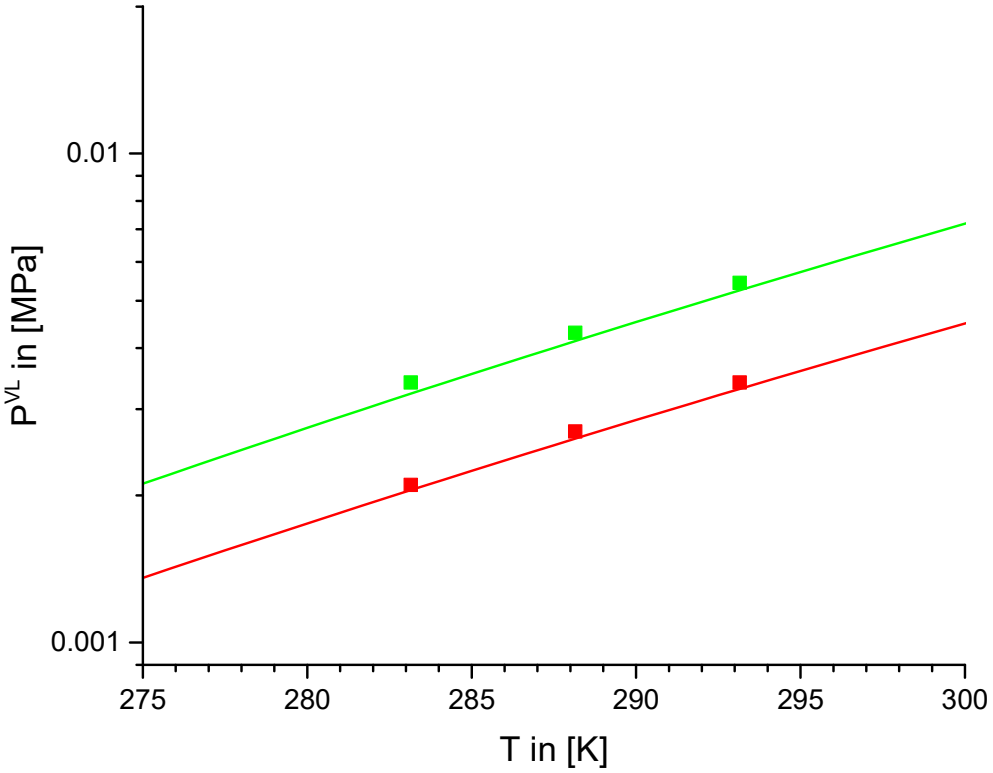

Figure 32: Vapor pressure of [BMIM][BF4] + methanol for two concentrations over temperature. The green lines and squares represent a IL-concentration of x_{IL}=0.7 and the red lines and squares represent a IL-concentration of x_{IL}=0.8, with the squares representing points measured by Revelli et al. [366] and the lines representing PC-SAFT calculations with the binary interaction parameters given in Table 9.

In Figure 33 the vapor pressure of the system [BMIM][BF4] + methanol is depicted over the ionic liquid concentration from x_{IL} = 0 to x_{IL} = 0.9. It can be seen, that while the vapor pressure can be calculated quite accurately in the area of high ionic liquid concentration, in the area of low ionic liquid concentrations the accuracy is lower. This is of course due to the fact that the fitting was done to the area of high IL-concentration. So the calculations in the area of low IL-concentrations are a prediction.

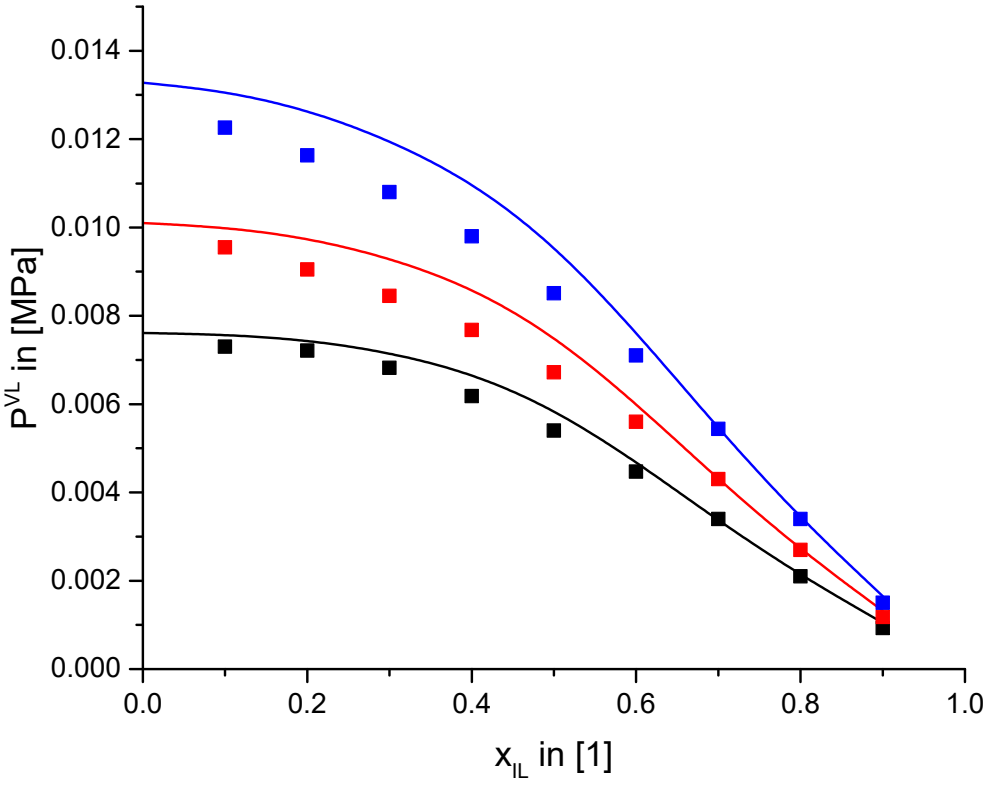

Figure 33: Vapor pressure of [BMIM][BF4] + methanol over composition. The black lines and black squares represent a temperature of T=283.15K, the red lines and red squares represent T=288.15K and the blue lines and blue squares represent T=293.15K. The squares are representing the points measured by Revelli et al. [366], the solid lines represent PC-SAFT calculations with the binary interaction parameters given in Table 9.

Because of the fact, that this good accuracy is only achieved with the use of binary interaction parameters, it is worth reminding, that the PC-SAFT parameters are only fitted to pure component data and a calculated VLE with only these parameters would be a complete prediction. With the good accuracy in the calculations of the vapor pressure in the ionic liquid concentrations range important for absorption chillers and the possibility of temperature extrapolation it is possible to reliably calculate the P,v,T-data of the VLE and of the absorption process. The results of these calculations are shown in Figure 34.

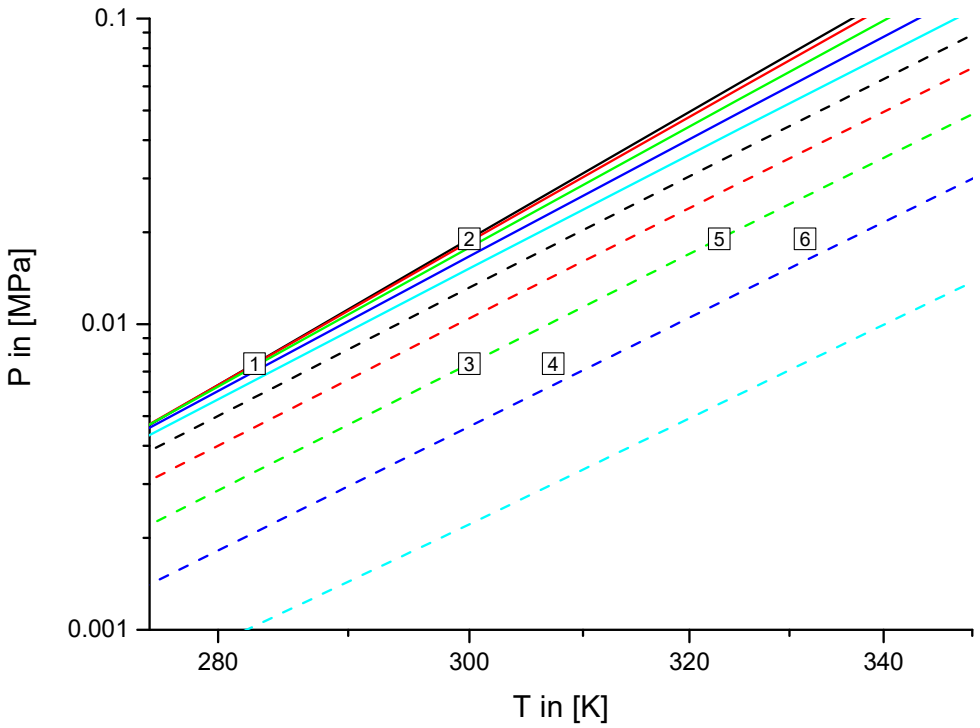

Figure 34: Absorption chilling process of [BMIM][BF4] + methanol, calculated with PC-SAFT, lines representing IL concentrations, solid black is x_{IL}=0, solid red is x_{IL}=0.1, solid green is x_{IL}=0.2, solid dark blue x_{IL}=0.3, solid light blue x_{IL}=0.4, dashed black x_{IL}=0.5, dashed red is x_{IL}=0.6, dashed green x_{IL}=0.7, dashed dark blue x_{IL}=0.8 and dashed light blue is x_{IL}=0.9. Squares with numbers represent the working points of absorption cycle with 1 being the evaporator, 2 being the condensor, 3 and 4 being the absorber and the 5 and 6 being the desorber.

The lines of constant ionic liquid concentrations are showing an interesting behavior. In the area of low ionic liquid concentrations the lines are getting close to each other for lower temperatures. An explanation for this behavior can be the presence of an LLE. This will be investigated later in this work (chapter 4.2.5). The absorption process under the defined boundaries show a temperature of T = 283 K inside of the evaporator.

Since [BMIM][BF4] is the only ionic liquid, for which experimental data for the VLE could be found [366], the calculations for the systems [OMIM][BF4], [BMIM][PF6], [HMIM][PF6], [BMMIM][PF6], [EMIM][OAc] + methanol are done as a prediction. The calculations for the systems containing [OMIM][BF4], [HMIM][PF6], [BMMIM][PF6] did show a P,v,T- behavior that was not compatible with an absorption process. Exemplary, the system [HMIM][PF6] + methanol is shown in Figure 35. It can be

seen, that for low ionic liquid concentrations, the vapor pressure is lowered but already the lines of constant concentration are getting close to each other for lower temperatures. This effect enhances with the rising of the ionic liquid concentrations to a point where the calculations suggest even a raise of the vapor pressure. This is obviously not the real behavior of the system and can be attributed to the fact, that no binary interaction parameters were available. Only the systems [EMIM][OAc] + methanol and [BMIM][PF6] + methanol were predicted to have a VLE that is compatible with an absorption process.

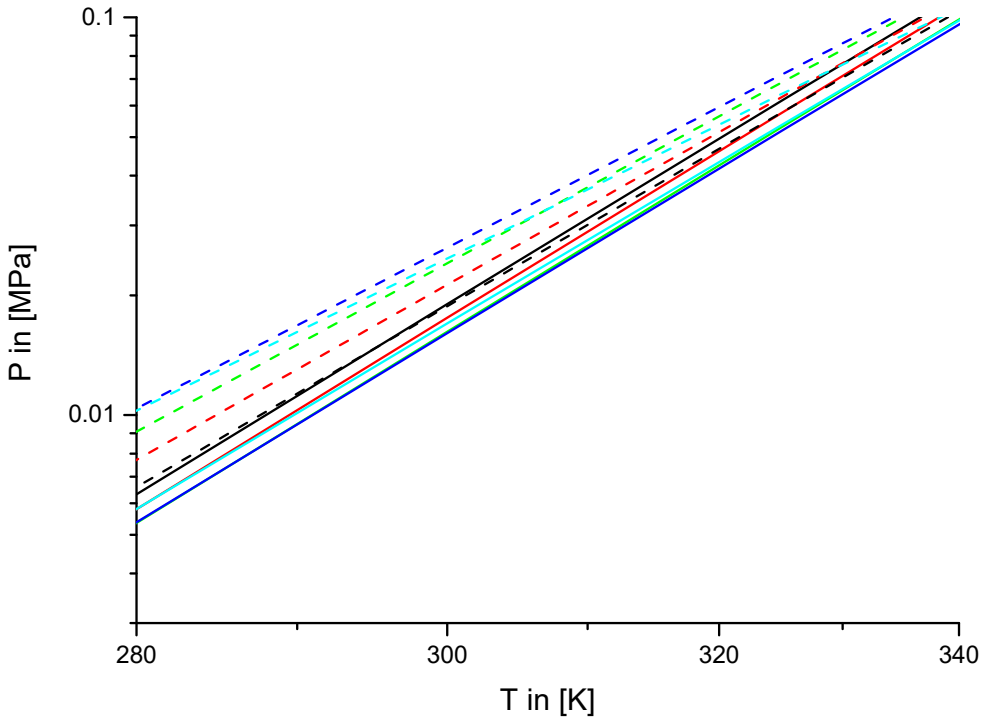

Figure 35: VLE of [HMIM][PF6] + methanol, calculated with PC-SAFT, lines representing IL concentrations, solid black is x_{IL}=0, solid red is x_{IL}=0.1, solid green is x_{IL}=0.2, solid dark blue x_{IL}=0.3, solid light blue x_{IL}=0.4, dashed black x_{IL}=0.5, dashed red is x_{IL}=0.6, dashed green x_{IL}=0.7, dashed dark blue x_{IL}=0.8 and dashed light blue is x_{IL}=0.9.

The calculated results for the system [EMIM][OAc] + methanol can be seen in Figure 36.

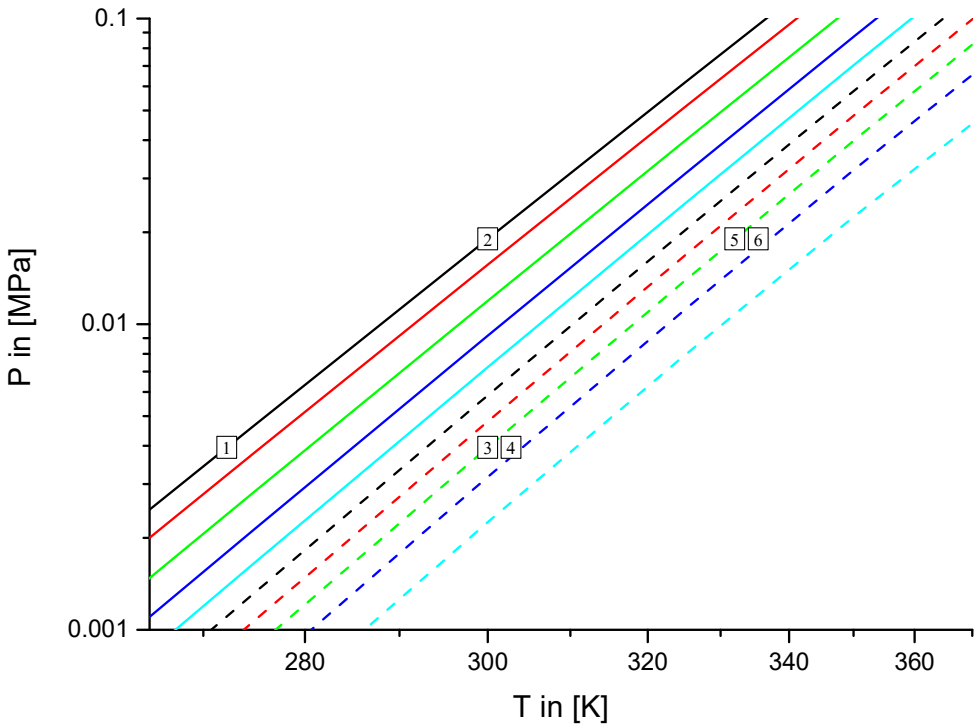

Figure 36: Absorption chilling process of [EMIM][OAc] + methanol, calculated with PC-SAFT, lines representing IL concentrations, solid black is x_{IL}=0, solid red is x_{IL}=0.1, solid green is x_{IL}=0.2, solid dark blue x_{IL}=0.3, solid light blue x_{IL}=0.4, dashed black x_{IL}=0.5, dashed red is x_{IL}=0.6, dashed green x_{IL}=0.7, dashed dark blue x_{IL}=0.8 and dashed light blue is x_{IL}=0.9. Squares with numbers represent the working points of absorption cycle with 1 being the evaporator, 2 being the condensor, 3 and 4 being the absorber and the 5 and 6 being the desorber.

Figure 36 shows a behavior with nearly parallel lines of constant concentration which is close to the desired behavior for an absorption cycle. For the absorption process, the calculated temperature inside of the evaporator is T = 272 K. The behavior of the system, with its nearly parallel lines of constant concentration is comparable to the system [BMIM][PF6] + methanol. The results for that system are pictured in Figure 37.

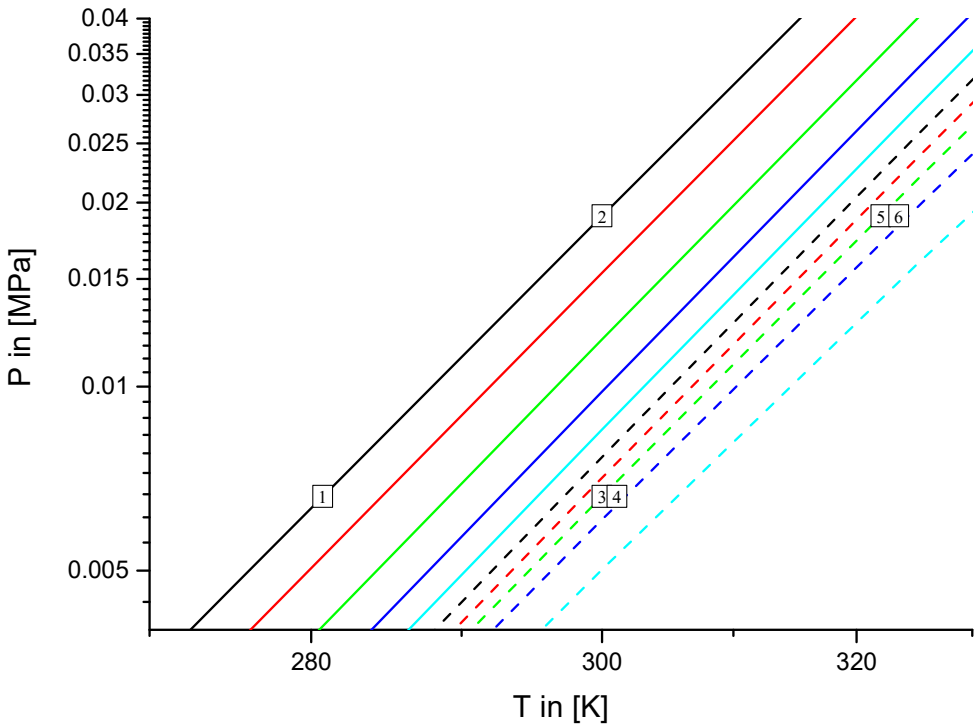

Figure 37: Absorption chilling process of [BMIM][PF6] + methanol, calculated with PC-SAFT, lines representing IL concentrations, solid black is x_{IL}=0, solid red is x_{IL}=0.1, solid green is x_{IL}=0.2, solid dark blue x_{IL}=0.3, solid light blue x_{IL}=0.4, dashed black x_{IL}=0.5, dashed red is x_{IL}=0.6, dashed green x_{IL}=0.7, dashed dark blue x_{IL}=0.8 and dashed light blue is x_{IL}=0.9. Squares with numbers represent the working points of absorption cycle with 1 being the evaporator, 2 being the condensor, 3 and 4 being the absorber and the 5 and 6 being the desorber.

In the Figure 37 it can be seen, that the VLE behavior of the system [BMIM][PF6] + methanol is again close to the desired behavior like for the [EMIM][OAc] + methanol depicted in Figure 36. The calculated evaporator temperature is T=281 K. The calculated evaporator temperature for the system containing [EMIM][OAc] is T=272 K, substantially lower than the calculated evaporator temperature of the system containing [BMIM][PF6]. This means, that for a cooling house with a desired cooling temperature of at least T=273.15 K, only the system containing [EMIM][OAc] seems to be able to maybe reach this temperature. According to the calculations, the evaporator only reaches a temperature difference of T=1 K, but one has to keep in mind, that the calculations are predictions from only pure component data without the use of adjusted binary interaction parameters. The actual cooling temperature may be lower than the estimation, but of course, it could also be higher. The absorption process of the [BMIM][BF4] + methanol shown in Figure 34 has a vaporizing

temperature similar to the [BMIM][PF6] system, but the comparability is debatable since only the system [BMIM][BF4] methanol system was calculated with binary interaction parameters. And the other 5 systems were calculated as prediction without binary interaction parameters.

4.2.4 VLE of ethanol + ionic liquid

For the system of [BMIM][BF4] + ethanol, experimental results for the VLE were found again in the works of Revelli et al. [366]. For the system containing ethanol they measured the vapor pressure for 4 temperatures T=283.15, 288.15, 293.15, 298.15 K over mole fractions from x_{IL}=0 to x_{IL}=0.9. Again the binary interaction parameters were fitted to the experimental results in composition range of x_{IL}=0.7-0.8 as it was done for the system [BMIM][BF4] + methanol. Just as the system with the methanol, the calculations were done with three binary interaction parameters (l_{ij}, $k_{ij}^{\text{dispersion}}$, $k_{ij}^{\text{association}}$) where the parameter to correct the combining rule for the temperature independent segment diameter (l_{ij}) was treated as constant with temperature and the two parameters to correct the combining rules for the depth of the square-well potential and the association energy ($k_{ij}^{\text{dispersion}}$ and $k_{ij}^{\text{association}}$ respectively) were treated as temperature dependent. The binary interaction parameters for the system [BMIM][BF4] + ethanol are given in Table 10.

Parameter	Value	Equation
l_{ij}	0.005	(24)
$k_{ij}^{\text{dispersion}}$	$-0.0013 \cdot T/\text{K} + 0.3994$	(25)
$k_{ij}^{\text{association}}$	$0.0021 \cdot T/\text{K} - 0.6764$	(27)

Table 10: Binary interaction parameters for [BMIM][BF4] + ethanol.

With the binary interaction parameters listed in Table 10, it was possible to reproduce the experimental results of Revelli et al. [366] with a satisfactory accuracy in the considered composition range. The results are shown in Figure 38.

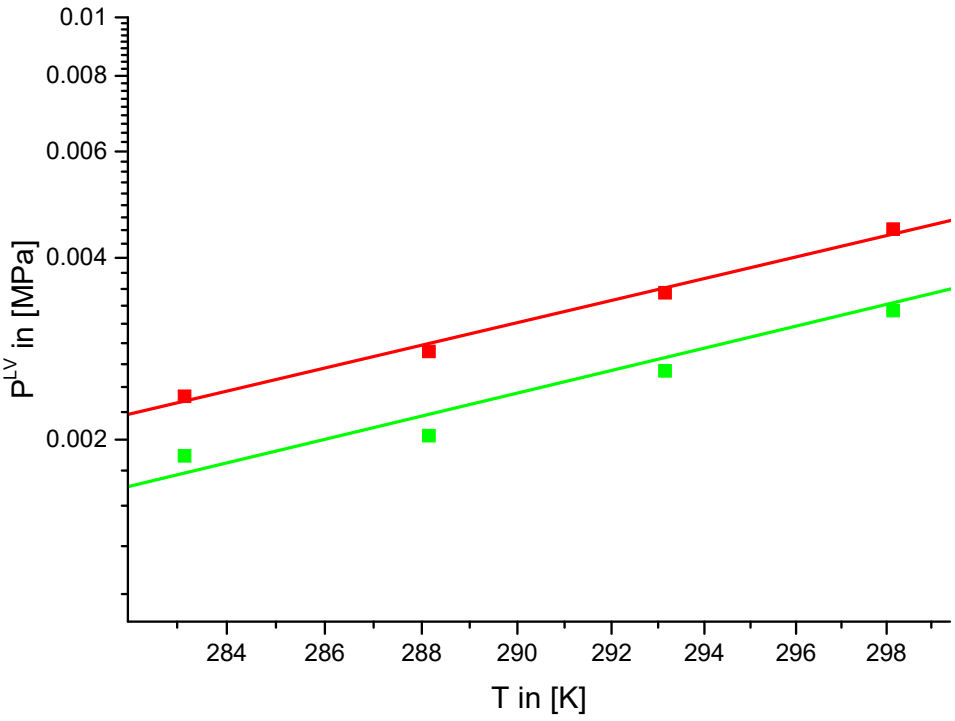

Figure 38: Vapor pressure of [BMIM][BF4] + ethanol for two concentrations over temperature. The red lines and red squares represent a IL-concentration of x_{IL}=0.7 and the green lines and green squares represent an IL-concentration of x_{IL}=0.8, with the squares representing the points measured by Revelli et al. [366] and the lines representing PC-SAFT calculations with the binary interaction parameters given in Table 10.

Although the parameters were fitted to results of only different compositions, they made it possible to calculate vapor pressures for the compositions from pure ethanol to 90% ionic liquids in mole fraction with a satisfactory accuracy as shown in Figure 39.

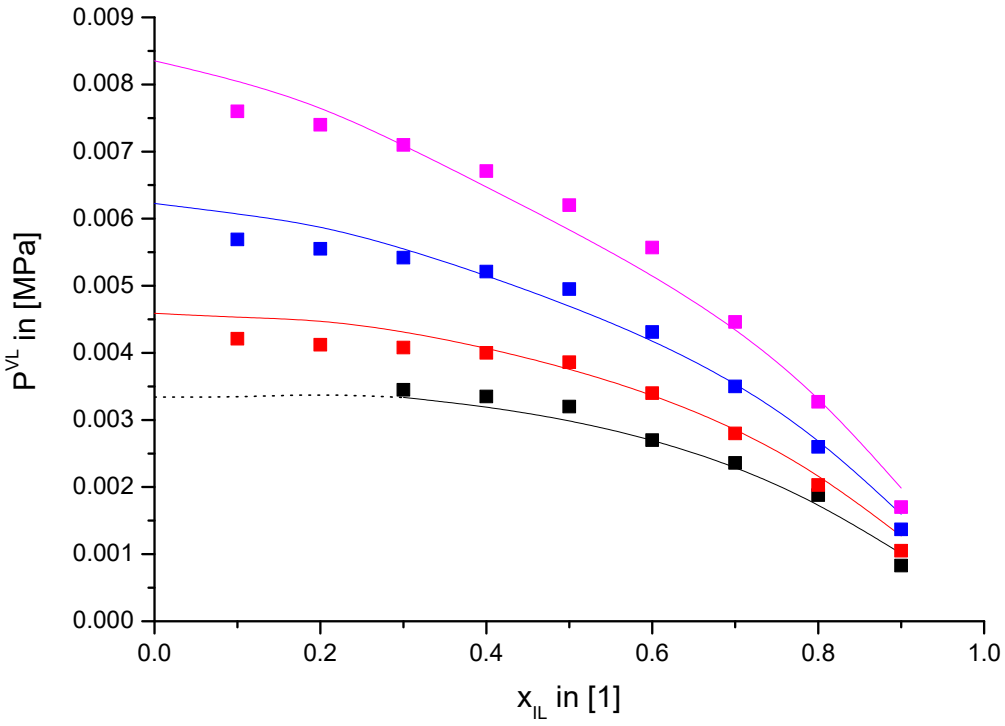

Figure 39: Vapor pressure of [BMIM][BF4] + ethanol over composition. The black lines and black squares represent a temperature of T=283.15 K, the red lines and red squares represent T=288.15 K, the blue lines and blue squares represent T=293.15 K and the pink lines and squares represent T=298.15 K. The squares are representing the points measured by Revelli et al. [366], the solid lines represent PC-SAFT calculations with the binary interaction parameters given in Table 10 and the dotted line represent calculations with the binary interaction parameters with a suspected LLE.

Figure 39 also shows another aspect of the system, especially the isothermal line for T = 283.15 K. The calculations are showing a slight raise in the vapor pressure. Revelli et al. [366] presumed that this was the area of a Liquid Liquid Equilibrium. Revelli et al. [366] fitted NRTL parameters to their experimental data sets and calculated the concentrations for the LLE at T = 283.15 K with the concentrations being x_{IL} = 0.1 and x_{IL} = 0.34. These calculations are in a good agreement with the calculations in this work, having identified the vapor pressure maximum in this concentration range as shown in Figure 39. The LLEs of these systems will be the subject of this work later (chapter 4.2.5).

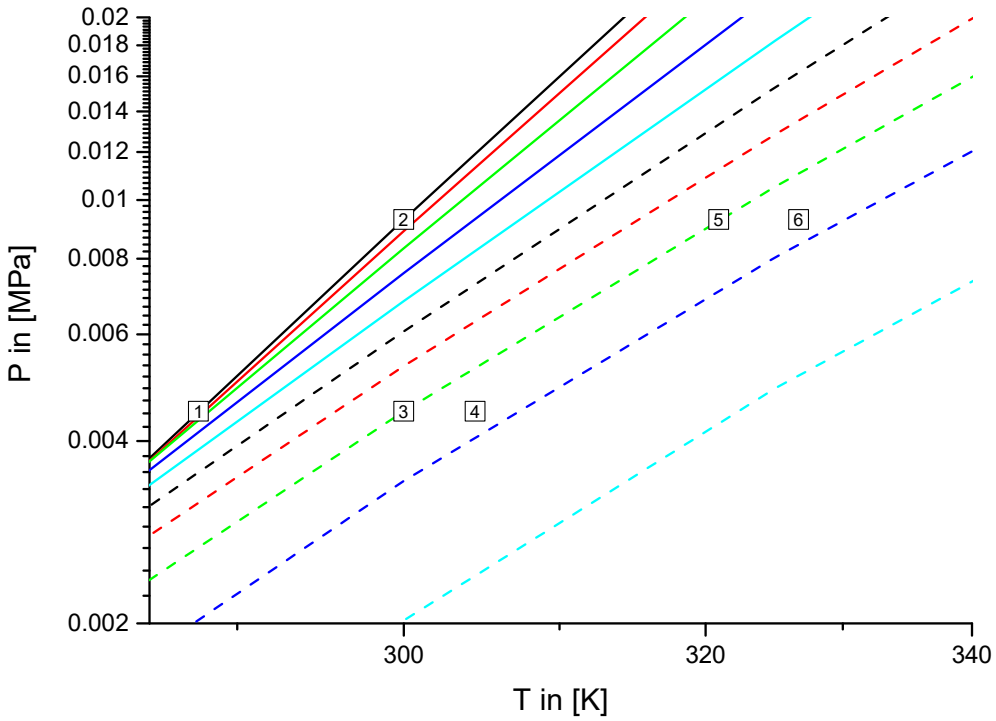

Figure 40: Absorption chilling process of [BMIM][BF4] + ethanol, calculated with PC-SAFT with interaction parameters given in Table 10, lines representing IL concentrations, solid black is x_{IL}=0, solid red is x_{IL}=0.1, solid green is x_{IL}=0.2, solid dark blue x_{IL}=0.3, solid light blue x_{IL}=0.4, dashed black x_{IL}=0.5, dashed red is x_{IL}=0.6, dashed green x_{IL}=0.7, dashed dark blue x_{IL}=0.8 and dashed light blue is x_{IL}=0.9. Squares with numbers represent the working points of absorption cycle with 1 being the evaporator, 2 being the condensor, 3 and 4 being the absorber and the 5 and 6 being the desorber.

The P,v,T-data of the working points for the process can be seen in Figure 40 together with the lines of constant concentrations for the vapor pressure for several concentrations. The lines of constant concentrations seem to come closer together for lower temperatures and low ionic liquid concentrations implying also the presence of a LLE. The temperature inside of the evaporator was calculated to be T = 288 K for this working pair.

Since the system [BMIM][BF4] + ethanol was the only system containing ethanol with available experimental P,v,T-data, the other systems had to be treated as predictions. For the systems containing ethanol, no VLEs like the one depicted in Figure 35 were calculated, making it possible to calculate the absorption cycles. This seems to imply, that ethanol might be a more suitable cooling agent, at least with the

ionic liquids considered in this work. The results for the system [OMIM][BF4] + ethanol can be seen in Figure 41.

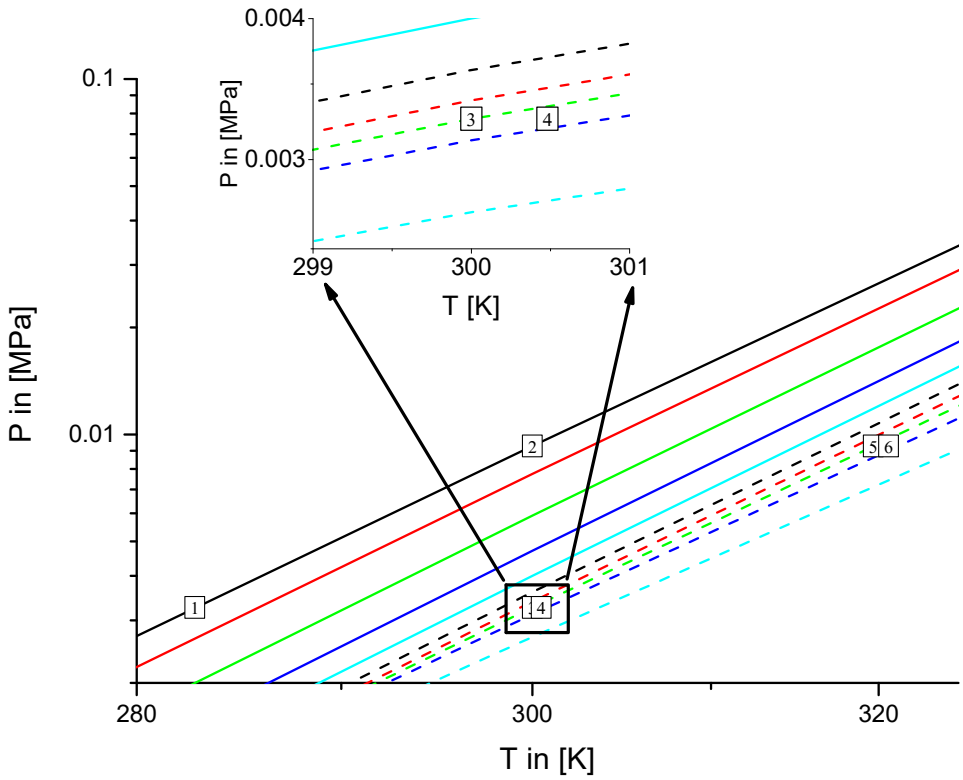

Figure 41: Absorption chilling process of [OMIM][BF4] + ethanol, calculated with PC-SAFT, lines representing IL concentrations, solid black is x_{IL}=0, solid red is x_{IL}=0.1, solid green is x_{IL}=0.2, solid dark blue x_{IL}=0.3, solid light blue x_{IL}=0.4, dashed black x_{IL}=0.5, dashed red is x_{IL}=0.6, dashed green x_{IL}=0.7, dashed dark blue x_{IL}=0.8 and dashed light blue is x_{IL}=0.9. Squares with numbers represent the working points of absorption cycle with 1 being the evaporator, 2 being the condensor, 3 and 4 being the absorber and the 5 and 6 being the desorber.

The ionic liquids in the system contain the same anion [BF4] and only differ in the length of the imidazolium terminal group (butyl and octyl). But a comparison between the two systems is difficult since only one of the systems was calculated with binary interaction parameters (Figure 40) while the other was treated as a prediction from only pure component parameters (Figure 41). But both systems are showing a behavior with the lines of constant concentration getting closer together at lower temperatures, for [BMIM][BF4] + ethanol (Figure 40) at the area of low ionic liquid concentration and for [OMIM][BF4] + ethanol (Figure 41) at the area of high ionic liquid concentration but with slightly higher temperatures. This could indicate that the concentration may be more important for the forming of a LLE. For both systems, an

indication for demixing behavior could be found by analyzing the calculated VLE data. The calculated evaporator temperature for the [OMIM][BF4] system is T=283 K, which is comparable to the system containing [BMIM][BF4] where the calculated evaporator temperature was T=288 K.

The results for the system containing [HMIM][PF6], can be seen at Figure 42.

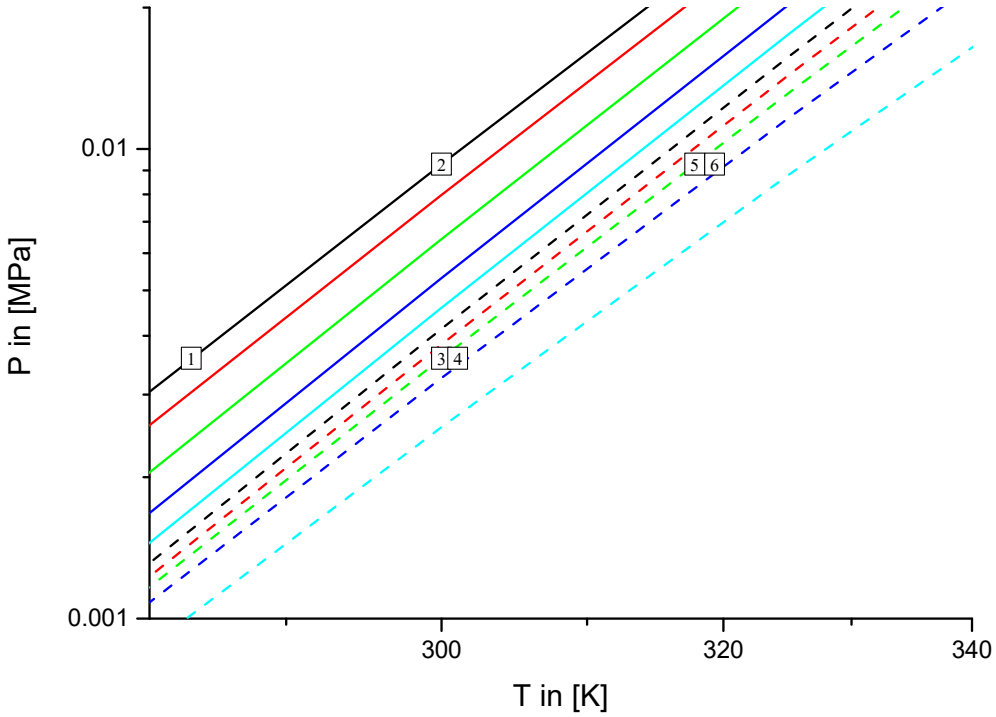

Figure 42: Absorption chilling process of [HMIM][PF6] + ethanol, calculated with PC-SAFT, lines representing IL concentrations, solid black is x_{IL}=0, solid red is x_{IL}=0.1, solid green is x_{IL}=0.2, solid dark blue x_{IL}=0.3, solid light blue x_{IL}=0.4, dashed black x_{IL}=0.5, dashed red is x_{IL}=0.6, dashed green x_{IL}=0.7, dashed dark blue x_{IL}=0.8 and dashed light blue is x_{IL}=0.9. Squares with numbers represent the working points of absorption cycle with 1 being the evaporator, 2 being the condensor, 3 and 4 being the absorber and the 5 and 6 being the desorber.

The system containing [HMIM][PF6] in Figure 42 is again showing the behavior of lines of constant concentration coming together at low temperatures and high ionic liquid concentrations. This behavior is similar to the system [OMIM][BF4] in Figure 41. The calculated evaporator temperature for the [HMIM][PF6] system is T = 284 K, again comparable to the two already examined systems.

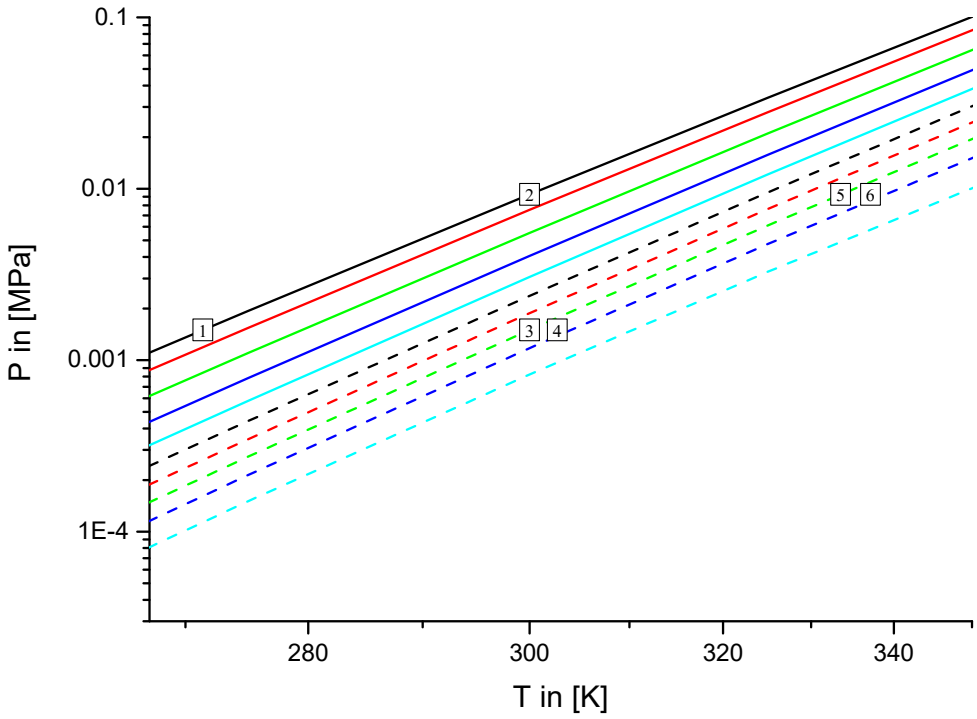

Figure 43: Absorption chilling process of [BMIM][PF6] + ethanol, calculated with PC-SAFT, lines representing IL concentrations, solid black is x_{IL}=0, solid red is x_{IL}=0.1, solid green is x_{IL}=0.2, solid dark blue x_{IL}=0.3, solid light blue x_{IL}=0.4, dashed black x_{IL}=0.5, dashed red is x_{IL}=0.6, dashed green x_{IL}=0.7, dashed dark blue x_{IL}=0.8 and dashed light blue is x_{IL}=0.9. Squares with numbers represent the working points of absorption cycle with 1 being the evaporator, 2 being the condensor, 3 and 4 being the absorber and the 5 and 6 being the desorber.

The system containing [BMIM][PF6] + ethanol displayed in Figure 43 shows a behavior a little different from the previous. All lines of constant concentration are nearly parallel and the system shows no sign of a possible LLE. Also the calculated evaporator temperature for this system is T=271 K, making it able to cool to much lower temperatures and therefore possibly to be a superior cooling agent to the three systems already examined.

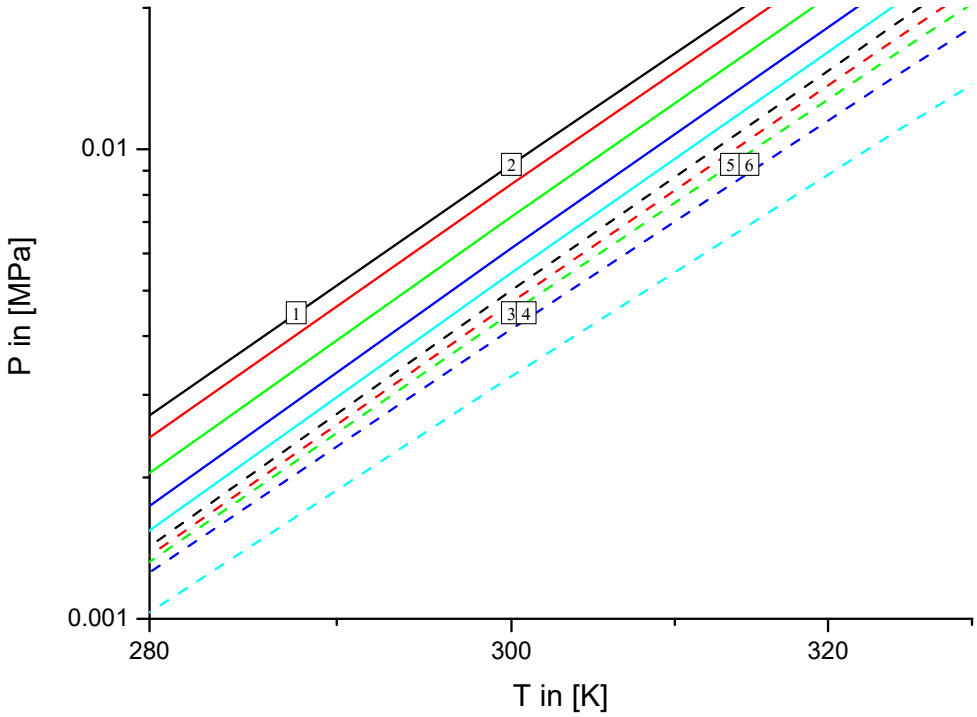

Figure 44: Absorption chilling process of [BMMIM][PF6] + ethanol, calculated with PC-SAFT, lines representing IL concentrations, solid black is x_{IL}=0, solid red is x_{IL}=0.1, solid green is x_{IL}=0.2, solid dark blue x_{IL}=0.3, solid light blue x_{IL}=0.4, dashed black x_{IL}=0.5, dashed red is x_{IL}=0.6, dashed green x_{IL}=0.7, dashed dark blue x_{IL}=0.8 and dashed light blue is x_{IL}=0.9. Squares with numbers represent the working points of absorption cycle with 1 being the evaporator, 2 being the condensor, 3 and 4 being the absorber and the 5 and 6 being the desorber.

The system containing [BMMIM][PF6] + ethanol in Figure 44 again shows lines of constant concentrations that are coming together at lower temperatures and high ionic liquid concentrations. The calculated temperature inside of the evaporator is T=288K, making it comparable to the three first evaluated systems, but higher than the [BMIM][PF6] system with a calculated evaporator temperature of T=271 K. Three systems containing ionic liquids with matching anions were predicted with the systems being [HMIM][PF6] + ethanol, [BMIM][PF6] + ethanol and [BMMIM][PF6] + ethanol varying in the number and length of the alkane terminal group of the cation. The systems containing [HMIM][PF6] and [BMMIM][PF6] did show indications of a possible LLE. Only the system containing [BMIM][PF6] did show a behavior, that was close to the desired one for an absorption cycle.

The last considered system is [EMIM][OAc] + ethanol. The predicted VLE with the working points can be found in Figure 45.

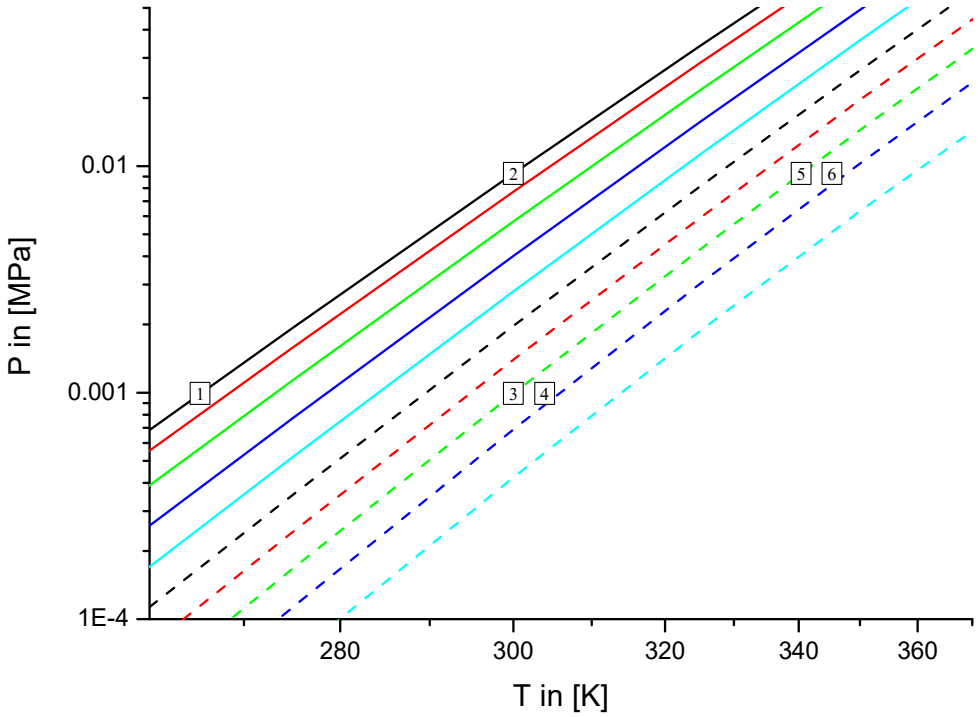

Figure 45: Absorption chilling process of [EMIM][OAc] + ethanol, calculated with PC-SAFT, lines representing IL concentrations, solid black is x_{IL}=0, solid red is x_{IL}=0.1, solid green is x_{IL}=0.2, solid dark blue x_{IL}=0.3, solid light blue x_{IL}=0.4, dashed black x_{IL}=0.5, dashed red is x_{IL}=0.6, dashed green x_{IL}=0.7, dashed dark blue x_{IL}=0.8 and dashed light blue is x_{IL}=0.9. Squares with numbers represent the working points of absorption cycle with 1 being the evaporator, 2 being the condensor, 3 and 4 being the absorber and the 5 and 6 being the desorber.

The system shows nearly parallel lines of constant concentration with no hints of a LLE. Predicted VLEs like seen here are a good hint, that the working pair of [EMIM][OAc] could be a promising candidate for an absorption chilling process. Also the temperature inside of the evaporator is the lowest of all considered systems with T=266 K.

4.2.5 Demixing behavior of alcohol + ionic liquid

The presence of a LLE in a system can be a knock out criterion for a working pair, if the LLE is inside of the temperature and concentration area that is used in the

absorption cycle. And since absorption cycles usually work in a very wide concentration range from pure cooling agent in the condenser and evaporator to very low concentrations of the cooling agent inside the absorber and desorber, this range will certainly overlap with an existing LLE nearly every time. Therefore information about the presence of LLE for the considered working pair is highly desirable. Some VLEs that were examined earlier showed lines of constant concentration that were coming together for lower temperatures which was identified as a sign of a possible LLE (Figure 34, Figure 40, Figure 41, Figure 42, Figure 44). To further investigate this, the LLEs were calculated with the PC-SAFT-EOS and the pure component parameters adjusted to the liquid densities and, if available, with binary interaction parameters. For the systems containing methanol, only the working pair with [BMIM][BF4] did show signs of a possible LLE. The results of the calculations can be seen in Figure 46.

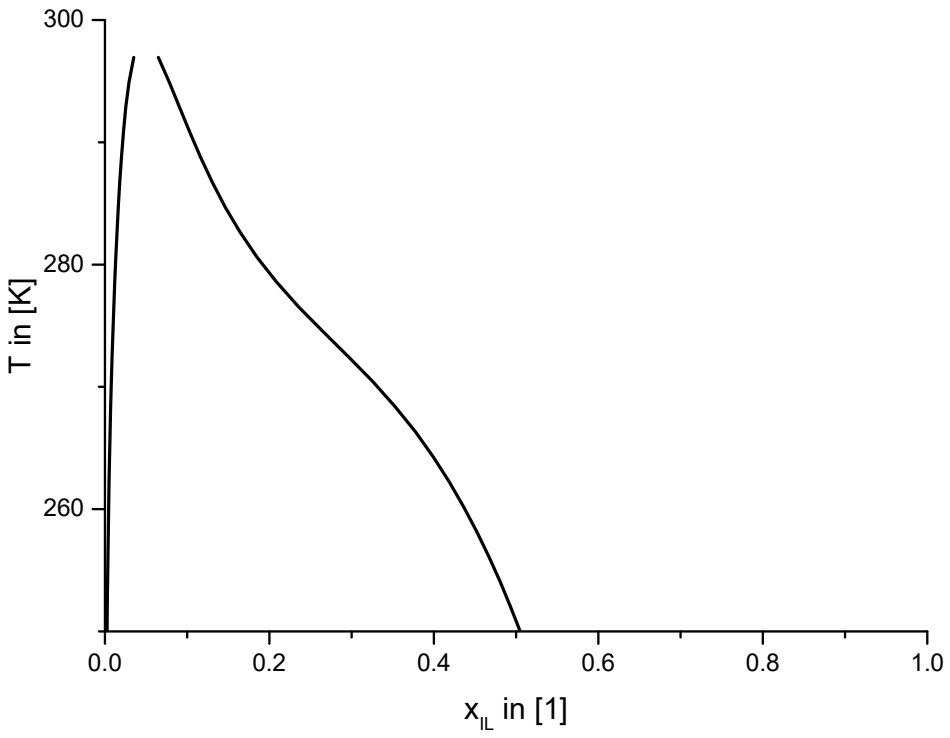

Figure 46: LLE of [BMIM][BF4] + methanol at P= 1 bar, the black lines represent PC-SAFT calculations with the binary interaction parameters given in Table 9.

It can be seen, that the calculated LLE is in the range of the possible LLE by the VLE calculations (Figure 40), at lower temperatures and low ionic liquid concentrations.

The critical point for the LLE seems to be close under T=300 K which is substantially higher than the calculated temperature inside of the evaporator which was T=288 K. The calculations seem to heavily imply, that the working pair of [BMIM][BF4] + methanol might not be suitable for the use inside of an absorption cooling cycle.

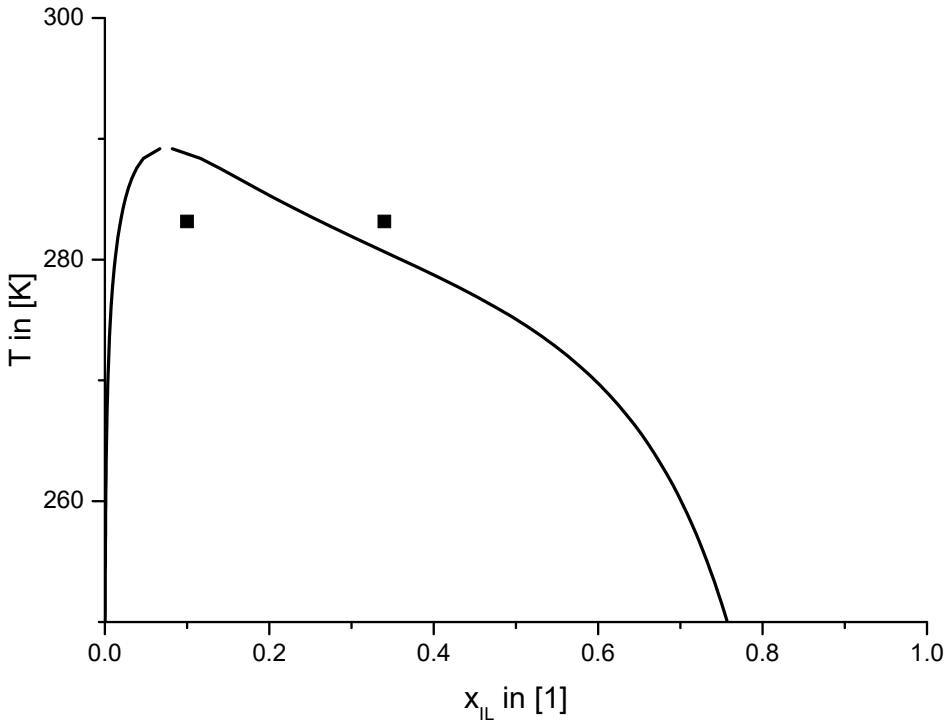

Figure 47: LLE of [BMIM][BF4] + ethanol at P=1bar, the black squares represent LLE calculations at T=283.15K from Revelli et al. [366] and the lines represent PC-SAFT calculations with the binary interaction parameters given in Table 10.

The calculated LLE of the system [BMIM][BF4] + ethanol is shown in Figure 47 together with the calculations of the LLE at T=283.15 K by Revelli et al. [366]. It can be seen, that the calculations in this work are in a qualitative agreement with the calculations of Revelli et al. [366]. Since both calculations are done as a prediction from the experimental VLE data, done with PC-SAFT in this work and NRTL in the case of Revelli et al. [366], the agreement of both predictions gives confidence in the calculations. It can be seen, that the critical point is predicted at roughly T=290K. The calculations of the absorption process did yield an evaporator temperature of T=288K. So if an absorption chiller with the working pair [BMIM][BF4] + ethanol is considered, further investigation about the actual temperature of the critical point

needs to be done, since it seems to be in a range that might compromise the whole process.

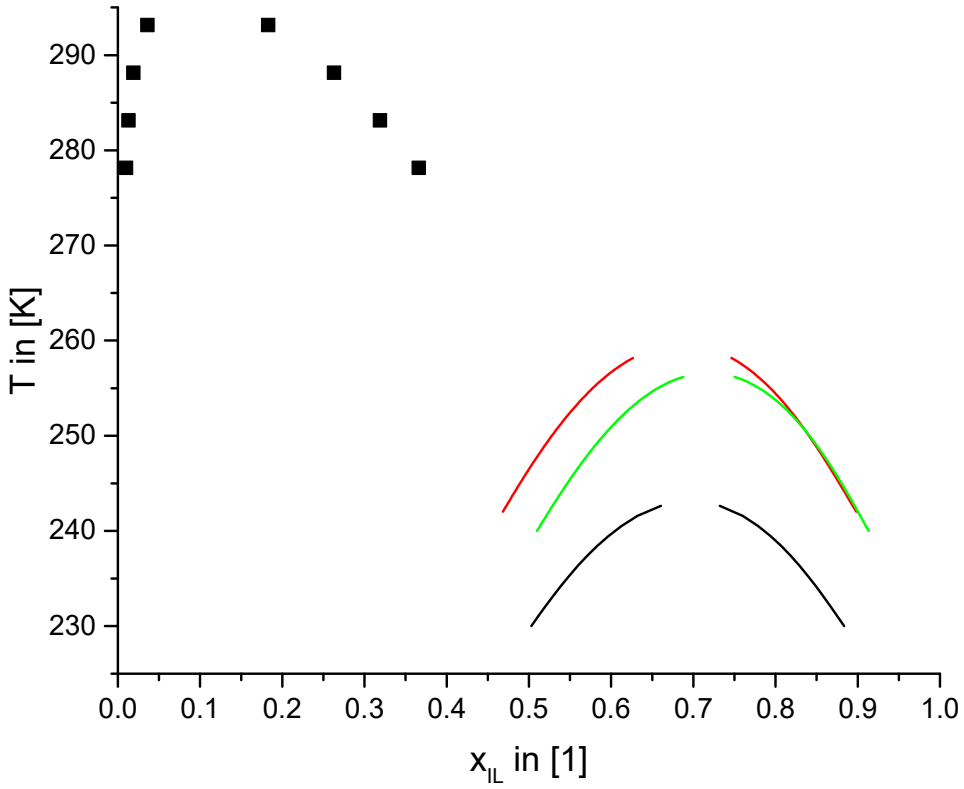

Figure 48: LLE of [HMIM][PF6], [BMMIM][PF6],[OMIM][BF4] + ethanol at P=1 bar, the black squares represent experimental LLE data of the system [HMIM][PF6] + ethanol of Pereiro and Rodriguez [295] and the lines represent PC-SAFT calculations for the system [HMIM][PF6] + ethanol, solid red line represents PC-SAFT-calculations for the system [BMMIM][PF6] + ethanol and solid green lines represent PC-SAFT calculations for the system [OMIM][BF4] + ethanol.

The calculated VLE of the system [HMIM][PF6] + ethanol (Figure 42) also implied the presence of a LLE. Pereiro and Rodriguez [295] also reported the presence of a LLE and did experimental evaluations on the composition at equilibrium. The experimental results of Pereiro and Rodriguez as well as the PC-SAFT calculations done in this work can be seen in Figure 48. It can be seen, that the predicted LLE does not fully agree with the experimental data. While the presence and the upper critical solution temperature (UCST) behavior is predicted correctly, the range of the concentration and the critical temperature do have large variations due to the fact, that the calculations were done without binary interaction parameters. The experiments show the miscibility gap at lower ionic liquid concentration and with a critical temperature of

around T=300 K while the calculations predicted it to be at high IL concentrations with a critical temperature around T=240 K. But it is worth reminding, that the LLE is a complete prediction from parameters fitted to pure components, in the case of the ionic liquids, these are merely the liquid densities.

For the systems [BMMIM][PF6] + ethanol and [OMIM][BF4] + ethanol, both depicted in Figure 48, both calculated VLEs (Figure 44, Figure 41) show a behavior that highly indicates the presence of LLEs. Again as with [HMIM][PF6] + ethanol (Figure 48) a LLE in the area of high IL concentration is predicted. The critical temperatures of both systems seem to be roughly between T=255K and T=260K. So if these two systems are considered as a working pair for the absorption cycle, further investigation of the nature of the miscibility gap needs to be done in order to secure the functionality of this pair. In the case of the system [BMIM][PF6] + ethanol, Sahandzhieva et al. [367] did observe and measure a LLE. The calculations with PC-SAFT however predict a fully miscible system, but it is vital to recall, that these calculations were done without binary interaction parameters.

4.3 Performance characterization and efficiency

The calculated coefficients of performance and minimal temperatures in the evaporator of the systems containing ethanol are listed in Table 11. It can be seen, that the COPs are of typical absorption chiller range, spanning a range from COP=0.67 to COP=0.92. This is in accordance to simulations done by Seiler et al. [368]. They used a model with similar simplifications and calculated a COP for the system of IL + methanol of COP=0.87. It is also apparent, that the minimal temperatures are not significantly lower than the lowest possible cooling temperatures of conventional water + lithium-bromide machines which provides evaporator temperatures around T = 2-12°C [369]. Only the system [EMIM][OAc] + ethanol could possibly truly improve the achievable lowest cooling temperatures. [BMIM][BF4] excluded, the systems were all calculated without the use of binary interaction parameters. So the results of these systems have to be seen more as a rough estimation than a correct calculation. But it already shows, that the absorption chillers containing the investigated ionic liquids do not promise a great improvement in the minimal cooling temperatures. A closer look at the results also suggests that lower minimal temperatures are also linked to lower COPs.

Ionic Liquid	T_{min} in [K]	COP
[EMIM][OAc] + ethanol	266	0.67
[BMIM][BF4] + ethanol	288	0.92
[OMIM][BF4] + ethanol	283	0.89
[BMIM][PF6] + ethanol	271	0.71
[BMMIM][PF6] + ethanol	288	0.90
[HMIM][PF6] + ethanol	284	0.86
[EMIM][OAc] + methanol	272	0.74
[BMIM][BF4] + methanol	283	0.64
[OMIM][BF4] + methanol	LLE	LLE
[BMIM][PF6] + methanol	281	0.86
[BMMIM][PF6] + methanol	LLE	LLE
[HMIM][PF6] + methanol	LLE	LLE

Table 11: Minimum cooling temperatures and COPs of chillers with ethanol and methanol, [BMIM][BF4] is highlighted, because it was calculated with binary interaction parameters for both systems containing methanol and ethanol.

The minimal temperatures and COPs for the systems containing methanol can be seen in Table 11, too. Because only three systems showed a behavior where an absorption process is even possible, it is hardly feasible to draw conclusions or make definitive statements. What can be said is that the correlation of lower minimal temperature and lower COP seems to be intact as well. Also the minimal temperature seems to rise with the vapor pressure of the cooling agent, which of course is to be expected.

Of the 6 ionic liquids mixed with ethanol, where the calculations suggest a behavior that enables an absorption process, only 3 are showing a behavior that is compatible with an absorption chilling process when containing methanol. So the calculations highly imply possible problems when working pairs consist of the examined ILs and methanol.

Considering all the systems reviewed in this work, it seems like ethanol is the superior cooling agent over methanol when paired with ionic liquids. The temperature inside of the evaporator, which is important for the lowest temperature reachable with a cooling process, is slightly lower for the systems containing [EMIM][OAc] but also slightly higher for the systems containing [BMIM][PF6] and [BMIM][BF4]. And of course a real absorption cooling machine would always be preferred to be used with ethanol as a cooling agent since the toxicity of methanol is substantially higher.

4.4 Influence of mixing behavior on cooling performance

Since the ultimate goal of an absorption chiller is to work with maximum efficiency to the lowest cooling temperature possible, the COPs and evaporator temperatures of the absorption cycles with the different working pairs are of utmost importance and since not every working pair comes with enough experimental results to fit the binary interaction parameters, the influence of these parameters on the COPs should be investigated. Because the previous calculations suggested a connection of the COP to the minimal cooling temperature, it will also be discussed in these examinations. To determine the influence of the binary interaction parameters a damping factor D was impinged on the individual parameters in the equations (24), (25), and (27).

$$\varepsilon_{ij}^{AB} = \frac{\varepsilon_{ii}^{AB} + \varepsilon_{jj}^{AB}}{2} \cdot \left(1 - k_{ij}^{\text{association}} \cdot D_{\text{k,Ass}}\right) \quad \textbf{(52)}$$

$$\varepsilon_{ij} = \sqrt{\varepsilon_{ii} \cdot \varepsilon_{jj}} \cdot \left(1 - k_{ij}^{\text{dispersion}} \cdot D_{\text{k,Disp}}\right) \quad \textbf{(53)}$$

$$\sigma_{ij} = \frac{\sigma_{ii} + \sigma_{jj}}{2} \left(1 - l_{ij} \cdot D_{\text{l}}\right) \quad \textbf{(54)}$$

This damping factor *D* is extending from $D_X = 0$ (no binary interaction parameter) over $D_X = 1$ (binary interaction parameters as fitted) to $D_X = 2$ (double binary interaction parameter as fitted) to account for the possibilities an over- or underestimation of the parameters. With this set-up it is possible to observe the influence of the binary interaction parameters correcting the combining rules for the association energy and the dispersion energy, while keeping the temperature dependence working. To distinguish the influence of the individual parameters as well as the influence of combinations, the damping factor has been applied to each of the individual parameters as well as the combination of the temperature dependent energy interaction parameters while keeping the parameter for the correction of the depth of the square well potential combining rule untouched and to all interaction parameters combined. All calculations were done for the system [BMIM][BF4] + ethanol since it was the only system where binary interaction parameters could be fitted to the experimental results of Revelli et al. [366] and where the LLE does not seem to hinder the use in an absorption cycle. The results for the influence of the binary interaction parameter on the dispersion energy can be seen in Figure 49.

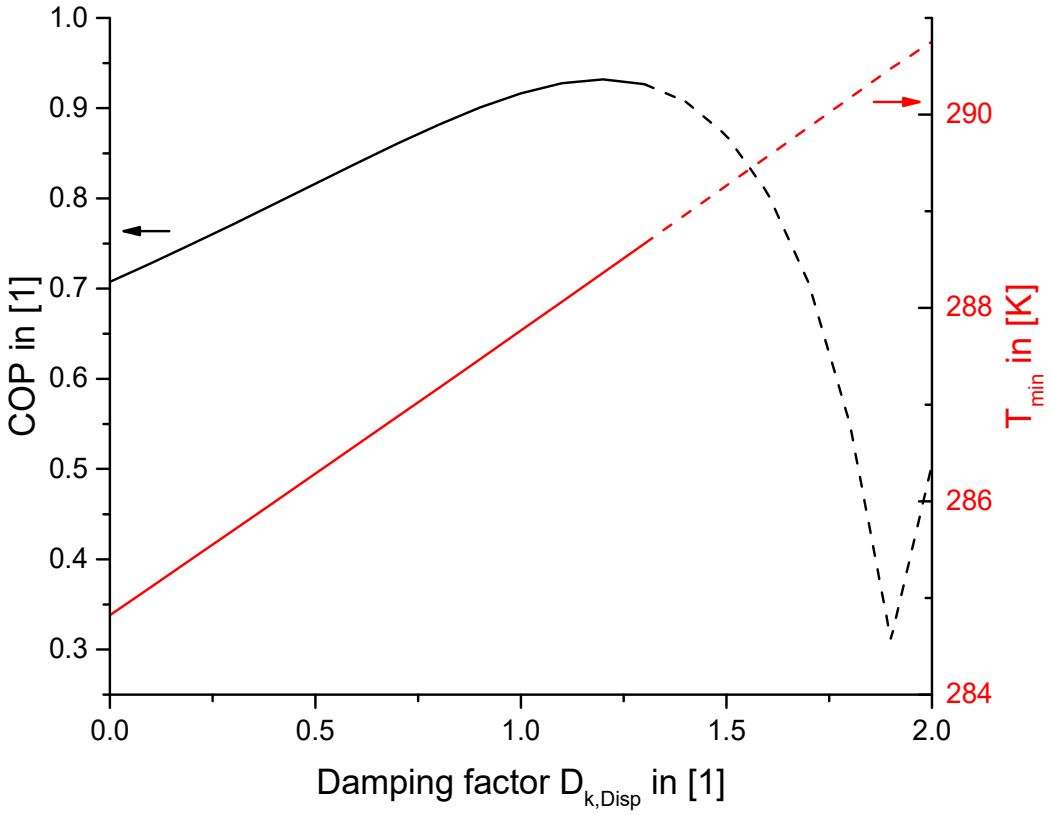

Figure 49: Influence of the binary energy interaction parameter $k_{ij}^{\text{dispersion}}$ on the COP and the minimal cooling temperature. Solid black lines represent the COP, dashed black lines the COP in a possible LLE area, solid red lines represent the minimal cooling temperature and the dashed red lines the minimal cooling temperature in the area of a possible LLE.

In Figure 49 we can see, that the COP is positively influenced by the binary interaction parameters, meaning that without the possibility of fitting the parameters, the performance of the absorption cycle would be underestimated. The difference between no binary interaction parameter and the binary interaction parameter as fitted in this work for the COP is $\Delta\text{COP} \approx 0.2$. This makes a huge difference in the energy efficiency of the process. The strong connection between the dispersion energy of the mixture and the COP could be the subject of further investigation, perhaps leading to a method of estimating performance qualities of a working pair based on the interaction energies. Another influence of the parameter is the possible presence of a LLE. The possibility for the LLE was positively influenced with an increasing interaction parameter up to the extended where the LLE would definitely make an absorption process impossible, indicated by dashed lines in Figure 49. The

Figure 49 also shows the connection of the temperature in the evaporator with the COP. An increase in the COP is always connected to an increase in the evaporator temperature, making the process more energy efficient but also decreasing the ability to cool to lower temperatures. This connection is only showing for absorption processes without a present LLE. The influence of the interaction parameter for the association energy can be seen in Figure 50.

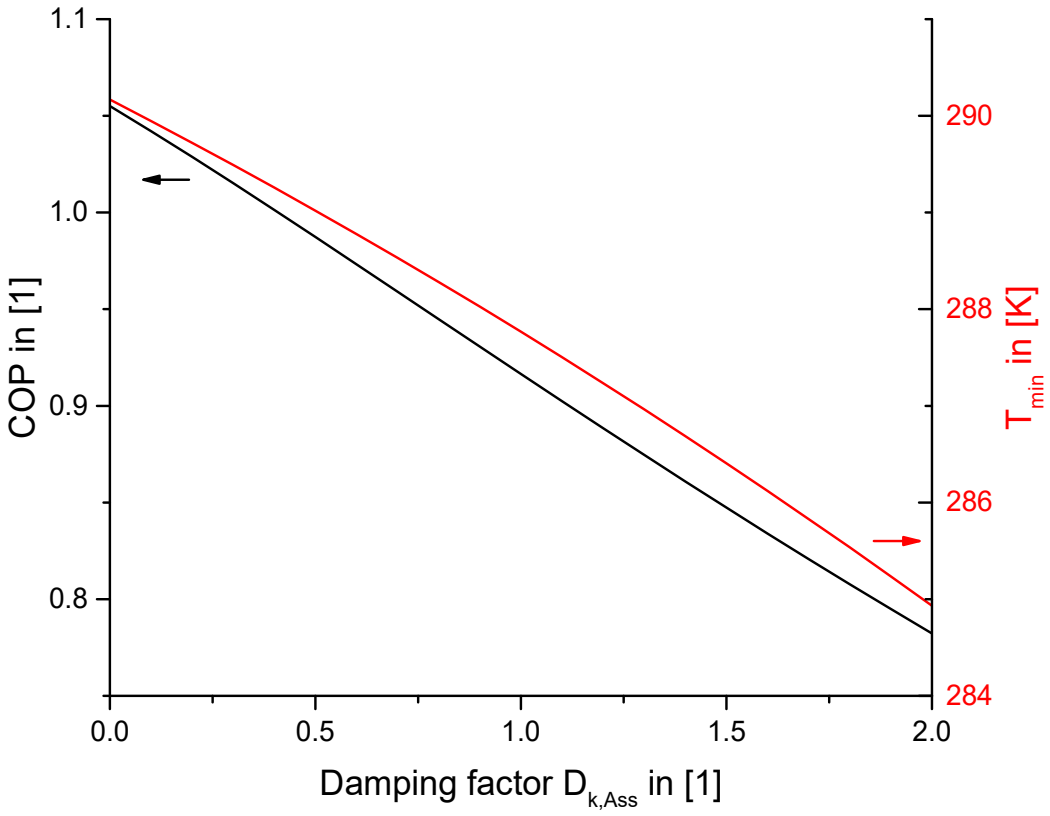

Figure 50: Influence of the binary energy interaction parameter $k_{ij}^{\text{association}}$ on the COP and the minimal cooling temperature. Solid black lines represent the COP, solid red lines represent the minimal cooling temperature.

The Figure 50 shows, that the COP is negatively influenced by the parameter for association energy. Since the variation of this parameter did not influence the possibility for a LLE, the calculations yielded exploitable results for the whole range of the damping factor D. It shows that the difference in the COP for no binary interaction parameter and the fitted parameter is already $\Delta\text{COP} \approx 0.2$ and even higher if the parameter in this work was underestimated. This again makes a huge difference for

the efficiency. Also the evaporator temperature is lowered with the decreasing COP, being around $\Delta T \approx 3\mathrm{K}$ lower for the parameter as used in this work than with no binary interaction parameter. And since the parameter for the dispersion energy seems to positively influence the COP and the parameter for the association energy seems to have a negative influence, it is vital to look at the influence of the combination of both parameters. The results for the influence of the combination of both parameters can be seen in Figure 51.

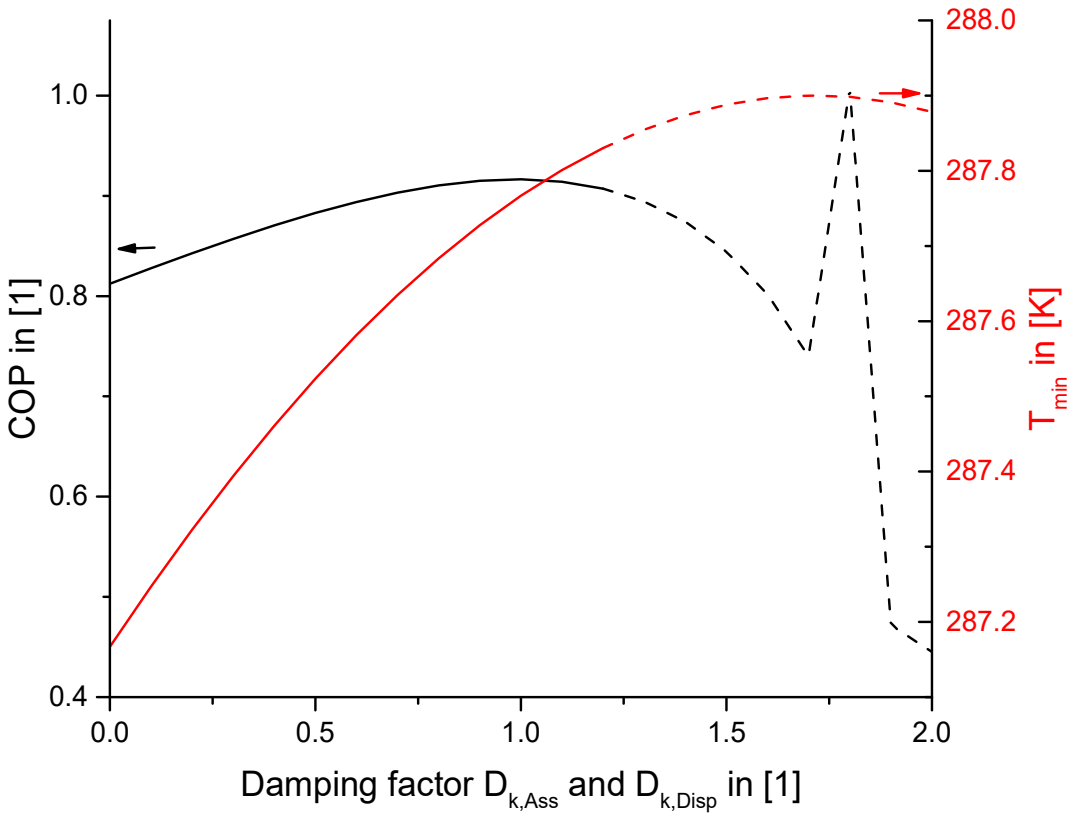

Figure 51: Influence of the binary energy interaction parameters $k_{ij}^{\mathrm{Dispersion}}$ and $k_{ij}^{\mathrm{Association}}$ together on the COP and the minimal cooling temperature. Solid black lines represent the COP, dashed black lines the COP in a possible LLE area, solid red lines represent the minimal cooling temperature and the dashed red lines the minimal cooling temperature in the area of a possible LLE area.

Figure 51 shows, that the combination of the binary interaction parameters correcting the mixing rule for the dispersion and association energy has a positive influence on the COP. It seems as if the influence of the dispersion energy parameter is bigger, but its effect is lightly extenuated by the association energy parameter. The difference of the COP between no binary energy interaction parameters and the

parameters as fitted in this work is $\Delta COP \approx 0.1$. Again, the difference can be even higher if the parameters have been underestimated in this work. But an underestimation would also mean a higher chance for a LLE in the system. Since the range of the possible LLE is the same in Figure 49 as in Figure 51, it can be concluded, that the influence of the binary interaction parameter for the association energy is small and therefore the influence of the association energy is small. A possible explanation for low association energies and therefore the low influence could be that the ions of the liquid tend to form ion pairs. The results for the influence of the interaction parameter correcting the combining rules on the depth of the square well potential can be seen in Figure 52.

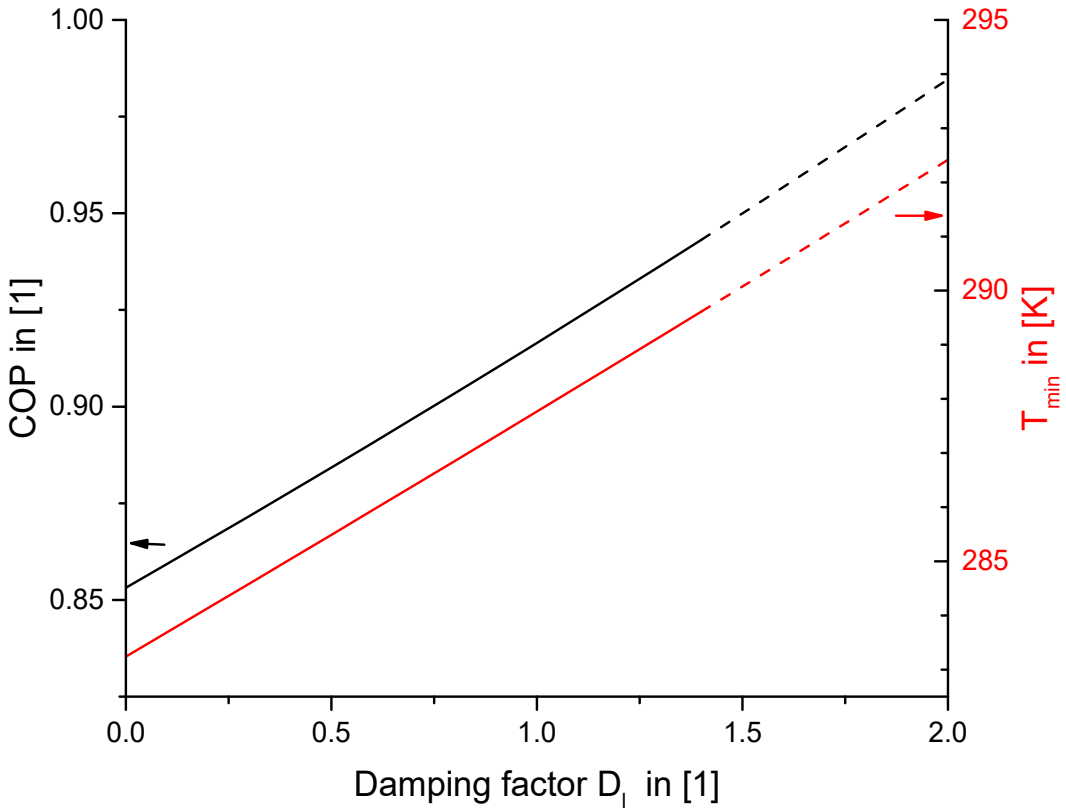

Figure 52: Influence of the binary segment interaction parameters l_{ij} on the COP and the minimal cooling temperature. Solid black lines represent the COP, dashed black lines the COP in a possible LLE area, solid red lines represent the minimal cooling temperature and the dashed red lines the minimal cooling temperature in the area of a possible LLE area.

Again, we see a positive influence on the COP and on the cooling temperature. The COP is raised by nearly $\Delta COP \approx 0.05$ and the minimal cooling temperature is raised

by nearly $\Delta T \approx 4\mathrm{K}$ between the interaction parameter fitted in this work and no binary interaction parameter for the square well potential. This shows, that the influence of every individual binary interaction parameter is not negligible. The results of the influence of all binary interaction parameters combined can be seen in Figure 53.

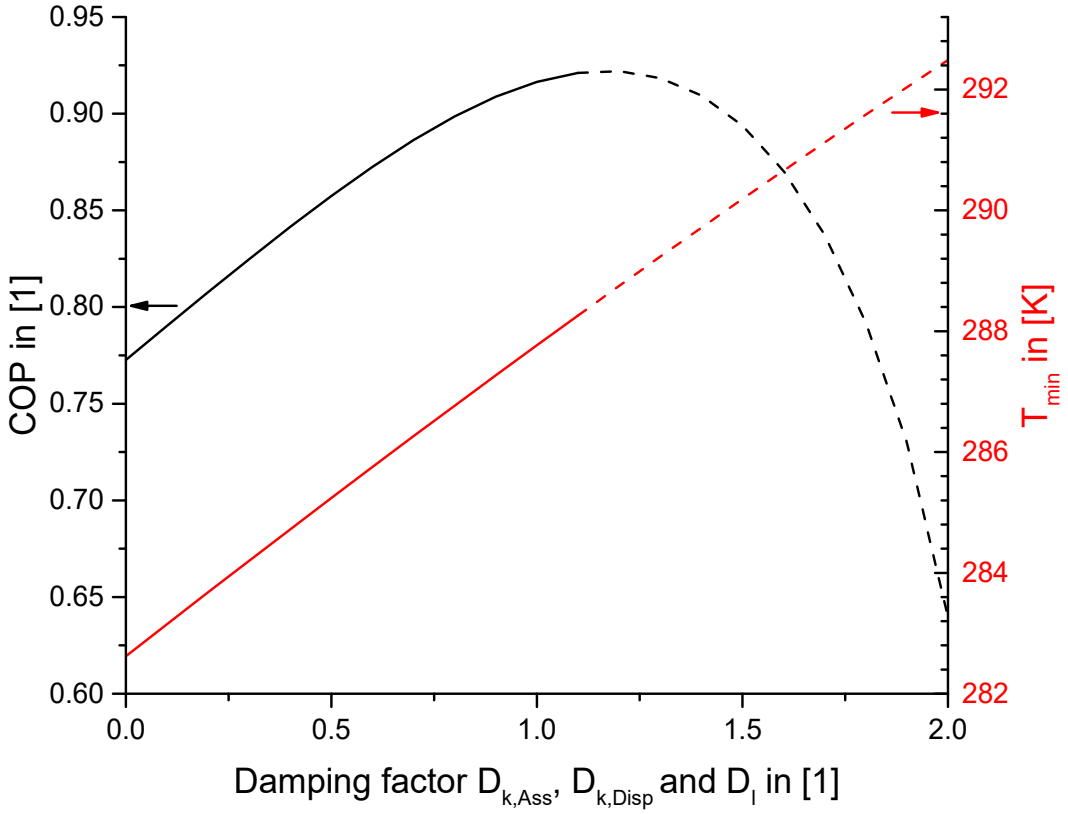

Figure 53: Influence of the binary interaction parameters l_{ij}, $k_{ij}^{\mathrm{Dispersion}}$ and $k_{ij}^{\mathrm{Association}}$ on the COP and the minimal cooling temperature. Solid black lines represent the COP, dashed black lines the COP in a possible LLE area, solid red lines represent the minimal cooling temperature and the dashed red lines the minimal cooling temperature in the area of a possible LLE area.

Figure 53 shows a positive influence on the COP and evaporator temperature from the binary interaction parameters. If the absorbing process is calculated only with the pure component parameters, the efficiency of the system will be underestimated and the ability to cool to lower temperatures will be overestimated. The difference in the COP between the binary interaction parameters as estimated earlier is $\Delta\mathrm{COP} \approx 0.15$ and the difference in the cooling temperatures is $\Delta T \approx 5\mathrm{K}$. All facts considered it can be said, that the influence on the COP and evaporator temperature from the binary

interaction parameters is not negligible. And since these values are the key aspects in choosing a suitable working pair for an absorption cycle it is necessary to work with experimental results for the binary VLE of the system. Doing the calculations with only the pure component parameters gives an estimate of the performance qualities and can be helpful in the early development stages and even give hints regarding a possible LLE. But even if VLE data is available, the calculations of the LLE can only give qualitative predications.

5 Conclusions and outlook

Within this work, the PC-SAFT framework was utilized to quickly generate a first look at the feasibility of certain working pairs for absorption refrigeration processes, consisting of alcohols and ionic liquids. The PC-SAFT parameters for the ionic liquids were fitted to experimental data for the pure component liquid densities at ambient pressure found in literature, the parameters for methanol and ethanol were taken directly from literature. These parameters were tested by calculating the liquid densities at higher pressure, the surface tensions and the speeds of sound, all for the pure ionic liquids. It could be shown, that the liquid densities at higher pressures and the surface tensions could be predicted with good accuracy and the speeds of sound, which in general is more complex to predict, could be predicted with a fair accuracy, giving faith in the fitted PC-SAFT parameters, even if there are some deviations with ionic liquid PC-SAFT parameters from literature. For the pure components a first step to predict the self-diffusion coefficients from pure component PC-SAFT parameters was undertaken, with good results for non-associating gases and liquids and associating gases, but with deviations in the predictions for associating liquids. Since alcohols and ionic liquids are associating components and the liquid diffusion an integral part for the absorption cycle no further steps were taken. For the binary systems, it could be shown, that the predictions of the diffusion coefficients from pure component PC-SAFT parameters is possible for equimolar mixtures composed of components for which self-diffusion coefficients could be predicted accurately. Since the limitations on the self-diffusion coefficients for associating liquids are still present for the mixtures, again no further steps were taken. For the absorption cycle, the VLE of the considered working pairs was calculated and it could be shown, that for the correct calculations of the VLE binary interaction parameters are mandatory. To give a representation of the VLE of the system [BMIM][BF4] + ethanol and [BMIM][BF4] + methanol with good quality, temperature dependent corrections of the combining rules for the energy of the dispersion interaction, temperature dependent corrections of the combining rules for the energy of the association interaction and a temperature independent correction for the combining rule of the depth of the potential well was needed. For the systems without fitted interaction parameters not all VLEs could be calculated due to the presence of LLE. It could be shown, that the PC-SAFT framework with only the pure component parameters from liquid densities is able to predict the presence of most of LLEs, if combined with interaction parameters even in

fair agreement with NRTL calculations. For the working pairs without a predicted LLE hindering an absorption cycle, the temperatures in the evaporator and the COP could be calculated for the given design parameters. The COP is comparable to simulation from literature [368]. Because of the simplifications in the model, a lower experimental COP is to be expected. This gives a first glimpse at the performance qualities of a considered working pair. All in all, it was possible to predict valuable data for the field stages of an absorption refrigerator design process for a working pair consisting of alcohols and ionic liquids suspending working pairs with LLEs and giving a first look at the performances of the working pairs left. The predictions of the VLE and the possible LLEs were all done with only parameters fitted to liquid densities, so in the case of a new working pair, first insights can be achieved with moderate experimental effort. For the performance of the absorption cycle, experimental data for the heat capacity are mandatory, increasing the experimental effort, but still within a reasonable limit. For even better results of the calculated VLE, temperature dependent binary interaction parameters are needed which come with a much larger experimental effort. So the suspension of working pairs because of present LLEs or unfavorable VLE predictions is a highly valuable insight for new working pairs.

For the system [BMIM][BF4] + ethanol together with its fitted binary interaction parameters, it was possible to show, that both the dispersion interaction as well as the association interaction do have a big influence on the COP. Both partially cancel each other out but are not negligible individually or combined. The influence of the combining of the depth of the square well potentials is also present, but not as determining as the association or dispersion interactions. It also became obvious, that a connection between the temperature in the evaporator and the COP of the system is present. A favorable increase in the COP is always connected to an unfavorable increase in the evaporator temperature and therefore in the possibly achievable cooling temperature.

To continue this work, several paths are possible. First it could be interesting what the reasons for the deviations in the ionic liquid pure component parameters are, since both the parameters from literature as well as the parameters established in this work were tested against experimental results with satisfiable results.

The method for first examination of possible working pairs established in this work has only been used to treat working pairs of methanol and ethanol and 8 different ionic liquids. For a broad use of this method it may be necessary to further put this method to the test for more ionic liquids and different alcohols. It could also provide highly desirable information for working pairs with cooling agents other than alcohols. Also, although the method was developed with ionic liquids as absorbents in mind, the basic principles are assignable to all compounds principally describable with the PC-SAFT framework or its derivations. So it could provide a valuable tool for a first assessment of possible working pairs not only consisting of alcohols and ionic liquids but a wide variety of possible cooling agents and absorbents.

The connection of the performance of an absorption cycle to the association and dispersion interactions could also be subject to further investigations. With more VLE-data available for specific working pairs, this connection could be further investigated and possibly a prediction method for the prediction of the performance qualities of certain working pairs could be developed.

For a more precise picture of the absorption cycle, more sophisticated modelling and simulation methods are needed. And for a realistic depiction they will have to incorporate transport processes in the absorption machine and will therefore need diffusion coefficients for the gases and the liquids. While a few first steps in predicting these transport properties have been done in this work, with good results for associating and non-associating gases in a pure or binary system as well as non-associating liquids and its mixtures, the fact that it was not yet possible to accurately predict the diffusion in associating pure and mixed liquids leaves the efforts at a stage where it is not possible to implement these predictions in the simulation of an absorption chiller. But since the transport properties are accessible with a laborious and money-consuming experimental effort only, a further development of the theory that was described in this work is highly desirable.

Appendix

A.1 Density data

Ionic liquids were a main focus of research over the last decades, and so a lot of experimental data was produced. To only incorporate data, that agrees well with that of other researchers, the data was gathered, a linear interpolation was done and only data sets that were within a defined deviation were considered for this work.

A.1.1 [OMIM][PF6]

For the ionic liquid [OMIM][PF6] the linear interpolation of all the found experimental data (Table A 1) following eaquation (47) yielded the parameters $A = -0.7269$ and $B = 1449.8$.

The sources for the experimental data and the mean deviation from the linear interpolation can be seen in Table A 1.

Author	Mean deaviation D_M in [1]	Temperature range in [K]
AlTuwaim et al. [276]	0.00048	298.15 – 333.15
Gardas et al. [240]	0.00171	293.15 – 393.15
Gu and Brennecke [306]	0.00675	298.2 – 343.2
Harris et al. [270]	0.00282	273.15 – 363.15
Malek et al. [347]	0.01207	293.15 – 323.15
Montalban et al. [238]	0.00221	293.15 – 343.15
Pereiro et al. [284]	0.00191	278.15 – 343.15
Pereiro and Rodriguez [285]	0.00215	293.15 – 303.15
Rocha et al. [287]	0.00239	293.15 – 363.15
Taguchi et al. [296]	0.00228	293.15 – 353.15
Tariq et al. [258]	0.00036	293.15 – 333.15
Tomida et al. [297]	0.00090	293.15 – 353.15
Tomida et al. [298]	0.00077	295.1 – 335.2

Table A 1:Sources of experimental data for the density of [OMIM][PF6] with mean deviation from linear interpolation (equation (47)).

Experimental data sets with a mean deviation greater than $D_M = 0.003$ will be omitted. This is the case for the data of Gu and Brennecke [306] and Malek et al.

[347]. Gu and Brennecke [306] are reporting problems with chloride impurities in the ionic liquid which may be a reason for the deviations. Malek et al. [347] mention that they are seeing the deviations as a result of halide and water impurities.

A.1.2 [OMIM][BF4]

For the ionic liquid [OMIM][PF6] the linear interpolation of all the experimental data found in the literature (Table A 2) is following eaquation (47) yielded the parameters $A = -0.6647$ and $B = 1301.1$.

The sources for the experimental data and the mean deviation from the linear interpolation can be seen in Table A 2.

Author	Mean deaviation D_M in [1]	Temperature range in [K]
Blanchard et al. [370]	0.01240	313.15 – 333.15
Gardas et al. [240]	0.00104	293.15 – 393.15
Gu and Brennecke [306]	0.01037	298.2 – 343.2
Harris et al. [270]	0.00060	273.15 – 363.15
Ijardar and Malek [343]	0.00434	293.15 – 323.15
Kumar [271]	0.00035	293.15 – 343.15
Malek et al. [344]	0.00493	298.15 – 318.15
Mokhtarani et al. [371]	0.01016	283.15 – 363.15
Montalban et al. [238]	0.00001	293.15 – 343.15
Ning et al. [272]	0.00050	303.15 – 333.15
Restolho et al. [372]	0.00229	298.15 – 328.15
Sanchez et al. [273]	0.00079	283.15 – 363.15
Sanmamed et al. [254]	0.00070	288.15 – 323.15
Singh and Kumar [274]	0.00194	298.15 – 318.15
Stoppa et al. [256]	0.00043	278.15 – 338.15
Tomida et al. [275]	0.00046	293.15 – 353.15

Table A 2: Sources of experimental data for the density of [OMIM][BF4] with mean deviation from linear interpolation (equation (47)).

Data with a mean deviation bigger than $D_M = 0.002$ will be omitted. As mentioned before, Gu and Brennecke [306] reported problems chloride impurities and Malek et

al. [344] attributed their deviations to possibly water and halide contents. The authors of the other omitted results do not give explanations for the deviations.

A.1.3 [BMIM][BF4]

For the ionic liquid [BMIM][BF4] the linear interpolation of all the experimental data found in literature (Table A 3) is following eaquation (47) yielded the parameters $A = -0.7118$ and $B = 1413.4$.

The sources for the experimental data and the mean deviation from the linear interpolation can be seen in

Author	Mean deaviation D_M in [1]	Temperature range in [K]
Afzal et al. [373]	0.00026	293.2 – 358.2
Aki et al. [374]	0.01378	298 2 – 333.2
Chaudhary et al. [342]	0.00413	293.15 – 323.15
Ciocirlan et al. [241]	0.00024	293.15 – 353.15
Curras et al. [375]	0.00084	283.15 – 333.15
Fredlake et al. [326]	0.00314	295.45 – 343.85
Gao et al. [376]	0.00219	298.15 – 313.15
Garcia-Miaja et al. [264]	0.00219	293.15 – 318.15
Gardas et al. [240]	0.00079	293.15 – 393.15
Gomes de Azevedo et al. [299]	0.00334	298.34 – 332.73
Harris et al. [242]	0.00036	288.15 – 363.16
Huo et al. [377]	0.00785	293.15 – 343.15
Huo et al. [279]	0.00793	298.15 – 353.15
Iglesias-Otero et al. [378]	0.00008	293.15 – 323.15
Jacquemin et al. [243]	0.00070	293.15 - 343.15
Jacquemin et al. [244]	0.00105	292.94 – 414.92
Jacquemin et al. [244]	0.00070	292.89 – 391.28
Kavitha et al. [245]	0.00063	298.15 – 313.15
Kim et al. [246]	0.00031	298.2 – 323.2
Klomfar et al. [379]	0.00206	281.45 – 352.74
Krishna et al. [247]	0.00050	298.15 – 323.15
Kumar [271]	0.00213	283.15 – 343.15

Li et al. [380]	0.01061	298.15 – 353.15
Li et al. [381]	0.01662	298.15 – 313.15
Lopes et al. [283]	0.00219	298.15 – 333.15
Lu et al. [382]	0.00331	293.15 – 313.15
Machida et al. [301]	0.00408	313.1 – 472.2
Matkowska and Hofman [302]	0.00240	290.65 – 353.15
Montalban et al. [238]	0.00014	298.15 – 343.15
Navarro et al. [248]	0.00035	298.15 – 323.15
Navia et al. [383]	0.00135	298.15 – 308.15
Nikitina et al. [384]	0.00574	278.15 – 358.15
Pal and Kumar [249]	0.00063	288.15 – 318.15
Palgunadi et al. [385]	0.00158	313.15 – 333.15
Perez-Sanchez et al. [250]	0.00058	291.151 – 310.145
Qi and Wang [251]	0.00003	288.15 – 303.15
Rilo et al. [303]	0.00502	298.15 – 323.15
Salgado et al. [252]	0.00007	278.15 – 373.15
Sanchez et al. [273]	0.00132	283.15 – 363.15
Sanmamed et al.[253]	0.00071	283.15 – 323.15
Sanmamed [254]	0.00036	293.15 – 323.15
Sariano et al. [386]	0.00091	298.2 – 353.2
Schreiner et al. [255]	0.00030	298.15 – 333.15
Song and Chen [387]	0.00083	293.15 – 343.15
Stoppa et al. [256]	0.00056	278.15 – 338.15
Sunkara et al. [257]	0.00055	298.15 – 323.15
Taib and Murugesan [388]	0.00213	293.15 – 353.15
Tariq et al. [258]	0.00048	293.15 – 333.15
Tian et al. [389]	0.00157	298.15 – 318.15
Tokuda et al. [259]	0.00060	288.15 – 313.15
Tomida et al. [260]	0.00055	293.15 – 353.15
Vakili-Nezhaad et al. [316]	0.00485	278.15 – 363.15
Wu et al. [261]	0.00027	303.15 – 333.15
Xu et al. [262]	0.00039	298.15 – 338.15
Yusoff et al. [390]	0.00502	303.15 – 363.15

Zafarani-Moattar and Shekaari [288]	0.00813	298.15 – 318.15
Zhang et al. [263]	0.00016	288.2 – 313.2
Zhao et al. [391]	0.00206	303.15 – 343.15
Zhou and Wang [392]	0.00156	293.15 – 353.15

Table A 3: Sources of experimental data for the density of [BMIM][BF4] with mean deviation from linear interpolation (equation (47)).

Data with a mean deviation bigger than $D_M = 0.0008$ will be omitted. The biggest deviations occur in the work of Lu et al. [381] while they pointed out that they are in a good agreement with Tokuda et al. [259]. While most of the density measurements are done with a vibrating tube densitometer (e.g. [271,377]), Lu et al. [382] used a capillary pycnometer. Kumar [271] attributes his deviations to water and halide impurities.

A.1.4 [BMIM][CF3SO3]

For the ionic liquid of [BMIM][CF3SO3] the linear interpolation of all the experimental data in the literature (Table A 4) is following eaquation (47) yielded the parameters $A = -0.7813$ and $B = 1532.3$.

The sources for the experimental data and the mean deviation from the linear interpolation can be seen in Table A 4.

Author	Mean deaviation D_M in [1]	Temperature range in [K]
Fredlak et al. [326]	0.002012	295.75 – 342.95
Garcia-Miaja et al. [264]	0.001377	293.15 – 318.15
Gardas et al. [240]	0.001030	293.15 – 393.15
Ge et al. [393]	0.003384	303.15 – 343.15
Gonzalez et al. [265]	0.000154	288.15 – 308.15
Gonzalez et al. [266]	0.000173	293.15 – 323.15
Jacquemin et al. [243]	0.001543	293.15 – 363.15
Klomfar et al. [267]	0.001372	293.37 – 342.95
Montalban et al. [238]	0.005392	293.15 – 343.15
Seoane et al. [268]	0.000077	293.15 – 343.15
Shamsipur et al. [394]	0.004178	283.15 – 363.15

Soriano et al. [386]	0.003695	298.2 – 353.2
Tariq et al. [258]	0.000104	293.15 – 333.15
Tokuda et al. [259]	0.001083	288.15 – 313.15
Tsamba et al. [395]	0.004024	293.15 – 343.14
Vercher et al. [396]	0.002109	288.15 – 338.15
Zech et al. [269]	0.001586	278.15 – 338.15

Table A 4: Sources of experimental data for the density of [BMIM][CF3SO3] with mean deviation from linear interpolation (equation (47)).

Data with a mean deviation bigger than $D_M = 0.002$ will be omitted. The biggest deviations occur at the work of Montalban et al. [238]. As well as Kumar [271] and Gu and Brennecke [306], they attribute the deviations to halide and water impurities. This is also the suggestion of Shamsipur et al. [394].

A.1.5 [BMIM][PF6]

For the ionic liquid of [BMIM][PF6] the linear interpolation of the experimental data found in literature (Table A 5:) is following equation (47) yielded the parameters $A = -0.8117$ and $B = 1608$.

The sources for the experimental data and the mean deviation from the linear interpolation can be seen in Table A 5: .

Author	Mean deaviation D_M in [1]	Temperature range in [K]
Afzal et al. [373]	0.001241	288.2 – 353.2
Aki et al. [374]	0.008599	298.2 – 333.2
Al-Rashed et al. [397]	0.002936	293.15 – 298.15
AlTuwaim et al. [276]	0.000897	298.15 – 333.15
Chaudhary et al. [277]	0.000923	293.15 – 323.15
Dzyuba and Bartsch [398]	0.002378	298.15 – 323.15
Fan et al. [399]	0.001032	283.15 – 353.15
Gu and Brennecke [306]	0.004012	298.2 – 343.2
Harris et al. [278]	0.000958	273.15 – 303.15
Huo et al. [377]	0.001925	293.15 – 343.15
Huo et al. [279]	0.000217	298.15 – 323.15
Jacquemin et al. [280]	0.000683	293.49 – 414.93

Jacquemin et al. [281]	0.000967	283.13 – 343.27
Jacquemin et al. [243]	0.001012	293.15 – 343.15
Jacquemin et al. [244]	0.000531	292.87 – 391.27
Kabo et al. [239]	0.000218	298.23 – 353.47
Kumar [271]	0.001045	298.23 – 353.47
Kumar et al. [400]	0.001092	298.15 – 318.15
Kumelan et al. [282]	0.000846	289.1 – 309.15
Li et al. [380]	0.003945	298.15 – 343.15
Lopes et al. [283]	0.000672	298.15 – 333.15
Machida et al. [301]	0.002940	312.8 – 472.3
Montalban et al. [238]	0.000179	293.15 – 343.15
Navia et al. [383]	0.001369	298.15 – 308.15
Pal et al. [345]	0.001314	288.15 – 308.15
Pereiro et al. [284]	0.000688	278.15 – 343.15
Pereiro and Rodriguez [285]	0.000957	293.15 – 303.15
Qi and Wang [251]	0.005351	288.15 – 303.15
Qiao et al. [307]	0.002511	313.2 – 413.2
Reyes et al. [286]	0.000628	303.15 – 363.15
Rocha et al. [287]	0.000933	293.15 – 363.15
Salgado et al. [252]	0.001490	278.15 – 373.15
Singh et al. [322]	0.001016	303 – 333
Singh and Kumar [401]	0.001092	298.15 – 318.15
Soriano et al. [386]	0.001038	298.2 – 353.2
Tariq et al. [258]	0.001781	293.15 – 333.15
Tokuda et al. [259]	0.001733	288.15 – 313.15
Tomida et al. [260]	0.000218	293.15 – 353.15
Tomida et al. [298]	0.003661	294.9 – 335.1
Troncoso et al. [237]	0.000365	283.15 – 323.15
Zafarani-Moattar and Shekaari [288]	0.000333	298.15 – 318.15
Zech et al. [269]	0.001365	278.15 – 338.15
Zhang et al. [263]	0.001216	288.2 – 313.2

Table A 5: Sources of experimental data for the density of [BMIM][PF6] with mean deviation from linear interpolation (equation (47)).

Data with a mean deviation bigger than $D_{\mathrm{M}} = 0.001$ will be omitted. As before, the deviations in the density measurements are usually attributed to impurities in the ionic liquids.

A.1.6 [HMIM][PF6]

For the ionic liquid of [HMIM][PF6] the linear interpolation of all the experimental data found in the literature (Table A 6) is following eaquation (47) yielded the parameters $A = -0.7831$ and $B = 1526.2$.

The sources for the experimental data and the mean deviation from the linear interpolation can be seen in Table A 6.

Author	Mean deaviation D_M in [1]	Temperature range in [K]
AlTuwaim et al. [276]	0.000795	298.15 – 333.15
Gardas et al. [240]	0.000947	293.15 – 393.15
Harris et al. [290]	0.000460	273.15 – 363.15
Klomfar et al. [291]	0.000470	277.88 – 364.46
Li et al. [292]	0.000121	293.15 – 343.15
Malek et al. [347]	0.004257	293.15 – 323.15
Montalban et al. [238]	0.000422	293.15 – 343.15
Muhammad et al. [293]	0.000643	298.15 – 358.15
Ning et al. [272]	0.000481	303.15 – 333.15
Pal and Kumar [348]	0.001457	288.15 – 318.15
Pereiro et al. [294]	0.000738	278.15 – 318.15
Pereiro and Rodriguez [295]	0.000784	293.15 – 303.15
Rocha et al. [287]	0.001199	293.15 – 363.15
Taguchi et al. [296]	0.000196	293.15 – 353.15
Tariq et al. [258]	0.000300	293.15 – 333.15
Tomida et al. [297]	0.001290	293.15 – 353.15
Tomida et al. [298]	0.001314	294.1 – 335.2
Vakili-Nezhaad et al. [316]	0.001007	278.15 – 363.15

Table A 6: Sources of experimental data for the density of [HMIM][PF6] with mean deviation from linear interpolation (equation (47)).

Data with a mean deviation bigger than $D_{\mathrm{M}} = 0.001$ will be omitted. As with all the other ionic liquids, the deviations are usually attributed to ionic liquid impurities.

A.2 Tables

Substance	σ in [Å]	m in [1]	ε/k_B in [K]	κ^{AB} in [1]	ε^{AB}/k_B in [K]	Ref.
Carbon dioxide*	3.1869	1.5131	163.33			[209]
Methane	3.7039	1	150.03			[59]
Ethane	3.5206	1.6069	191.2			[59]
Ethylene*	3.4523	1.5425	179.37			[209]
Propane	3.6184	2.002	208.11			[59]
Butane	3.7086	2.3316	222.88			[59]
Argon	3.484	0.9285	122.23			[402]
Nitrogen	3.2975	1.2365	89.492			[403]
Helium	3.58	0.1852	32.84			[404]
Hydrogen	2.601	1.306	23.42			[405]
Nitrous oxide	2.6699	2.3547	160.85			[402]
Oxygen	3.1711	1.1457	113.98			[403]
Carbon monoxide	3.2507	1.3097	92.15			[59]
Methanol (2B)	3.23	1.5255	188.9	0.035176	2899.5	[60]
Ethanol (2B)	3.1771	2.3827	198.24	0.032384	2653.4	[60]
Water (4C)	3.0007	1.0656	366.51	0.01	1800	[406]

Table A 7: PC-SAFT pure component parameters used for non-IL components. * - including polar term.

6 Wissenschaftliche Veröffentlichungen

6.1 Publikationen

S. Enders, T. Grunert, H. Rudolph
Prediction of interfacial tensions between demixed ternary mixtures.
Zeitschrift für Physikalische Chemie, International journal of research in physical chemistry and chemical physics 227 (2013), 269-284.

H. Rudolph, S. Enders
Prediction of the self-diffusion coefficients of pure fluids and binary gas mixtures using Polar Perturbed Chain-Self Associating Fluid Theory Equation of State
Molecular Physics.

H. Rudolph, S. Enders
Thermodynamic modelling for the selection of working pairs (ionic liquid and alcohol) in adsorption chillers at low temperatures
Fluid Phase Equilibria in Vorbereitung

6.2 Vorträge

T. Grunert, H. Rudolph, S. Enders
Grenzflächeneigenschaften ternärer Systeme,
Process-Net: Fachausschuss Extraktion
Clausthal-Zellerfeld (Deutschland) 18.-20. September 2012

H. Rudolph, T. Grunert, S. Senders
Calculation of Interfacial Properties for Material Transport
Thermophysical properties for Technical Thermodynamics
Rostock (Deutschland) 27.–28. März 2013.

H. Rudolph, S. Enders
Modelling of physical properties of ionic liquid solutions related to the absorption cooling cycle
20th European Conference on Thermophysical Properties
Porto (Portugal) 31. August – 04. September 2014.

H. Rudolph, C.Walowski, S. Enders
Prediction of Self-Diffusion Coefficients from Chapman-Enskog-Theory in combination with PC-SAFT or LCT-EOS,
Thermodynamics,
Kopenhagen (Dänemark) 15.-18. September 2015.

6.3 Posterbeiträge

H. Rudolph, S. Enders
Modelling of physical properties of ionic liquid solutions related to the absorption cooling cycle
International Conference on Chemical Thermodynamics and The South African Institution of Chemical Engineers,
Durban (Südafrika) 27. Juli – 01. August 2014.

H. Rudolph, S. Enders
Anwendung der PC-SAFT EOS für Mischungen aus ionischer Flüssigkeit und einem kurzkettigen Alkohol
Process-Net Fachausschuss “Thermodynamik”
Stuttgart (Deutschland) 22.-24. September 2014.

C.Walowski, **H. Rudolph**, S. Enders
Prediction of Self-Diffusion Coefficients from Chapman-Enskog-Theory in combination with PC-SAFT or LCT-EOS
Thermodynamics
Kopenhagen (Dänemark) 15.-18. September 2015.

H. Rudolph, C. Walowski, S. Enders
Berechnung von Diffusionskoeffizienten reiner Stoffe
Process-Net Fachausschuss “Thermodynamik”
Bochum (Deutschland) 05.-07. Oktober 2015.

References

[1] N. Ak, A. Demirbas, Energy Sources Part A 38 (2016) 1730-1738.
[2] D.T. Allen, J. Air Waste Manage. Assoc. 66 (2016) 549-575.
[3] L.D. Claxton, Mutation Research 763 (2016) 103-147.
[4] A. Horvath, E. Rachlew, Ambio 45 (2016) 38-49.
[5] E. Cuce, Int. J. Ambient Energy 37 (2016) 428-435.
[6] J. Sun, L. Fu, S. Zhang, Renewable Sustainable Energy Rev. 16 (2012) 1899-1906.
[7] M. Seiler, A. Kühn, F. Ziegler, X. Wang, Ind. Eng. Chem. Res. 52 (2013) 16519-16546.
[8] M. Seiler, P. Schwab, "*New Working Pairs for Absorption Chillers*", Handbook of green chemistry, Volume 6: Ionic Liquids. WILEY-VCH (2010), 221-232.
[9] W.G.W. Wytze, F.S.A.F. Onink, A.B. de Haan, "*Green Seperation Processes with Ionic Liquids*", Handbook of green chemistry, Volume 6: Ionic Liquids. WILEY-VCH (2010) 139-190.
[10] M. Uerdingen, "*Ionic Liquids as Lubricants*", Handbook of green chemistry, Volume 6: Ionic Liquids. WILEY-VCH (2010) 203-220.
[11] D. Rooney, J. Jacquemin, R. Gardas, "*Thermophysical properties of Ionic Liquids*", Ionic Liquids, Springer Verlag Berlin, Heidelberg (2009) 185-212.
[12] T. Mu, B. Han, "*Structures and Thermodynamic Properties of Ionic Liquids*", Structures and Interactions of Ionic Liquids, Springer Verlag Berlin, Heidelberg (2014) 107-140.
[13] S. Zhang, N. Sun, X. He, X. Lu, X. Zhang, J. Phys. Chem. Ref. Data 35 (2006) 1475-1517.
[14] S. Gabriel; J. Weiner, Chem. Ber. 21 (1888) 2669–2679.
[15] P. Walden, Bull. Acad. Sci. St. Petersburg 8 (1914) 405-422.
[16] R. Caminiti, L. Gontrani, "*The Structure of Ionic Liquids*", Springer Science & Business Media (2014).
[17] C.A. López-Rico, J. Galindo-De-La-Rosa, E. Ortiz-Ortega, L. Álvarez-Contreras, J. Ledesma-García, M. Guerra-Balcázar, L.G. Arriaga, N. Arjona, Electrochim. Acta 207 (2016) 164-176.
[18] M. Li, B. Yang, J. Hao, Y. Lu, Z. Long, Y. Liu, J. Nanosci. Nanotechnol. 16 (2016) 6238-6245.
[19] L. Zhang, T. You, T. Zhou, X. Zhou, F. Xu, ACS Appl. Mater. Interfaces 8 (2016) 13918-13925.
[20] D. Rabari, T. Banerjee, Ind. Eng. Chem. Res. 53 (2014) 18935-18942.
[21] I.R. Sitepu, S. Shi, B.A. Simmons, S.W. Singer, K. Boundy-Mills, C.W. Simmons, FEMS Yeast Res. 14 (2014) 1286-1294.
[22] Z. Lei, X. Xi, C. Dai, J. Zhu, B. Chen, AIChE J. 60 (2014) 2994-3004.
[23] M. Francisco, A.S.B. González, S.L. García De Dios, W. Weggemans, M.C. Kroon, RSC Advances 3 (2013) 23553-23561.
[24] J.A.P. Coutinho, P.J. Carvalhoa, N.M.C. Oliveira, Phys. Chem. Chem. Phys. 8 (2006) 642–649.
[25] N.V. Plechkova K.R. Seddon, Chem. Soc. Rev. 37 (2008) 123–150.
[26] P. García-Gutiérrez, J. Jacquemin, C. McCrellis, I. Dimitriou, S.F.R. Taylor, C. Hardacre, R.W.K. Allen, Energy Fuels 30 (2016) 5052-5064.
[27] T. Mulukutla, J. Chau, D. Singh, G. Obuskovic, K.K. Sirkar, J. Membr. Sci. 493 (2015) 321-328.
[28] J. Wang, D. Zheng, L. Fan, L. Dong, J. Chem. Eng. Data 55 (2010) 2128–2132.

[29] X. Zhang, D. Hu, Appl. Therm. Eng. 31 (2011) 3316-3321.
[30] X. Zhang, D. Hu, Appl. Therm. Eng. 37 (2012) 129-135.
[31] A. Yokozeki, M.B. Shiflett, Appl. Energy 84 (2007) 1258–1273.
[32] A. Yokozeki, M.B. Shiflett, Ind. Eng. Chem. Res. 46 (2007) 1605-1610.
[33] A. Yokozeki, M.B. Shiflett, Ind. Eng. Chem. Res. 49 (2010) 9496–9503.
[34] A. Yokozeki, Appl, Energy 80 (2005) 383–399.
[35] Y.J. Kim, S. Kim, Y.K. Joshi, A.G. Fedorov, P.A. Kohl, Energy 44 (2012) 1005-1016.
[36] S. Kim, Y. Kim, Y.K. Joshi, A.G. Fedorov, P.A. Kohl. ASME. J. Electron. Packag.134 (2012), 031009-1-9.
[37] S. Kim, N. Patel, P.A. Kohl, Ind. Eng. Chem. Res. 52 (2013) 6329−6335.
[38] Y. J. Kim, M. Gonzalez, Int. J. Refrig. 48 (2014) 26-34.
[39] S. Kim, P.A. Kohl, Ind. Eng. Chem. Res. 52 (2013) 13459−13465.
[40] M. Preißinger, S. Pöllinger, D. Brüggemann, Int. J. Energy Res. 37 (2013) 1382–1388.
[41] S.K. Swarnka, S.S. Murthy, R.L. Gardas, G. Venkatarathnam, Appl. Therm. Eng. 72 (2014) 250-257.
[42] T. Weith, M. Preißinger, S. Pöllinger, D. Brüggemann, Heat Transfer Eng. 35 (2014) 1462-1472.
[43] E. Ruiz, V.R. Ferro, J. de Riva, D. Moreno, J. Palomar, Appl. Energy 123 (2014) 281–291.
[44] K.A. Kurnia, S.P. Pinho, J.A.P. Coutinho, Green Chem. 16 (2014) 3741-3745.
[45] G. Mozurkewich, L.D. Simoni, M.A. Stadtherr, W F. Schneider, Int. J. Refrig. 46 (2014) 196-206.
[46] G. Jackson, W.G. Chapman, K.E. Gubbins, Mol. Phys. 65 (1988) 1-31.
[47] W.G. Chapman, G. Jackson, K.E. Gubbins, Mol. Phys. 65 (1988) 1057-1079.
[48] W.G. Chapman, K.E. Gubbins, G. Jackson, M. Radosz, Ind. Eng. Chem. Res 29 (1990) 1709-1721.
[49] M.S. Wertheim, J. Stat. Phys. 35 (1984) 19-34.
[50] M.S. Wertheim, J. Stat. Phys. 35 (1984) 35-47.
[51] M.S. Wertheim, J. Stat. Phys. 42 (1986) 459-476.
[52] M.S. Wertheim, J. Chem. Phys. 87 (1987) 7323-7331.
[53] A. Gil-Villega, A. Galindo, P.J. Whitehead, S.J. Mills, G. Jackson, A.N. Burgess, J. Chem. Phys. 106 (1997) 4168-4186.
[54] A. Galindo, L.A. Davies, A. Gil-Villegas, G. Jackson, Mol. Phys. 93 (1998) 241-252.
[55] H Adidharma, M Radosz, Ind. Eng. Chem. Res. 37, (1998) 4453–4462.
[56] X. Ji, H. Adidharma, Chem. Eng. Sci. 64 (2009) 1985-1992.
[57] X. Ji, H. Adidharma, Fluid Phase Equilib. 293 (2010) 141-150.
[58] X. Ji, H. Adidharma, Fluid Phase Equilib. 315 (2012) 53-63.
[59] J. Gross, G. Sadowski, Ind. Eng. Chem. Res. 40 (2001) 1244–1260.
[60] J. Gross, G. Sadowski, Ind. Eng. Chem. Res. 41 (2002) 5510–5515.
[61] F. J. Blas, L. F. Vega, J. Chem. Phys., 115, (2001), 4355-4358.
[62] Z.-Q. Hu, J—C- Yang, Y—G- Li, Fluid Phase Equilibria 205, (2003), 25–36
[63] S.S. Chen, A. Kreglewski, Ber. Bunsen-Ges. Phys. Chem. 81 (1977) 1048-1052.
[64] L.F. Cameretti, G. Sadowski, J.M. Mollerup, Ind. Eng. Chem. Res. 44 (2005) 3355-3362.
[65] S. Seyfi, G.R. Pazukim, S.F. Aghamiri, M. Beheshti, J. Dispersion Sci. Technol. 31 (2010) 536-550.

[66] O. Guzman, J.E. Ramos Lara, F. del Rio, J. Phys. Chem. B 119 (2015) 5864-5872.
[67] I. Polishok, J. Phys. Chem. A 117 (2013) 2223-2232.
[68] I. Polishuk, Ind. Eng. Chem. Res. 51 (2012) 13527-13537.
[69] I. Polishuk, J. Supercrit. Fluids 67 (2012) 94-107.
[70] F.M. Maia, I. Tsivintzelis, O. Rodrigueza, E.A. Macedo, G.M. Kontogeorgis, Fluid Phase Equilib. 332 (2012) 128−143.
[71] K. Paduszynski, U. Domanska, J. Phys. Chem. B 116 (2012) 5002-5018.
[72] M.C. dos Ramos, F.J. Blas, J. Supercrit. Fluids 55 (2010) 141-150.
[73] G. Das, S. Hlushuk, M.C. dos Ramos, C. McCabe, AIChE J. 61 (2015) 3053-3072.
[74] M. Chorazewski, J. Troncoso, J. Jacquemin, Ind. Eng. Chem. Res. 54 (2015) 720-730.
[75] M. Abolala, K. Peyrondi, F. Varaminian, Fluid Phase Equilib. 394 (2015) 61-70.
[76] J.M.A. Schreckenberg, S. Dufal, A.J. Haslam, C.S. Adjiman, G. Jackson, A. Galindo, Mol. Phys. 112 (2014) 2339-2364.
[77] A. Lymperiadis, C.S. Adjiman, A. Galindo, G. Jackson, J. Chem. Phys. 127 (2007) 234903-1-22.
[78] S.S. Ashrafmansouri, S. Raeissi, J. Supercrit. Fluids 63 (2012) 53-63.
[79] X. Ji, H. Adidharma, Chem. Eng. Sci. 102 (2013) 24-31.
[80] U. Domanska, K Paduszynski, M. Krolikowsli, A Wroblewska, Ind. Eng. Chem. Res. 55 (2016) 5736-5747.
[81] U. Domanska, M. Zawadzki, K. Paduszynski, M. Krolikowski, J. Phys. Chem. B 116 (2012) 8191-8200.
[82] K. Paduszynski, M. Okuniewski, U. Domanska, Fluid Phase Equilib. 403 (2015) 167-175.
[83] K. Paduszynski, J. Chiyen, D. Ramjugernath, T.M. Letcher, U. Domanska, Fluid Phase Equilib. 305 (2011) 43-52.
[84] K.Paduszynski, E.V. Lukoshko, M. Krolikowski, U. Domanska, J. Chem. Thermodynamics 90 (2015) 317-326.
[85] K. Paduszynski, E. V. Lukoshko, M. Krolikowski, U. Domanska, J. Szydlowski, J. Chem. Phys. B 119 (2015) 543-551.
[86] K. Paduszynski, M. Okuniewski, U. Domanska, Ind. Eng. Chem. Res. 52 (2013) 18482-18491.
[87] K. Paduszynski, M. Okuniewski, U. Domanska, J. Phys. Chem. B 117 (2013) 7034-7046.
[88] K. Paduszynski, M. Okuniewski, U. Domanska, J. Phys. Chem. B 117 (2013) 3884-3891.
[89] K. Paduszynski, M. Okuniewski, U. Domanska, J. Chem. Thermodynamics 92 (2016) 81-90.
[90] K. Paduszynski, U. Domanska, J. Phys. Chem. B 115 (2011) 12537-12548.
[91] E. Lukoshko, F. Mutelet, K. Paduszynski, U. Domanska, Fluid Phase Equilib. 399 (2015) 105-114.
[92] M. Krolikowska, K. Paduszynski, M. Krolikowski, P. Lipinske, J. Antonowicz, Ind. Eng. Chem. Res 53 (2014) 18316-18325.
[93] S. Mahato, A. Kumar, T. Banorjee, J. Taiwan Inst. Chem. Eng. 59 (2016) 69-78.
[94] R. Shakiari, M.R. Dehghani, B. Behzadi, Ind. Eng. Chem. Res. 51 (2012) 10274-10282.
[95] P.B. Sanchez, M.R. Curras, M.M. Mato, J. Salgado, J. Garcia, Fluid Phase Equilib. 405 (2015) 37-45.

[96] M.R. Curras, P. Husson, A.H.A. Padua, M.F. Costa Gomes, J. Garcia, Ind. Eng. Chem. Res. 53 (2014) 10791-10802.
[97] I. Domínguez, B. Gonazalez, B. Orge, C. Held, M. Vogues, E. A. Macedo, Fluid Phase Equilib. 424 (2016) 32-40.
[98] A.P. Carneiro, O. Rodriguez, C. Held, G. Sadowski, E.A. Macedo, J. Chem. Eng. Data 59 (2014) 2942-2954.
[99] A.P. Carneiro, C. Held, O. Rodriguez, G. Sadowski, E.A. Macedo, J. Phys. Chem. B 117 (2013) 9980-9995.
[100] H. Passos, I. Khan, F. Mutelet, M.B. Oliveira, P.J. Carvalho, L.M.N.B.F. Santos, C. Held, G. Sadowski, M.G. Freire, J.A.P. Coutinho, Ind. Eng. Chem. Res. 53 (2014) 3737-3748.
[101] A. Nann, C. Held, G. Sadowski, Ind. Eng. Chem. Res. 52 (2013) 18472-18481.
[102] A. Nann, J. Mündges, C. Held, S.P. Verevkin, G. Sadowski, J. Phys. Chem. B 117 (2013) 3173-3185.
[103] M.M. Joshipura, Indian Chem. Eng. 57 (2015) 154-163.
[104] V.H. Alvarez, M.D.A. Saldana, J. Supercrit. Fluids 66 (2012) 29-35.
[105] A. Khelassi-Sefaoui, F. Mutelet, I. Mokbel, J. Jose, L. Negadi, J. Chem. Thermodynamics 72 (2014) 134-138.
[106] Y. Chen, F. Mutelet, J.N. Jaubert, J. Chem. Eng. Data 59 (2014) 603-612.
[107] Y. Chen, F. Mutelet, J.N. Jaubert, Fluid Phase Equilib. 354 (2013) 191-198.
[108] Y. Chen, F. Mutelet, J.N. Jaubert, J. Phys. Chem. B 116 (2012) 14375-14388.
[109] L.M.C. Pereira, V. Martins, K.A. Kurnia, M.B. Oliveira, A.M.A. Dias, F. Llovell, L.F. Vega, P.J. Carvalho, J.A.P. Coutinho, J. Supercrit. Fluids 110 (2016) 56-64.
[110] L.M.C. Pereira, M.B. Oliveira, F. Llovell, L.F. Vega, J.A.P. Coutinho, J. Supercrit. Fluids 92 (2014) 231-241.
[111] L.M.C. Pereira, M.B. Oliveira, A.M.A. Dias, F. Llovell, L.F. Vega, P.J. Carvalho, J.A.P. Coutinho, Int. J. Greenhouse Gas Control 19 (2013) 299-309.
[112] N. Mac Dowell, F. Llovell, N. Sun, J.P. Hallet, A. George, P.A. Hunt, T. Welton, B.A. Simmons, L.F. Vega, J. Phys. Chem. B 118 (2014) 6206-6221.
[113].M.B. Oliveira, E.A. Crespo, F. Llovell, L.F. Vega, J.A.P. Coutinho, Fluid Phase Equilib. 426 (2016) 100-109.
[114] M.B. Oliveira, F. Llovell, J.A.P. Coutinho, L.F. Vega, J. Phys. Chem. B 116 (2012) 9089-9100.
[115] M.B. Oliveira, M. Dominguez-Perez, M.G. Freire, F. Llovell, O. Cabeza, J.A. Lopes-da-Silva, L.F. Vega, J.A.P. Coutinho, J. Phys. Chem. B 116 (2012) 12133-12141.
[116] F. Llovell, L.V. Vega, J. Chem. Eng. Data 59 (2014) 3220-3231.
[117] F. Llovell, M.B. Oliveira, J.A.P. Coutinho, L.F. Vega, Catal. Today 255 (2015) 87-96.
[118] F. Llovell, R.M. Marcos, N. MacDowell, L.F. Vega, J. Phys. Chem. B 116 (2012) 7709-7718.
[119] F. Llovell, O. Vilaseca, L.F. Vega, Sep. Sci. Technol. 47 (2011) 399-410.
[120] F. Llovell, E. Valente, O. Vilaseca, L.F. Vega, J. Phys. Chem. B 115 (2011) 4387-4398.
[121] L.F. Vega, O. Vilaseca, F. Llovell, J.S. Andreu, Fluid Phase Equilib. 294 (2010) 15-30.
[122] J.S. Andreu, L.F. Vega, J. Phys. Chem. B 112 (2008) 15398-15406.
[123] J.S. Andreu, L.F. Vega, J. Phys. Chem. C 111 (2007), 16028-16034.
[124] A. Magheri, M.S. Sadeghi, Fluid Phase Equilib. 252 (2007) 152-161.

[125] A. Magheri, Z. Safaei, S. Sarhangian, Cryogenics 48 (2008) 48-55.
[126] A. Magheri, Z. Safaei, J. Mol. Liq. 142 (2008) 95-102.
[127] A. Magheri, M. Hamzehloo, Fluid Phase Equilib. 302 (2011) 195-201.
[128] A. Magheri, F. ZiaMajidi, E. Pashaei, J. Mol. Liq. 191 (2014) 59-67.
[129] A. Magheri, F. ZiaMajidi, Fluid Phase Equilib. 356 (2013) 109-116.
[130] Y.U. Paulechka, G.J. Kabo, A.V. Blokhin, O.A. Vydrov, J. Chem. Eng. Data. 48 (2003) 457-462.
[131] G.J. Kabo, A.V. Blokhin, Y.U. Paulechka, A.G. Kabo, M.P. Shymanovich, J. Chem. Eng. Data 49 (2004) 453-461.
[132] C. Held, L.F. Cameretti, G. Sadowski, Fluid Phase Equilib. 270 (2008) 87-96.
[133] C. Held, G. Sadowski, Fluid Phase Equilib. 279 (2009) 141-148.
[134] G. Shen, C. Held, X. Lu, X. Ji, Mol. Phys. 114 (2016) 2492-2499.
[135] G. Shen, C. Held, X. Lu, X. Ji, Fluid Phase Equilib. 405 (2015) 73-82.
[136] G. Shen, C. Held, J.P. Mitkola, X. Lu, X. Ji, Ind. Eng. Chem. Res. 53 (2014) 20258-20268.
[137] X. Ji, C. Held, Fluid Phase Equilib. 410 (2016) 9-22.
[138] C.M.S.S. Neves, C. Held, S. Mohammad, M. Schleinitz, J.A.P. Coutinho, M.G. Freire, Phys. Chem. Chem. Phys. 17 (2015) 32044-32052.
[139] S. P. Verevkin, A.Y. Sazonova, A.K. Frolokova, D.H. Zaitsau, I.V. Prikkodko, C. Held, Ind. Eng. Chem. Res. 54 (2015) 3498-3504.
[140] X. Ji, C. Held, G. Sadowski, Fluid Phase Equilibria 335 (2012) 64-73.
[141] X. Ji, C. Held, G. Sadowski, Fluid Phase Equilib. 335 (2012) 64-73.
[142] Y. Hiruya, A. Kuto, Y. Sato, T.M. Aida, M. Watanabe, R.L. Smith Jr., Sep. Purif. Technol. 155 (2015) 139-148.
[143] L.F. Vega, F. Llovell, Fluid Phase Equilib. 416 (2016) 150-173.
[144] S.P. Tan, H. Adidharma, M. Radosz, Ind. Eng. Chem. Res. 47 (2008) 8063-8082.
[145] M. A. Gebbie, M. Valtiner, X. Banquy, E. T: Fox, W. A: Henderson, J. N, Israelachvili, PNAS 110, (2013), 9674-9679.
[146] E.O. Stejskal, J.E. Tanner, J. Chem. Phys. 42 (1965) 288-292.
[147] P.H. Oosting, N.J. Trappeniers, Physica A 51 (1971) 418-431.
[148] B. Arends, K.O. Prins, N.J. Trappeniers, Physica A 107 (1981) 307-318.
[149] N. Karger, T. Vardag, H.D. Lüdermann, J. Chem. Phys. 93 (1990) 3437-3444.
[150] M. Holz, S.R. Heil, A. Sacco, Phys. Chem. Chem. Phys. 2 (2000) 4740-4742.
[151] K. Yoshida, C. Wakai, N. Mantubayasi, M. Nakahara, J. Chem. Phys. 123 (2005) 164506-1-10.
[152] J. Kestin, K. Knierim, E.A. Mason, B. Najafi, S.T. Ro, M. Waldman, J. Phys. Chem. Ref. Data 13 (1984) 229-303.
[153] S.H. Chen, T.A. Postol, K. Sköld, Phys. Rev. A 16 (1977) 2112.
[154] A. Boushehri, J. Bzowski, J. Kestin, E.A. Mason, J. Phys. Chem. Ref. Data 16 (1987) 445-466.
[155] J. Bzokski, J. Kestin, E.A. Mason, F.J. Uribe, J. Phys. Chem. Ref. Data 19 (1990) 1179-1232.
[156] W.J. Massman, Atmospheric Envir. 32 (1998) 1111-1127.
[157] O. Suarez-Iglesias, I. Medina, M. de los Angeles Sanz, C. Pizarro, J.L. Bueno, J. Chem. Eng. Data 60 (2015) 2757-2817.
[158] H.P. Deutsch, K. Binder, J. Chem. Phys. 94 (1991) 2294-2304.
[159] R.J. Speedy, Mol. Phys. 62 (1987) 509-515.
[160] J.J. Erpenbeck, W.W. Wood, Phys. Rev. A 43 (1991) 4254.
[161] G. Salin, D. Gilles, J. Phys. A, 39 (2006) 4517.

[162] P. Ungerer, C.N. Draghi, B. Rousseau, G. Ahunbay, V. Lachet, J. Mol. Liquids 134 (2007) 71-89.
[163] G. A. Fernandez, J. Vrabec, H. Hasse, Int. J. Thermophys. 25 (2004) 175-186.
[164] Y. M. Munoz-Munoz, G. Guevara-Carrion, M. Llano-Restrepo, J. Vrabec, Fluid Phase Equilib 404 (2015) 150-160.
[165] G. A. Fernandez, J. Vrabec, H. Hasse, Int. J. Thermophys. 26 (2005) 1389-1407.
[166] L.X. Dang, T.M. Chang, J. Chem. Phys. 106 (1997) 8149-8159.
[167] S. Pařez, G. Guevara-Carrion, H. Hasse, J. Vrabec, Phys. Chem. Chem. Phys. 15 (2013) 3985-4001.
[168] O. Lobanova, C. Avendaño, T. Lafitte, E.A. Müller, G. Jackson, Mol. Phys. 113 (2015) 1228-1249.
[169] G. Guevara-Carrion, C. Nieto-Draghi, J. Vrabec, H. Hasse, J. Phys. Chem. 112 (2008) 16664-16674.
[170] M. Dzugutow, Nature 381 (1996) 137-139.
[171] J.J. Hoyu, M. Asta, B. Sadigh, Phys. Rev. Letters 85 (2000) 594-597.
[172] Y. Rosenfeld, Chem. Phys. Lett. 48 (1977) 467-468.
[173] J. Naghizadeh, S.A. Rice, J. Chem. Phys. 36 (1962) 2710-2720.
[174] R. Zwanzig, J. Chem. Phys. 79 (1983) 4507-4508.
[175] U. Mohanty, Phys. Rev. A 32 (1985) 3055.
[176] T.X. Xiang, J. Chem. Phys. 109 (1998) 7876-7884.
[177] V.S. Galkin, M.S. Shavaliev, Fluid Dynamics 33 (1998) 469-487.
[178] J.M. Zielinski, B.F. Hanley, AIChE J. 45 (1999) 1-12.
[179] J.L. Bretonnet, J. Chem. Phys. 117 (2002) 9370-9373.
[180] K. Harstad, J. Bellan, Ind. Eng. Chem. Res. 43 (2004) 645-654.
[181] Y. Qin, B.C. Eu, J. Phys. Chem. B 113 (2009) 4751-4755.
[182] D. Enskog, Kgl. Svenska Verenskapsakad. Handl. 4 (1922) 63.
[183] S. Chapman, T.G. Cowling, *The Mathematical Theory of Non-Uniform Gases*, (1970), 259-268.
[184] L. Monchick, E.A. Mason, J. Chem. Phys. 35 (1961) 1676-1697.
[185] M.H. Ernst, J.R. Dorfman, E.G.D. Cohen, Physica 31 (1965) 493-521.
[186] E.N. Fuller, P.D. Schettler, L.C. Giddings, Ind. Eng. Chem. 58 (1966) 19-27.
[187] J.H. Dymond, J. Chem. Phys. 60 (1974) 969-973.
[188] G.A. Parsafar, Z. Kalantar, Fluid Phase Equilibr. 253 (2007) 108-117.
[189] Y.X. Yu, G.H. Gao, Fluid Phase Equilibr. 166 (1999) 111-124.
[190] H. Liu, C.M. Silva, E.A. Macedo, Chem. Eng. Sci. 53 (1998) 2403-2422.
[191] E. Ruckenstein, H. Liu, Ind. Eng. Chem. Res. 36 (1997) 3927-3936.
[192] S.K. Oh, S.W. Campbell, Fluid Phase Equilibr. 129 (1997) 69-88.
[193] L.S. Wang, Z.X. Lang, T.M. Guo, Fluid Phase Equilibr. 117 (1996) 364-372.
[194] E.G.D. Cohen, Physica A 194 (1993) 229-257.
[195] J.W. Dufty, K.C. Mo, K.E. Gubbins, J. Chem. Phys. 94 (1991) 3132-3140.
[196] G.M. Kremer, E. Rosa, Jr., J. Chem. Phys. 89 (1988) 3240-3247.
[197] D.M. Heyes, J. Chem. Soc., Faraday Trans. 2 83 (1987) 1985-2009.
[198] H. Van Beijeren, Phys. Rev. Letters 51 (1983) 1503.
[199] J.H. Dymond, Physica 75 (1974) 100-114.
[200] D.K. Hoffman, C.F. Curtiss, Physics of Fluids 7 (1964) 1887-1897.
[201] W. Sheng, G.J. Chen, H.C. Lu, Int. J. Thermophysics 1 (1989) 133-144.
[202] E. Goldman, L. Sirovich, Physics of Fluids 10 (1967) 1928-1940.
[203] H. Van Beijeren, M.H. Ernst, Physica 68 (1973) 437-456.
[204] W.A. Wakeham, J. Phys. B 6 (1973) 372.

[205] M. Lopez De Haro, E.G.D. Cohen, J.M. Kincaid, J. Chem. Phys. 78 (1983) 2746-2759.
[206] J.M. Kincaid, S. Pérez, E.G.D. Cohen, Phys. Rev. A 38 (1988) 3628.
[207] A. Firoozabadi, K. Ghorayeb, K. Shukla, AIChE J. 46 (2000) 892-900.
[208] M.M. Papari, D.M. Aghaiee, B. Haghighi, A. Boushehri, Fluid Phase Equilibr. 232 (2005) 122-135.
[209] J. Gross, AIChE J. 51 (2005) 2556-2568.
[210] J. Gross, J. Vrabec, AIChE J. 52 (2006) 1194-204.
[211] T. Goel, C.N. Patra, T. Mukherjee and C. Chakravarty, J. Chem. Phys. 129 (2008) 164904.
[212] E. Voyiatzis, F. Müller-Plathe, M.C. Böhm, Macromolecules 46 (2013) 8710-8723.
[213] N.I. Diamantonis, G.C. Boulougouris, D.M. Tsangaris, M.J.E. Kadi, H. Saadawi, S. Negahban, I.G. Economou, Chem. Eng. Res. Des. 91 (2013) 1793-1806.
[214] R.A. Reis, B. Nobrega, J.V. Oliveira, F.W. Tavares, Chem. Eng. Sci. 60 (2005) 4581-4592.
[215] N.F. Carnahan, K.E. Starling, J. Chem. Phys. 51 (1979) 635-636.
[216] R.L. Cotterman, B.J. Schwartz, J.M. Prausnitz, AIChE J. 32 (1986) 1787-1798.
[217] S. Huang, M. Radosz, Ind. Eng. Chem. Res 29 (1990) 2284-2294.
[218] J. D. Van der Waals, "*Over de Continuiteit van den Gas en Vloiestoftoestand (On the Continuity of the Gas and Liquid State)",* Doctoral Dissertation, Leiden University, Leiden, The Netherlands, (1873).
[219] J.W. Cahn, J.E. Hilliard, J. Chem. Phys. 28 (1958) 258-267.
[220] S. Chapman, T.G. Cowling, "*The Mathematical Theory of Non-Uniform Gases"*, 259-268 (1970).
[221] J. Gross, personal communications, 2015.
[222] Institute for Occupational Safety and Health of Germany, TRGS 900, BArBl. Issue 1/2006 (2006), 41-55.
[223] M. Khamooshi, K. Parham, U. Atikol, Adv. Mech. Eng. 5 (2013) 620592.
[224] K.E. Herold, R. Radermacher, „*Absorption Chillers and Heat Pumps*", CRC Press (1996).
[225] J.M.M. Araujo, A.B. Pereiro, F. Alves, I.M. Marrucho, L.P.N. Rebelo, J. Chem. Thermodyn. 57 (2013) 1-8.
[226] M.C. Castro, H. Rodriguez, A. Arce, A. Soto, Ind. Eng. Chem. Res. 53 (2014) 11850-11861.
[227] A.P. Fröba, M.H. Rausch, K. Krzeminski, D. Assenbaum, P. Wasserscheid, A. Leipertz, Int. J. Thermophys. 31 (2010) 2059-2077.
[228] M.G. Freire, A.R.R. Teles, M.A.A. Rocha, B. Schroder, C.M.S. Neves, P.J. Carvalho, D.V. Evtuguin, L.M.N.B.F. Santos, J.A.P. Coutinho, J. Chem. Eng. Data 56 (2011) 4813-4822.
[229] F.S. Oliveira, L.P.N. Rebelo, I.M. Marrucho, J. Chem. Eng. Data 60 (2015) 781-789.
[230] A.B. Pereiro, J.M.M. Araujo, F.S. Oliveira, C.E.S. Bernardes, J.M.S.S. Esperanca, J.N.C. Lopes, I.M. Marrucho, L.P.N. Rebelo, Chem. Commun. 48 (2012) 3656-3658.
[231] A. Pinkert, K.L. Ang, K.N. Marsh, S. Pang, Phys. Chem. Chem. Phys. 13 (2011) 5136-5143.
[232] A. M. Pinto, H. Rodriguez, A. Arce, A. Soto, J. Chem. Thermodyn. 77 (2014) 197-205.

[233] E. Quijada-Maldonado, S. Van der Boogaart, J. H. Lijbers, G. W. Meindersma, A. B. De Haan, J. Chem. Thermodyn. 51 (2012) 51-58.
[234] D. Rabari, N. Patel, M. Joshipura, T. Banerjee, J. Chem. Eng. Data 59 (2014) 571-578.
[235] J.G. Rosenboom, W. Afzal, J.M. Prausnitz, J. Chem. Thermodyn. 47 (2012) 320-327.
[236] M.B. Shiflett, A. Yokozeki, J. Chem. Eng. Data 54 (2009) 108-114.
[237] J. Troncoso, C.A. Cerdeiriña, Y.A. Sanmamed, L. Romaní, L.P.N. Rebelo, J. Chem. Eng. Data 51 (2006) 1856-1859.
[238] M.G. Montalban, C.L. Bolivar, F.G.D. Banos, G. Villora, J. Chem. Eng. Data 60 (2015) 1986-1996.
[239] G.J. Kabo, A.V. Blokhin, Y.U. Paulechka, A.G. Kabo, M.P. Shymanovich, J.W. Magee, J. Chem. Eng. Data 49 (2004) 453-461.
[240] R.L. Gardas, M.G. Freire, P.J. Carvalho, I.M. Marrucho, I.M. Fonseca, A.G. Ferreira, J.A.P. Coutinho, J. Chem. Eng. Data 52 (2007) 80-88.
[241] O. Ciocirlan, O. Croitoru, O. Iulian, J. Chem. Eng. Data 59 (2014) 1165-1174.
[242] K.R. Harris, M. Kanakubo, L.A. Woolf, J. Chem. Eng. Data 52 (2007) 2425-2430.
[243] J. Jacquemin, R. Ge, P. Nancarrow, D.W. Rooney, M.F.C. Gomes, A.A.H. Padua, C. Hardacre, J. Chem. Eng. Data 53 (2008) 716-726.
[244] J. Jacquemin, P. Husson, A.A.H. Padua, V. Majer, Green Chem. 8 (2006) 172-180.
[245] T. Kavitha, T. Vasantha, P. Venkatesu, R.S.R. Devi, T. Hofman, J. Mol. Liq. 198 (2014) 11-20.
[246] K.S. Kim, B.K. Shin, H. Lee, Korean J. Chem. Eng. 21 (2004) 1010-1014.
[247] T.S. Krishna, M.G. Sankar, K.T.S. Raju, S.G. Rao, B. Munibhadrayya, J. Mol. Liq. 206 (2015) 350-358.
[248] P. Navarro, M. Larriba, S. Garcia, J. Garcia, F. Rodriguez, J. Chem. Eng. Data 57 (2012) 1165-1173.
[249] A. Pal, B. Kumar, J. Chem. Eng. Data 57 (2012) 688-695.
[250] G. Perez-Sanchez, J. Troncoso, P. Losada-Perez, P. Mendez-Castro, L. Romani, J. Chem. Thermodyn. 65 (2013) 131-137.
[251] F. Qi, H. Wang, J. Chem. Thermodyn. 41 (2009) 265-272.
[252] J. Salgado, T. Regueira, L. Lugo, J. Vijande, J. Fernandez, J. Garcia, J. Chem. Thermodyn. 70 (2014) 101-110.
[253] Y. A. Sanmamed, D. Gonzalez-Salgado, J. Troncoso, L. Romani, A. Baylaucq, C. Boned, J. Chem. Thermodyn. 42 (2010) 553-563.
[254] Y. A. Sanmamed, D. Gonzalez-Salagado, J. Troncoso, C.A. Cerdeirina, L. Romani, Fluid Phase Equilib. 252 (2007) 96-102.
[255] C. Schreiner, S. Zugmann, R. Hartl, H.J. Gores, J. Chem. Eng. Data 55 (2010) 1784-1788.
[256] A. Stoppa, O. Zech, W. Kunz, R. Buchner, J. Chem. Eng. Data 55 (2010) 1768-1773.
[257] G.R. Sunkara, M.M. Tadavarthi, V.K. Tadekoru, S.K. Tadikonda, S.R. Bezawada, J. Chem. Eng. Data 60 (2015) 886-894.
[258] M. Tariq, P.A.S. Forte, M.F.C. Gomes, J.N.C. Lopes, L.P.N. Rebelo, J. Chem. Thermodyn. 41 (2009) 790-798.
[259] H. Tokuda, S. Tsuzuki, M.A.B.H. Susan, K. Hayamizu, M. Watanabe, J. Phys. Chem. B 110 (2006) 19593-19600.

[260] D. Tomida, A. Kumagai, K. Qiao, C. Yokoyama, Int. J. Thermophys. 27 (2006) 39-47.
[261] J.Y. Wu, Y.P. Chen, C.S. Su, J. Solution Chem. 44 (2015) 395-412.
[262] W.G. Xu, L. Li, X.X. Ma, J. Wei, W.B. Duan, W. Guan, J.Z. Yang, J. Chem. Eng. Data 57 (2012) 2177-2184.
[263] Y. Zhang, T. Zhang, P. Gan, H. Li, M. Zhang, K. Jin, S. Tang, J. Chem. Eng. Data 60 (2015) 1706-1714.
[264] G. Garcia-Miaja, J. Troncoso, L. Romani, Fluid Phase Equilib. 274 (2008) 59-67.
[265] E.J. Gonzalez, A. Dominguez, E.A. Macedo, J. Chem. Eng. Data 57 (2012) 2165-2176.
[266] E.J. Gonzalez, N. Calvar, A. Dominguez, E.A. Macedo, J. Chem. Thermodyn. 61 (2013) 64-73.
[267] J. Klomfar, M. Souckova, J. Patek, J. Chem. Eng. Data 55 (2010) 4054-4057.
[268] R.G. Seoane, S. Corderi, E. Gomez, N. Calvar, E.J. Gonzalez, E.A. Macedo, A. Dominguez, Ind. Eng. Chem. Res. 51 (2012) 2492-2504.
[269] O. Zech, A. Stoppa, R. Buchner, W. Kunz, J. Chem. Eng. Data 55 (2010) 1774-1778.
[270] K.R. Harris, M. Kanakubo, L.A. Woolf, J. Chem. Eng. Data 51 (2006) 1161-1167.
[271] A. Kumar, J. Solution Chem. 37 (2008) 203-214.
[272] H. Ning, M. Hou, Q. Mei, Y. Liu, D. Yang, B. Han, Sci. China Chem. 55 (2012) 1509-1518.
[273] L.G. Sanchez, J.R. Espel, F. Onink, G.W. Meindersma, A.B. de Haan, J. Chem. Eng. Data 54 (2009) 2803-2812.
[274] T. Singh, A. Kumar, J. Chem. Thermodyn. 40 (2008) 417-423.
[275] D. Tomida, S. Kenmochi, T. Tsukada, K. Qiao, Q. Bao, C. Yokoyama, Int. J. Thermophys. 33 (2012) 959-969.
[276] M.S. Aituwaim, K.H.A.E. Alkhaldi, A.S. Al-Jimaz, A.A. Mohammad, J. Chem. Eng. Data 59 (2014) 1955-1963.
[277] G.R. Chaudhary, S. Bansal, S.K. Mehta, A.S. Ahluwalia, J. Chem. Thermodyn. 50 (2012) 63-70.
[278] K.R. Harris, L.A. Woolf, M. Kanakubo, J. Chem. Eng. Data 50 (2005) 1777-1782.
[279] Y. Huo, S. Xia, P. Ma, J. Chem. Eng. Data 53 (2008) 2535-2539.
[280] J. Jacquemin, P. Husson, V. Mayer, I. Cibulka, J. Chem. Eng. Data 52 (2007) 2204-2211.
[281] J. Jacquemin, P. Husson, V. Majer, M.F. Costa Gomes, Fluid Phase Equilib. 240 (2006) 87-95.
[282] J. Kumelan, A.P.S. Kamps, D. Tuma, G. Maurer, Fluid Phase Equilib. 228-229 (2005) 207-211.
[283] J.N.C. Lopes, T.C. Cordeiro, J.M.S.S. Esperanca, H.J.R. Guedes, S. Huq, L.P.N. Rebelo, K.R. Seddon, J. Phys. Chem. B 109 (2005) 3519-3525.
[284] A.B. Pereiro, J.L. Legido, A. Rodriguez, J. Chem. Thermodyn. 39 (2007) 1168-1175.
[285] A. B. Pereiro, A. Rodriguez, J. Chem. Eng. Data 52 (2007) 600-608.
[286] G. Reyes, M. Cartes, C. Rey-Castre, H. Segura, A. Mejia, J. Chem. Eng. Data 58 (2013) 1203-1211.
[287] M.A.A. Rocha, F.M.S. Ribeiro, A.I.M.C.L. Ferreira, J.A.P. Coutinho, L.M.N.B.F. Santos, J. Mol. Liq. 188 (2013) 196-202.

[288] M.T. Zafarani-Moattar, H. Shekaari, J. Chem. Thermodyn. 38 (2006) 1377-1384.
[289] M. Souckova, J. Klomfar, J. Patek, J. Chem. Thermodyn. 77 (2014) 31-39.
[290] K.R. Harris, M. Kanakubo, L.A. Woolf, J. Chem. Eng. Data 52 (2007) 1080-1085.
[291] J. Klomfar, M. Souckova, J. Patek, J. Chem. Eng. Data 59 (2014) 2263-2274.
[292] J.G. Li, Y.F. Hu, S. Ling, J.Z. Zhang, J. Chem. Eng. Data 56 (2011) 3068-3072.
[293] A. Muhammad, M.I.A. Mutalib, C.D. Wilfred, T. Murugesan, A. Shafeeq, J. Chem. Thermodyn. 40 (2008) 1433-1438.
[294] A.B. Pereiro, E. Tojo, A. Rodriguez, J. Canosa, J. Tojo, J. Chem. Thermodyn. 38 (2006) 651-661.
[295] A.B. Pereiro, A. Rodriguez, J. Chem. Thermodyn. 39 (2007) 978-989.
[296] R. Taguchi, H. Machida, Y. Sato, R.L. Smith, J. Chem. Eng. Data 54 (2009) 22-27.
[297] D. Tomida, A. Kumagai, S. Kenmochi, K. Qiao, C. Yokoyama, J. Chem. Eng. Data 52 (2007) 577-579.
[298] D. Tomida, S. Kenmochi, T. Tsukada, K. Qiao, C. Yokoyama, Int. J. Thermophys. 28 (2007) 1147-1160.
[299] R. Gomes de Azevedo, J.M.S.S. Esperanca, V. Najdanovic-Visak, Z.P. Visak, H.J.R. Guedes, M. Nunes da Ponte, L.P.N. Rebelo, J. Chem. Eng. Data 50 (2005) 997-1008.
[300] J. Klomfar, M. Souckova, J. Patek, J. Chem. Eng. Data 56 (2011) 426-436.
[301] H, Machida, Y. Sato, R.L. Smith, Fluid Phase Equilib. 264 (2008) 147-155.
[302] D. Matkowska, T. Hofman, J. Mol. Liq. 165 (2011) 161-167.
[303] E. Rilo, A.G.M. Ferreira, I.M.A. Fonseca, O. Cabeza, Fluid Phase Equilib. 296 (2010) 53-59.
[304] I.M. Abdulagatov, A. Tekin, J. Safarov, E. Hassel, Int. J. Thermophys. 29 (2008) 505-533.
[305] J. Klomfar, M. Souckova, J. Patek, J. Chem. Eng. Data 57 (2012) 708-720.
[306] Z. Gu, J.F. Brennecke, J. Chem. Eng. Data 47 (2002) 339-345.
[307] Y. Qiao, F. Yan, S. Xia, S. Yin, P. Ma, J. Chem. Eng. Data 56 (2011) 2379-2385.
[308] A. Tekin, J. Safarov, A. Shahverdiyev, E. Hassel, J. Mol. Liq. 136 (2007) 177-182.
[309] M.G. Freire, P.J. Carvalho, A.M. Fernandes, I.M. Marrucho, A.J. Queimada, J.A. Coutinho, J. Colloid Interface Sci. 314 (2007) 621-630.
[310] H.F.D. Almeida, A.R.R. Teles, J.A. Lopes-da-Silva, J.A.P. Coutinho, M.G. Freire, J. Chem. Thermodyn. 54 (2012) 49-54.
[311] G. Law, P. R. Watson, Langmuir,17 (2001) 6138-6141.
[312] D. Fu, H. Wang, L. Du, J. Chem. Thermodyn. 71 (2014) 1-5.
[313] M.H. Ghatee, A.R. Zolghadr, Fluid Phase Equilib. 263 (2008) 168-175.
[314] K.S. Kim, D. Demberelnyamba, B.K. Shin, S.H. Yeon, S. Choi, J.H. Cha, H. Lee, C.S. Lee, J.J. Shim, Korean J. Chem. Eng. 23 (2006) 113-116.
[315] J. Klomfar, M. Souckova, J. Patek, J. Chem. Thermodyn. 42 (2010) 323 -329.
[316] G. Vakili-Nezhaad, M. Vatani, M. Asghari, I. Ashour, J. Chem. Thermodyn. 54 (2012) 148-154.
[317] J.Y. Wang, X.J. Zhang, Y.M. Liu, Y.Q. Hu, J. Chem. Eng. Data 56 (2011) 3734-3737.
[318] M. Souckova, J. Klomfar, J. Patek, Fluid Phase Equilib. 303 (2011) 184-190.
[319] J. Klomfar, M. Souckova, J. Patek, J. Chem. Eng. Data 54 (2009) 1389-1394.

[320] L. George, P. R. Watson, Langmuir 17 (2001) 6138-6141.
[321] P. Kilaru, G.A. Baker, P. Scovazzo, J. Chem. Eng. Data 52 (2007) 2306-2314.
[322] M. Singh, S. Mandal, Y. Verma, A. Gupta, R. Singh, S. Chandra, J. Chem. Eng. Data 59 (2014) 2349-2359.
[323] J. Klomfar, M. Souckova, J. Patek, Fluid Phase Equilib. 385 (2015) 62-71.
[324] Y.A. Sanmamed, P. Navia, D. González-Salgado, J. Troncoso, L. Romaní, J. Chem. Eng. Data 55 (2009) 600-604.
[325] H.C. Hu, A.N. Soriano, R.B. Leron, M.H. Li, Thermochim. Acta 519 (2011) 44-9.
[326] C.P. Fredlake, J.M. Crosthwaite, D.G. Hert, S.N.V.K. Aki, J.F. Brennecke, J. Chem. Eng. Data 49 (2004) 954-964.
[327] C.A. Nieto de Castro, M.J.V. Lourenco, A.P.C. Ribeiro, E. Langa, S.I.C. Vieira, J. Chem. Eng. Data 55 (2010) 653-661.
[328] Y.U. Paulechka, A.G. Kabo, A.V. Blokhin, G.J. Kabo, M.P. Shevelyova, J. Chem. Eng. Data 55 (2010) 2719-2724.
[329] Z.H. Zhang, Z.C. Tan, Y.S. Li, L.X. Sun, J. Therm. Anal. Calorim. 85 (2006) 551-557.
[330] Y.U. Paulechka, A.V. Blokhin, G.J. Kabo, Thermochim. Acta 604 (2015) 122-128.
[331] D. Waliszewski, I. Stepniak, H. Piekarski, A. Lewandowski, Thermochim. Acta 433 (2005) 149-152.
[332] L.P.N. Rebelo, V. Najdanovic-Visak, Z.P. Visak, M. Nunes da Ponte, J. Szydlowski, C.A. Cerdeirina, J. Troncoso, L. Romani, J.M.S.S. Esperanca, H.J.R. Guedes, H.C. de Sousa, Green Chem. 6 (2004) 369-381.
[333] Y.H. Yu, A.N. Soriano, M.H. Li, Thermochim. Acta 482 (2009) 42-48.
[334] G. Garcia-Miaja, J. Troncoso, L. Romani, J. Chem. Thermodyn. 41 (2009) 334-341.
[335] K.S. Kim, Korean J. Chem. Eng. 26 (2009) 770-774.
[336] K.S. Kim, B.K. Shin, F. Ziegler, Fluid Phase Equilib. 218 (2004) 215-220.
[337] D. Waliszewski, J. Chem. Thermodyn. 40 (2008) 203-207.
[338] J.M. Crosthwaite, M.J. Muldoon, J.K. Dixon, J.L. Anderson, J.F. Brennecke, J. Chem. Thermodyn. 37 (2005) 559-568.
[339] J.D. Holbrey, W.M. Reichert, R.G. Reddy, R.D. Rogers, "*Ionic Liquids as Green Solvents*", Progress and Prospects, ACS Symposium Series, Vol. 856 (2003), Ch. 11, Pg. 121-133, American Chemical Society, Washington D. C.
[340] Z.H. Zhang, T. Cui, J.I. Zhang, H. Xiong, G.P. Li, L.X. Sun, F. Xu, Z. Cao, F. Li, J.J. Zhao, J. Therm. Anal. Calorim. 101 (2010) 1143-1148.
[341] Tables, T. R. C., "*Selected values of properties of chemical compounds"*, Thermodynamic Research Center Data Project, Texas A&M University, College Station, (1974).
[342] G.R. Chaudhary, S. Bansal, S.K. Mehta, A.S. Ahluwalia, J. Solution Chem. 43 (2014) 340-359.
[343] S.P. Ijardar, N.I. Malek, J. Chem. Thermodyn. 71 (2014) 236-248.
[344] N.I. Malek, S.P. Ijardar, S.B. Oswal, J. Chem. Eng. Data 59 (2014) 540-553.
[345] A. Pal, R. Gaba, T. Singh, A. Kumar, J. Mol. Liq. 154 (2010) 41-46.
[346] M.T. Zafarani-Moattar, H. Shekaari, J. Chem. Eng. Data 50 (2005) 1694-1699.
[347] N.I. Malek, A. Singh, R. Surati, S.P. Ijardar, J. Chem. Thermodyn. 74 (2014) 103-118.
[348] A. Pal, B. Kumar, Fluid Phase Equilib. 334 (2012) 157-165.
[349] A.J. de Villiers, C.E. Schwarz, A.J. Burger, G.M. Kontogeorgis, Fluid Phase Equilib 338 (2013) 1-5.

[350] P. Etesse, J.A. Zega, R. Kobayashi, J. Chem. Phys. 97 (1992) 2022-2029.
[351] R. Span, W. Wagner, J. Phys. Chem. Ref. Data 25 (1995) 1509-1596.
[352] R. Dawson, F. Khoury, R. Kobayashi, AIChE J. 16 (1970) 725-729.
[353] D.E. Woessner, B.S. Snowden, Jr., R.A. George, J.C. Melrose, I & EC Fund. 8 (1969) 779-786.
[354] R.C. Robinson, W.E. Stuart, I & EC Fund. 7 (1968) 90-95.
[355] N. Asahi, Y. Nakamura, J. Chem. Phys. 109 (1998) 9879-9887.
[356] S.L. Wallen, B.J. Palmer, B.C. Garrett, C.R. Yonker, J. Phys. Chem. 100 (1996) 3959-3964.
[357] M.M. Hoffmann, M.S. Conradi, J. Phys. Chem. B 102 (1998), 263-271.
[358] K. Yoshida, N. Mantubayasi, M. Nakahara, J. Chem. Phys. 125 (2005), 074307.
[359] K. Yoshida, N. Mantubayasi, M. Nakahara, J. Chem. Phys. 129 (2008), 214501.
[360] V.J. Berry, Jr., R.C. Koeller, AIChE J. 6 (1960), 274-280.
[361] B. Haghighi, M. Fathabadi, M.M. Papari, Fluid Phase Equilibr. 203 (2002), 205-225.
[362] W.W. Wakeham, D.H. Slater, J. Physics B 7 (1974), 297-306.
[363] V.R. Maynard, E. Grushka, Adv. Chromatogr. 12 (1975), 99-140.
[364] E.N. Fuller, K. Ensley, J.C. Giddings, J. Phys. Chem. 73 (1969), 3679-3685.
[365] S.L. Seager, L.R. Geertson, J.C. Giddings, J. Chem. Eng. Data 8 (1963), 168-169.
[366] A.-L. Revelli, F. Mutelet, J.-N. Jaubert, J. Chem. Thermodyn. 42 (2010), 177-181.
[367] K. Sahandzhieva, D. Tuma, S. Breyer, A. P. S. Kamps, G. Maurer, J. Chem. Eng. Data 51 (2006), 1516-1525.
[368] M. Seiler, A. Kühn, F. Ziegler, X. Wang, Ind. Eng. Chem. Res. 52 (2013), 16519−16546.
[369] M. De Vega, J.-A. Almendros-Ibáñez, G. Ruiz, Energy Convers. Manage. 47 (2006), 3393-3407.
[370] L. A. Blanchard, Z. Gu, J. F. Brennecke, J. Phys. Chem. B 105 (2001), 2437-2444.
[371] B. Mokhtarani, M. M. Mojtahedi, H. R. Mortaheb, M. Mafi, F. Yazdani, F. Sadeghian, J. Chem. Eng. Data 53 (2008), 677-682.
[372] J. Restolho, A. P. Serro, J. L. Mata, B. Saramago, J. Chem. Eng. Data 54 (2009), 950-955.
[373] W. Afzal, X. Liu, J. M. Prausnitz, J. Chem. Thermodyn. 63 (2013), 88-94.
[374] S. N. V. K. Aki, B. R. Mellein, E. M. Saurer, J. F. Brennecke, J. Phys. Chem. B 108 (2004), 20355-20365.
[375] M. R. Curras, M. F. Costa Gomes, P. Husson, A. A. H. Padua, J. Garcia, J. Chem. Eng. Data 55 (2010), 5504-5512.
[376] H. Gao, F. Qi, H. Wang, J. Chem. Thermodyn. 41 (2009), 888-892.
[377] Y. Huo, S. Xia, P. Ma, J. Chem. Eng. Data 52 (2007), 2077-2082.
[378] M. A. Iglesias-Otero, J. Troncoso, E. Carballo, J. Solution Chem. 36 (2007), 1219-1230.
[379] J. Klomfar, M. Souckova, J. Patek, Fluid Phase Equilib. 282 (2009), 31-37.
[380] W. Li, Z. Zhang, B. Han, S. Hu, Y. Xie, G. Yang, J. Phys. Chem. B 111 (2007), 6452-6456.
[381] Y. Li, H. Ye, P. Zeng, F. Qi, J. Solution Chem. 39 (2010), 219-230.
[382] H. Lu, Y. Guo, X. An, W. Sheng, J. Chem. Eng. Data 55 (2010), 2482-2488.
[383] P. Navia, J. Troncoso, L. Romani, J. Chem. Eng. Data 52 (2007), 1369-1374.

[384] V. A. Nikitina, A. Nazet, T. Sonnleitner, R. Buchner, J. Chem. Eng. Data 57 (2012), 3019-3025.
[385] J. Palgunadi, J. E. Kang, D. Q. Nguyen, J. H. Kim, B. K. Min, S. D. Lee, H. Kim, H. S. Kim, Thermochim. Acta 494 (2009), 94-98.
[386] A. N. Soriano, B. T. Doma Jr., M.-H. Li, J. Chem. Thermodyn. 41 (2009), 301-307.
[387] D. Song, J. Chen, J. Chem. Thermodyn. 77 (2014), 137-143.
[388] M. M. Taib, T. Murugesan, J. Chem. Eng. Data 57 (2012), 120-126.
[389] S. Tian, Y. Hou, W. Wu, S. Ren, K. Pang, J. Chem. Eng. Data 57 (2012), 756-763.
[390] R. Yusoff, M. K. Aroua, A. Shamiri, A. Ahmady, N. S. Jusoh, N.. F. Asmuni, L. C. Bong, S. H. Thee, J. Chem. Eng. Data 58 (2013), 240-247.
[391] Y. Zhao, X. Zhang, S. Zeng, Q. Zhou, H. Dong, X. Tian, S. Zhang, J. Chem. Eng. Data 55 (2010), 3513-3519.
[392] Q. Zhou, L.-S. Wang, J. Chem. Eng. Data 51 (2006), 905-908.
[393] M.-L. Ge, R.-S. Zhao, Y.-F. Yi, Q. Zhang, L.-S. Wang, J. Chem. Eng. Data 53 (2008), 2408-2411.
[394] M. Shamsipur, A. A. M. Beigi, M. Teymouri, S. M. Pourmortazavi, M. Irandoust, J. Mol. Liq. 157 (2010), 43-50.
[395] M. Tsamba, S. Sarraute, M. Traikia, P. Husson, J. Chem. Eng. Data 59 (2014), 1747-1754.
[396] E. Vercher, P. J. Miguel, F. J. Llopis, A. V. Orchilles, A. Martinez-Andreu, J. Chem. Eng. Data 57 (2012), 1953-1963.
[397] O. A. Al-Rashed, M. A. A. Fahim, M. Shaaban, Fluid Phase Equilib. 363 (2014), 248-262.
[398] S. V. Dzyuba, R. A. Bartsch, ChemPhysChem 3 (2002), 161-166.
[399] W. Fan, Q. Zhou, J. Sun, S. Zhang, J. Chem. Eng. Data 54 (2009), 2307-2311.
[400] A. Kumar, T. Singh, R. L. Gardas, J. A. P. Coutinho, J. Chem. Thermodyn. 40 (2008), 32-39.
[401] T. Singh, A. Kumar, J. Mol. Liq. 153 (2010), 117-123.
[402] W.A. Fouad, M. Yarrison, K.Y. Song, K.R. Cox, W.G. Chapman, AIChE J. 61 (2015), 3038-3052.
[403] J. Stoll, J. Vrabec, H. Hasse, AIChE J. 49 (2003), 2187-2198.
[404] P.F. Arce, M. Aznar, J Supercrit. Fluids 52 (2010), 18-29.
[405] C. Le Thi, S. Tamouza, J.P. Passarello, P. Tobaly, J.C. de Hemptinne, Ind. Eng. Chem. Res 45 (2006), 6803-6810.
[406] O.G. Nino-Amézquita, D. Putten, S. Enders, Fluid Phase Equilibr. 332 (2012), 40-47.

Eidesstattliche Versicherung

gemäß § 5 Abs. 2 Ziff. 4 der Promotionsordnung des Karlsruher Instituts für Technologie für die Fakultät für Chemieingenieurwesen und Verfahrenstechnik

1. Bei der eingereichten Dissertation zu dem Thema *„Bereitstellung thermodynamischer Daten für die Auswahl des Arbeitspaares bei Absorptions-kältemaschinen“* handelt es sich um meine eigenständig erbrachte Leistung.

2. Ich habe nur die angegebenen Quellen und Hilfsmittel benutzt und mich keiner unzulässigen Hilfe Dritter bedient. Insbesondere habe ich wörtlich oder sinngemäß aus anderen Werken übernommene Inhalte als solche kenntlich gemacht.

3. Die Arbeit oder Teile davon habe ich bislang nicht an einer Hochschule des In- oder Auslands als Bestandteil einer Prüfungs- oder Qualifikationsleistung vorgelegt.

4. Ich habe die Regeln zur Sicherung guter wissenschaftlicher Praxis im Karlsruher Institut für Technologie (KIT) in der gültigen Fassung beachtet.

5. Die Richtigkeit der vorstehenden Erklärungen bestätige ich.

6. Die Bedeutung der eidesstattlichen Versicherung und die strafrechtlichen Folgen einer unrichtigen oder unvollständigen eidesstattlichen Versicherung sind mir bekannt. Ich versichere an Eides statt, dass ich nach bestem Wissen die reine Wahrheit erklärt und nichts verschwiegen habe.

Berlin, den 27. Juni 2017

Hendryk Rudolph

Eidesstattliche Versicherung

Belehrung

Die Universitäten in Baden-Württemberg verlangen eine Eidesstattliche Versicherung über die Eigenständigkeit der erbrachten wissenschaftlichen Leistungen, um sich glaubhaft zu versichern, dass der Promovend die wissenschaftlichen Leistungen eigenständig erbracht hat.

Weil der Gesetzgeber der Eidesstattlichen Versicherung eine besondere Bedeutung beimisst und sie erhebliche Folgen haben kann, hat der Gesetzgeber die Abgabe einer falschen eidesstattlichen Versicherung unter Strafe gestellt. Bei vorsätzlicher (also wissentlicher) Abgabe einer falschen Erklärung droht eine Freiheitsstrafe bis zu drei Jahren oder eine Geldstrafe.

Eine fahrlässige Abgabe (also Abgabe, obwohl Sie hätten erkennen müssen, dass die Erklärung nicht den Tatsachen entspricht) kann eine Freiheitsstrafe bis zu einem Jahr oder eine Geldstrafe nach sich ziehen.

Die entsprechenden Strafvorschriften sind in § 156 StGB (falsche Versicherung an Eides Statt) und in § 161 StGB (fahrlässiger Falscheid, fahrlässige falsche Versicherung an Eides Statt) wiedergegeben.

§ 156 StGB: Falsche Versicherung an Eides Statt
Wer vor einer zur Abnahme einer Versicherung an Eides Statt zuständigen Behörde eine solche Versicherung falsch abgibt oder unter Berufung auf eine solche Versicherung falsch aussagt, wird mit Freiheitsstrafe bis zu drei Jahren oder mit Geldstrafe bestraft.
§ 161 StGB: Fahrlässiger Falscheid, fahrlässige falsche Versicherung an Eides Statt
Abs. 1: Wenn eine der in den § 154 bis 156 bezeichneten Handlungen aus Fahrlässigkeit begangen worden ist, so tritt Freiheitsstrafe bis zu einem Jahr oder Geldstrafe ein.
Abs. 2: Straflosigkeit tritt ein, wenn der Täter die falsche Angabe rechtzeitig berichtigt. Die Vorschriften des § 158 Abs. 2 und 3 gelten entsprechend.

Berlin, den 27. Juni 2017

Hendryk Rudolph